# Investigating the role of lineage in the cortical integration of thalamic inputs


*Author:*
Matthew J. Buchan

*Supervisor:*
Prof. Colin J.Akerman

*A thesis submitted in fulfillment of the requirements*
*for the degree of Doctor of Philosophy*

*in the*

Department of Pharmacology
University of Oxford

Hilary Term 2022

# Declaration of Authorship

I, Matthew J. Buchan, declare that this thesis titled, "Investigating the role of lineage in the cortical integration of thalamic inputs" and the work presented in it are wholly my own, aside from parts that were completed in collaboration. I clearly acknowledge where others have made contributions, as follows:

- **Section 2.2**: Dr Sarah Newey designed and constructed the CAG-Lhx2 plasmids.
- **Figure 4.1A**: Dr Kashif Mahfooz acquired images.
- **Figure 4.2**: Dr Kashif Mahfooz acquired *in vitro* electrophysiology data.
- **Figure 4.4**: Dr Sophie Avery performed *in utero* electroporations, postnatal intrathalamic injections, and acquired *in vitro* electrophysiology data.
- **Figure 5.4A**: Gemma Gothard acquired images.
- **Figure 5.5**: Dr Kashif Mahfooz acquired *in vitro* electrophysiology data.
- **Figure 5.7**: Dr Kashif Mahfooz performed postnatal intrathalamic injections and acquired *in vitro* electrophysiology data.

"*The struggle itself toward the heights is enough to fill a man's heart. One must imagine Sisyphus happy.*"

Albert Camus

# Abstract

Primary sensory cortex receives and integrates inputs from first-order and higher-order thalamic nuclei. First-order inputs convey sensory information from the periphery and exhibit simple response properties, whereas higher-order inputs exhibit more complex response properties, provide contextual feedback, and can modulate first-order inputs. The data presented within this thesis show that the way in which cortical neurons integrate these thalamic inputs, reflects the progenitor cell from which the cortical neurons derive. Within layer 4 of mouse primary somatosensory cortex, excitatory neurons that derive from apical intermediate progenitors exhibit multi-whisker response properties and receive higher-order thalamic input, in a manner consistent with their dendritic morphology. These properties depend upon the expression levels of the transcription factor Lhx2, which when increased, abolishes the higher-order properties of apical intermediate progenitor-derived neurons, and disrupts the induction of sensory-evoked plasticity. These data reveal a lineage-dependent mechanism that establishes the integration and functional contribution of higher-order thalamic inputs within cortex.

# Acknowledgements

All of the experiments in this thesis, the things that I have learned, and how I have changed as a person would simply not have happened if not for the guidance of my supervisor, Colin. Your ability to dive into new areas of research with thoughtful abandon is an inspiration, and the mastery of detail you seem to be able to retain is simply unfair to the rest of us. I am grateful that you were understanding of my desire to pursue other creative projects outside of the lab, that sometimes required considerable commitments of time. Ever supportive, if you thought my priorities needed to be re-aligned, this was almost always done with sensitivity:

> "I know that you have a lot of work to do. I'm just checking that you also know that you have a lot of work to do".

Perhaps the best compliment I can give you, is that whenever you come up in conversation with other people, the first words always mention how kind and approachable you are. It is difficult to overstate the significance of this in your role as a mentor, and as a friend.

I cannot hope to list all of the other ways in which I have become indebted to various people throughout my DPhil. So, in true Akerman Lab style, it will have to be a 'quick' whip round.

To all members of the Akerman Lab (past and present), thank you for being such wonderful colleagues. Some honourable mentions include: Joram, for teaching me near-enough everything useful that I know about data analysis and programming (not to mention the many many open fires, successful or otherwise); Kashif, for being an incredibly patient teacher to an incredibly impatient student; Richard, for always being willing to pick a smaller hill to die on than me, and Gemma, for

killing him there; Alex VK, for encouraging the benefits of multi-faith worship with respect to electrical noise; Sarah, for always being around to set the world to rights and to help me with all things relating to molecular biology, not least loading the dishwasher; and Paul, for always being the person willing to ask questions, even if they relate to my disgusting code. I am also hugely appreciative of the efforts of John, Martyn and Hicham, without whom the Pharmacology Department would grind to a halt.

I should also thank Professors Gareth Miles and Keith Sillar at the University of St Andrews. Whilst they will inevitably be disappointed to know that I have spent the last few years studying a vestigial lump of grey matter that sits on top of the spinal cord, without their encouragement and guidance during my 'formative' years, I likely would not have ended up where I am today.

Following the conclusion of my experiments, I spent a 'hiatus' working at IBM Research. I am particularly grateful to Joe Pavitt, Graham White, Dave Braines, and Helen Stanton for providing me with that opportunity, and giving me the resources to explore the ways in which the worlds of neuroscience and AI collide.

Outside of the lab, I have been utterly reliant on several key support networks (which shall be referred to by groupchat name only for the sake of everyone involved): The Bovril Boys (old and new), The Flaky Housewives, QCCCCACC, and QC Spon Bois. In addition, those that know me will appreciate that music represents a huge part of my life in Oxford. In particular, I would like to thank Professor Owen Rees and all of the singers that I have had the pleasure of working with during my time as a member of The Queen's College Chapel Choir, and beyond.

I have wonderful friends, scattered across the world. However, a few people have been particularly influential over the course of my DPhil: Steph, for being a constant companion, and an important source of bread, in the dark days of pandemic restrictions; Rory, for bringing out what can only be described as my indulgent side; and Sarah, for always telling me things as they are.

Thank you to my parents, who quite clearly underestimated the extent to which I would run with the advice:

"We don't mind what you do as long as you find it interesting".

I can never repay what you have offered me in terms of support and understanding (if not the contents of this doorstop). What I will say, is that these experiences have given me the tools to continue following that advice long into the future.

Finally, I must thank Emma for being so supportive throughout the write-up of my DPhil. In all likelihoods you don't want to hear anything about neuroscience ever again, but no promises.

# Contents

# List of Figures

For my family and friends...

# Chapter 1

# General introduction

To be evolutionarily successful, an organism must reliably represent the sensory world and use that knowledge to guide behaviour and learning. This process requires that the brain encodes information not only about features of the sensory stimuli, but also about the context in which these stimuli occur. Understanding how these two types of information are integrated within networks of neurons represents a fundamental goal within systems and sensory neuroscience.

Sensory processing is organised in a hierarchical manner (Felleman and Van Essen 1991; Harris et al. 2019). Sensory information travels from the periphery through sequential stages of processing to higher brain areas in a feedforward manner (Sherman and Guillery 1996; Sherman and Guillery 1998). At each stage, convergent inputs from multiple sources are integrated, leading to the construction of increasingly complex stimulus representations that incorporate different features of the sensory environment (Siegle et al. 2021). In turn, higher areas send feedback projections that influence the processing of incoming sensory information, for example in response to changing context (Cauller 1995; Gilbert and Li 2013; Keller et al. 2020; Kwon et al. 2016; Nurminen et al. 2018; Vangeneugden et al. 2019). This hierarchical organisation is typified by the mammalian cortex, where these principles are well understood at a large scale; anatomical patterns of feedforward and feedback connectivity can be used to construct models that accurately describe the distribution of functional attributes across brain areas, and the complexity of stimulus representations at different stages of sensory processing (Harris et al.

2019; Markov et al. 2014; Siegle et al. 2021). Despite this, it is unclear how these organisational principles are implemented at the cellular and synaptic level.

In the rodent cortex, neurons receive convergent inputs from the thalamus that are associated with distinct types of information (Petersen 2007). Inputs from first-order thalamic nuclei relay sensory information from the periphery (Armstrong-James et al. 1992; Sherman and Guillery 1998), whereas inputs from higher-order thalamic nuclei incorporate contextual information, such as arousal levels and movement (Diamond et al. 1992; Lavallée et al. 2005; Petty et al. 2021; Usrey and Sherman 2019). Interestingly, neighbouring cortical neurons exhibit considerable heterogeneity in terms of the relative amount of higher-order input that they receive (Audette et al. 2018; Viaene et al. 2011a; Viaene et al. 2011b; Viaene et al. 2011c). This has fundamental consequences for their sensory response properties (Castejon et al. 2016; Mease et al. 2016; Zhang and Bruno 2019), yet the mechanisms that determine how individual neurons sample different thalamic inputs are unknown.

One potential explanation is that the thalamic inputs to a cortical neuron are reflective of the neuron's developmental history, or lineage. All cortical neurons are born from a heterogeneous pool of progenitor cells during embryonic development (Franco and Müller 2013; Gal 2006; Greig et al. 2013; Noctor et al. 2004; Stancik et al. 2010). Previous work has shown that the local synaptic connectivity between cortical neurons reflects the progenitor from which they derive (Cadwell et al. 2020; Ellender et al. 2019; Yu et al. 2009), suggesting that they sample inputs differently, and in a manner that reflects their lineage. However, it is unclear to what extent lineage governs the connectivity of sensory processing circuits and therefore the hierarchical organisation of cortical circuitry. This thesis aims to investigate how lineage relates to the thalamic inputs received by excitatory neurons in the mouse somatosensory cortex, by performing longitudinal studies that enable the properties of mature cortical neurons to be related to the progenitors from which they were derived during embryonic development.

## 1.1 Thalamocortical interactions

Sensory processing is underpinned by extensive reciprocal connectivity between the cortex and the thalamus (Halassa and Sherman 2019; Harris and Shepherd 2015; Sherman 2012; Sherman 2016). The evolutionary expansion of the cortex is often associated with the emergence of higher cognitive functions, such as abstract reasoning, language generation and the construction of social networks (Bicks et al. 2015; Buckner and Krienen 2013; Hage and Nieder 2016; Krubitzer and Prescott 2018; Mansouri et al. 2017). However, the expansion of the thalamus has mirrored that of the cortex, and it is increasingly clear that the thalamus plays a critical role in facilitating communication between different cortical areas (Halassa and Kastner 2017; Rikhye et al. 2018; Sherman 2016). This section will introduce each structure in turn, and give a brief account of their functional organisation, before discussing how models of their interaction have changed in recent years.

### 1.1.1 General organisation of the cortex

The cortex is one of the most prominent features of the mammalian brain. It has a pronounced laminar structure and is divided into modular areas that correspond to distinct functional properties (Brodmann 1909; Harris and Shepherd 2015). Despite this, the fundamental organisation of cortical neurons into interconnected networks is broadly conserved across different cortical areas and mammalian species (Douglas and Martin 2004; Harris and Mrsic-Flogel 2013; Harris and Shepherd 2015; Thomson and Lamy 2007). This observation led to the proposal of the canonical microcircuit model (Douglas et al. 1989), whereby stereotypic patterns of synaptic connectivity between cortical layers act as evolutionarily conserved building blocks that give rise to a collection of serially homologous cortical areas (Nelson 2002; Oberlaender et al. 2012). One advantage of this model is that if different areas of cortex are organised in a similar way, insights from one area might inform our understanding of others (Harris and Shepherd 2015). Equally, area-specific variations upon general organisational principles might bring an understanding of

how the organisation of synaptic connectivity at a fine-scale relates to the functional specialisation of a given cortical area (Brown and Hestrin 2009; Kampa et al. 2006; Ko et al. 2011; Yoshimura et al. 2005). To this end, an enormous body of work has been dedicated to investigating the neuronal composition of cortical circuits at different spatial scales (Braitenberg and Schüz 1998; Lee et al. 2021; Oh et al. 2014; Peng et al. 2021; Zingg et al. 2014).

Neurons have been classified according to many different criteria, often used in combination, to define a collection of distinct cell types with shared phenotypic characteristics (Bota and Swanson 2007; Fishell and Heintz 2013; Migliore and Shepherd 2005; Nelson et al. 2006; Somogyi and Klausberger 2005; Stevens 1998). The work of early 20th century neuroanatomists such as Santiago Ramón y Cajal represent some of the earliest attempts to characterise neurons based on their morphology, visualised using histological stains (Cajal and Azoulay 1955). In the decades since, the development of new anatomical, physiological, and molecular methods, have facilitated the classification of neurons with increasing granularity, toward the creation of a unified taxonomy (Tasic et al. 2016; Tasic et al. 2018; Yao et al. 2021; Yuste et al. 2020; Zeng and Sanes 2017).

Excitatory neurons, often termed principal cells, constitute roughly 80 % of the neurons in the cortex. They release the transmitter glutamate, typically exhibit selective activity in response to features of the sensory environment, and form extensive local and long-range synaptic connections. The remaining 20 % of cortical neurons comprises interneurons that use the inhibitory neurotransmitter gamma-aminobutyric acid (GABA), and mostly form local connections. Importantly, excitatory and inhibitory neurons in each cortical layer can be further divided into numerous subclasses, the classification of which constitutes an area of active research (Greig et al. 2013; Huang 2014; Tasic et al. 2016; Tasic et al. 2018; Zeng and Sanes 2017).

A vast anatomical and functional literature, predominantly in rodents, has begun to uncover the general principles through which the connectivity between excitatory

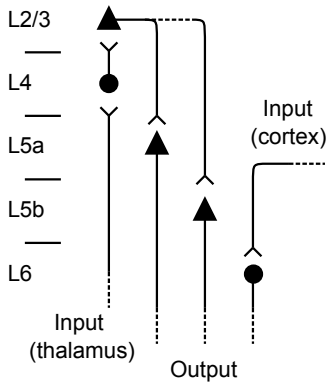


**Figure 1.1: Precise patterns of connectivity constrain the flow of information through the cortical circuit.** L4 is the primary input layer of the cortex. Neurons in L4 receive input from the thalamus, and project to L2/3. Pyramidal neurons in L2/3 send projections to L5a and L5b. L6 is predominantly driven by long-range input. L5 and L6 represent the output layers of the cortical circuit, projecting widely to other cortical areas and subcortical targets. It is important to acknowledge that these constraints are not absolute, multiple entry and exit points exist at each stage of the circuit (discussed in Harris and Shepherd 2015).

cortical neurons in different cortical layers is organised (reviewed in Feldmeyer 2012; Harris and Mrsic-Flogel 2013; Harris and Shepherd 2015; Thomson and Lamy 2007), bringing insight as to how information propagates through the cortex (**Figure 1.1**). Layer 4 (L4) is considered the primary input layer of the cortex. Excitatory L4 neurons typically receive dense feedforward input from the thalamus (Ferster et al. 1996; Sherman and Guillery 1996; Usrey et al. 2000; Viaene et al. 2011b; Viaene et al. 2011c), and project heavily to L2/3 (Feldmeyer 2012; Jiang et al. 2015). Meanwhile, neurons in L2/3 send descending projections to L5, avoiding L4 (Douglas and Martin 2004; Hooks et al. 2011; Thomson and Lamy 2007). L6 receives little descending excitatory input, being driven mostly by long-range projections from surrounding cortical areas (Hooks et al. 2011; Thomson 2010; Vélez-Fort et al. 2014; Zhang and Deschênes 1998). L1 does not contain any excitatory neurons. Instead, inputs from a variety of long-range sources converge onto the apical dendrites of neurons located in L2/3 and L5 (Ibrahim et al. 2016; Roth et al. 2016; Zhang et al. 2014; Zhu and Zhu 2004). Excitatory neurons in L5 and L6 represent the output of the cortical circuit, projecting widely to a variety of long-range cortical and subcortical targets (Hattox and Nelson 2007; Kasper et al.

1994; Kim et al. 2015; Kim et al. 2018; Thomson 2010; Zhang and Deschênes 1998). Notably, L5 is typically sub-divided into L5a and L5b, reflecting differences in their long-range connectivity. Whilst there is extensive recurrent connectivity between neurons within layers, connections between layers are predominantly asymmetric, constraining the flow of information through the cortical circuit (Douglas et al. 1989; Harris and Shepherd 2015).

### 1.1.2 General organisation of the thalamus

The thalamus is made up of a collection of forebrain nuclei that are typically divided into dorsal and ventral regions (Jones 1985). The dorsal thalamus comprises around fifty nuclei, grouped into seven major divisions. These nuclei primarily contain populations of excitatory glutamatergic neurons that send projections to the cortex and a number of subcortical structures, including the amygdala and striatum (Clascá et al. 2012; Halassa and Sherman 2019; Rikhye et al. 2018; Sherman and Guillery 2005). Meanwhile, the ventral thalamus comprises a shell of inhibitory neurons, collectively known as the thalamic reticular nucleus (TRN), that provide the major inhibitory input to excitatory neurons in the dorsal thalamus (Crabtree 2018; Lee et al. 2014; Pinault 2004; Pinault and Deschênes 1998).

A fundamental distinction between the thalamus and cortex is that the thalamus lacks the recurrent excitatory connectivity that is characteristic of cortical circuits. Consequently, the information encoded by individual thalamic neurons can be broadly understood as a function of their long-range excitatory connectivity (Halassa and Sherman 2019; Rikhye et al. 2018). This has led to the creation of numerous classification schemes based on the input and output connectivity of different thalamic nuclei (Sherman 2016; Sherman and Guillery 1996; Sherman and Guillery 1998; Sherman and Guillery 2005). Perhaps the most widely adopted scheme, is that which distinguishes thalamic nuclei as being either first-order or higher-order, depending upon the source of their inputs. First-order thalamic nuclei receive their major input from subcortical sources (e.g., the retina, or brainstem) and are considered the primary route from the sensory periphery to the cortex,

transferring sensory information via neurons with simple response properties (Ferster et al. 1996; Sherman and Guillery 1996; Sherman and Guillery 1998; Sherman and Guillery 2013; Usrey et al. 2000). In contrast, higher-order thalamic nuclei receive converging inputs from multiple sources that can be of a cortical or subcortical origin (Diamond et al. 1992; Groh et al. 2014; Lavallée et al. 2005; Mo and Sherman 2019; Theyel et al. 2010; Usrey and Sherman 2019). In addition, they are typically subject to considerable modulation by non-sensory variables, such as arousal, and movement. As such, neurons of higher-order nuclei display more complex response properties, thought to reflect the encoding of both sensory and contextual information (Diamond et al. 1992; Petty et al. 2021; Roth et al. 2016).

The majority of subcortical inputs to the cortex originate in the thalamus. However, the rules governing the connectivity between the brain's many thalamic nuclei and its many cortical areas are not fully understood. Nonetheless, a working model exists that is based upon two key organisational principles. Firstly, cortical areas and thalamic nuclei are grouped according to functional specialisation such that each sensory modality, aside from olfaction, has a corresponding first-order and higher-order thalamic nucleus (Jones 1985). For example, the somatosensory cortex is served by the first-order ventral posterior medial nucleus (VPM) and the higher-order posteromedial nucleus (POm; Petersen 2007). Secondly, first-order and higher-order nuclei exhibit distinct patterns of cortical innervation, often referred to as core and matrix, respectively (Castro-alamancos and Connors 1997; Herkenham 1986; Jones 1985). Neurons in first-order nuclei have spatially dense axonal projections that primarily target L4 and L5b, which are constrained by topographical representations of the sensory environment (e.g., barrels in somatosensory cortex; discussed in **Section 1.2**; Sermet et al. 2019; Woolsey and Van der Loos 1970). In contrast, higher-order nuclei send spatially diffuse projections that span the cortical layers. They are typically associated with having major arborisations in L1 and L5a, however it has been shown that neurons in all layers of cortex can receive higher-order inputs (Audette et al. 2018; Sermet et al. 2019)

It is important to acknowledge that, whilst useful, the classification of first-order

and higher-order nuclei is not always consistent. Although first-order nuclei appear to be entirely first-order (i.e., predominantly receive subcortical inputs and send core-like projections), higher-order nuclei typically include a mixture of higher-order and first-order circuitry (Groh et al. 2014; Halassa and Sherman 2019; Jaramillo et al. 2019; Kelly et al. 2003; Rovó et al. 2012; Sherman 2016). Indeed, previously unappreciated heterogeneity, particularly within higher-order thalamic nuclei, has inspired efforts to build models of thalamic function based on the connectivity patterns of individual thalamic neurons (Halassa and Sherman 2019; Roy et al. 2022). This thesis adopts the convention of referring to first-order thalamic nuclei as those that exclusively contain first-order circuitry, and referring to higher-order thalamic nuclei as those that contain either a mixture of first-order and higher-order circuits, or that exclusively comprise higher-order circuitry.

### 1.1.3 Thalamocortical models of sensory processing

In traditional models of sensory processing the thalamus is characterised as a simple relay, with ascending inputs from first-order thalamic nuclei conveying sensory information from the periphery to areas of primary sensory cortex. This information is then processed through a sequential hierarchy of sensory, motor and association cortices, via a series of direct connections between cortical areas, ultimately resulting in the modulation or execution of behaviour (Sherman 2016). However, it is now clear that the thalamus serves an ongoing role in sensory processing. It is increasingly appreciated that direct connections between cortical areas are often mirrored by parallel, transthalamic pathways that pass through higher-order thalamic nuclei. For example, in the mouse somatosensory system, projections via the higher-order nucleus, POm, facilitate the transfer of information from primary somatosensory cortex (S1) to secondary somatosensory cortex (S2; Theyel et al. 2010; Viaene et al. 2011a). Similar observations in visual, auditory, and sensorimotor cortices, suggest that transthalamic pathways represent a general feature of thalamocortical organisation (Bender 1983; Casanova et al. 2001; Chalupa et al. 1972; Mo and Sherman 2019). Notably, this presents a mechanism by which

information can be further processed or modulated by thalamic activity (e.g., by convergent long-range inputs in POm, or local inhibitory inputs from the TRN) that is not available to direct connections between or within cortical areas (Buchan 2020; Kirchgessner et al. 2020).

Furthermore, in contrast to the entirely feedforward model discussed above, recurrent connectivity has been observed between the cortex and thalamus, whereby higher-order thalamic nuclei send feedback projections to the area of cortex from which they receive their primary input (Guo et al. 2018; Guo et al. 2020; Sherman 2016). So-called cortico-thalamo-cortical (CTC) circuits have been widely characterised in frontal cortex, which led to the suggestion that they are necessary for the dynamic regulation of cognitive processes specific to higher cortical areas, such as attention, executive function, and decision-making (Collins and Anastasiades 2019; Halassa and Kastner 2017; Rikhye et al. 2018; Svoboda and Li 2018). However, higher-order thalamic nuclei are also known to send numerous feedback projections to primary sensory areas (Audette et al. 2018; Petersen 2007; Sermet et al. 2019). These projections are known to play a role in shaping the response properties of individual neurons (see **Section 1.2**; Castejon et al. 2016; Mease et al. 2016; Zhang and Bruno 2019), but have also been implicated in a number of fundamental cognitive processes, including attention, nociception, conscious perception and sensory-evoked plasticity (Castejon et al. 2016; Frangeul et al. 2014; Gambino et al. 2014; Nakajima and Halassa 2017; Suzuki and Larkum 2020). This apparent functional diversity reflects not only the variety of inputs received by higher-order nuclei (Chiaia et al. 1991; Diamond et al. 1992; Groh et al. 2014; Lavallée et al. 2005; Olsen and Witter 2016; Trageser and Keller 2004; Usrey and Sherman 2019), but also the heterogeneity of cortical circuits receiving higher-order inputs (Audette et al. 2018; Buchan et al. 2021; Sermet et al. 2019).

## 1.2 Primary somatosensory cortex as a model of sensory processing

Mice and other nocturnal rodents are critically dependent upon tactile information from the whiskers on their snout to perform basic tasks like exploring their surroundings and detecting objects. Indeed, it is thought that the somatosensory whisker system evolved as a consequence of the limited availability of visual information during much of a rodent's life. The whiskers are afforded by far the largest topographic representation in the cortex, with each whisker corresponding to discrete anatomical regions within L4 of S1 (Woolsey and Van der Loos 1970). This precise organisation has led to the somatosensory system becoming a well-established model for exploring the relationship between the development, anatomy, synaptic connectivity, and function of thalamocortical circuits (discussed in Erzurumlu and Gaspar 2020). In particular, the convergence of inputs from VPM and POm onto individual neurons within L4 (Audette et al. 2018; Viaene et al. 2011a; Viaene et al. 2011b), make it an invaluable system for investigating the relative contributions of first-order and higher-order thalamic nuclei to sensory processing. This section will outline the pathways that convey sensory information from the whiskers to S1, describe their organisation and development, and discuss how their interaction is thought to influence the sensory response properties of individual neurons over time.

### 1.2.1 Parallel pathways convey whisker-related information to the cortex

The most striking feature of rodent S1 is its somatotopic organisation. Dense clusters of thalamic axons in L4 are surrounded by aggregations of neurons that give rise to cytoarchitectonic structures, called barrels. Seminal work by Woolsey and Van der Loos demonstrated that the relationship between whiskers and barrels is isomorphic, with each whisker being represented by a specific barrel, and the layout of the barrel field in S1 closely mirroring that of the whiskers on the contralateral snout (Woolsey and Van der Loos 1970). Remarkably, this relationship can be

traced through well-defined pathways that are responsible for conveying sensory information from the whiskers to the cortex (Petersen 2007).

Whisker follicles in the mystacial pad are innervated by the infraorbital branch of the trigeminal ganglion, which provides excitatory glutamatergic input to various nuclei of the brainstem trigeminal complex (Erzurumlu et al. 1980; Lund and Webster 1967). From there, distinct pathways relay sensory information to S1 via different nuclei within the somatosensory thalamus. The lemniscal pathway originates in the principal trigeminal nucleus (PrV) before projecting to the first-order thalamic nucleus, VPM (Veinante and Deschênes 1999). Both PrV and VPM exhibit a somatotopic arrangement characterised by the presence of structures called barrelettes and barreloids, respectively (Emmers 1965; Van Der Loos 1976; Waite 1973). Thus, the lemniscal pathway operates as a collection of parallel circuits, or labelled lines, such that neurons within a given barreloid receive input from the corresponding barrelette (Welker 1971). Neurons in VPM subsequently send dense core-like projections to S1 that predominantly cluster in L4, forming the basis of the barrel field (**Figure 1.2**; Woolsey and Van der Loos 1970). Meanwhile, the paralemniscal pathway originates in the rostral interpolar trigeminal nucleus (rSpV), which projects to the higher-order thalamic nucleus, POm (Jacquin et al. 1989; Williams et al. 1994). Projections from POm to S1 are matrix-like, and span the cortical layers (**Figure 1.2**; Audette et al. 2018; Bureau et al. 2006; Petreanu et al. 2009). However, within L4 POm inputs are primarily associated with the inter-barrel regions, called septa (Koralek et al. 1988; Petersen 2007). Notably, somatotopy is absent from both rSpV and POm.

Consistent with these anatomical differences, the lemniscal and paralemniscal pathways have been shown to convey distinct types of sensory information to S1. In keeping with its preserved somatotopic organisation, the lemniscal pathway is predominantly associated with information from single whiskers. Indeed, recordings from neurons in PrV and VPM have demonstrated that spiking responses are mostly observed following deflection of a specific, principal whisker (PW; Armstrong-James et al. 1992; Armstrong-James and Fox 1987; Diamond et al.

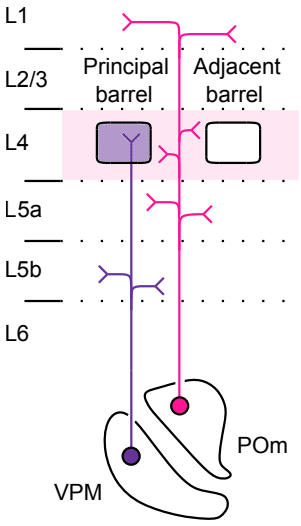


**Figure 1.2: S1 L4 receives anatomically segregated input from VPM and POm.** VPM sends dense, core-like projections to S1 that predominantly cluster in L4. This topographic restriction forms the basis of the barrel field. VPM also sends a major projection to L5b. Projections from POm to S1 are matrix-like, with primary arborisations in L1 and L5a. Within L4, POm inputs are associated with septal regions. Figure adapted from (Pouchelon et al. 2014).

1992; Ito 1988; Simons et al. 1992; Simons and Carvell 1989; Welker 1971). In contrast, the paralemniscal pathway is thought to convey multi-whisker information, consistent with its lack of somatotopy (Diamond et al. 1992; Erzurumlu et al. 1980; Jouhanneau et al. 2014; Veinante and Deschênes 1999; Williams et al. 1994). For example, whilst neurons in POm are often highly responsive to a PW, they also spike in response to the deflection of multiple surrounding, or adjacent whiskers (AWs; Diamond et al. 1992). Importantly, POm also receives inputs from numerous other cortical and subcortical sources, which are integrated with incoming sensory information from rSpV (Alloway et al. 2004; Groh et al. 2014; Lavallée et al. 2005; Lohse et al. 2018; Sobolewski et al. 2015; Theyel et al. 2010; Trageser and Keller 2004; Urbain and Deschênes 2007), thus generating more complex stimulus representations than those observed in VPM. For example, inputs from motor cortex provide information about the active movement of whiskers, and projections from the zona incerta modulate the activity of neurons in POm, in a manner that depends on the arousal state of the animal.

The complementary distribution of inputs from VPM and POm to L4 of S1, led

to the suggestion that barrels and septa represent segregated circuits for the processing of single and multi-whisker information, respectively (Bureau et al. 2006; Petersen 2007; Petreanu et al. 2009). This was reinforced by the observation that L4 excitatory neurons with soma located in septa are more likely to exhibit multi-whisker response properties than those within the barrel core, consistent with the sampling of POm inputs (Fox et al. 2003). However, it became clear that the response properties of neurons in S1 vary continuously throughout the extent of the barrel field (Kerr et al. 2007; Sato et al. 2007). Moreover, in contrast to PrV (Arabzadeh et al. 2005; Jones et al. 2004), L4 responses to whisker deflection typically exhibit considerable trial-to-trial variability (Petersen et al. 2003; Sachdev et al. 2004), suggesting that neurons in L4 are subject to a degree of modulation that is not present within the lemniscal pathway. This indicates that there is a degree of convergence between the lemniscal and paralemniscal pathways onto individual neurons within L4.

In order to understand how inputs from VPM and POm might interact to shape the sensory responses of L4 excitatory neurons, initial studies measured the relative response latency of individual excitatory neurons in VPM, POm, and S1 following whisker deflection (Armstrong-James et al. 1992; Armstrong-James and Callahan 1991; Diamond et al. 1992). This produced elegant functional maps that highlighted the likely anatomical routes through which excitatory activity spreads to, and within, S1 (summarised in **Figure 1.3**). Briefly, in the first 0-10 ms following single whisker deflection, activity propagates radially from VPM to the corresponding barrel in L4. In comparison, neurons in POm respond with a longer latency (10-20 ms), likely reflecting the integration of inputs, in this case from rSpV and S1 L5. Subsequently, activity spreads laterally to adjacent barrels via the coincident action of recurrent excitatory inputs originating in POm and from within local cortical circuitry. Therefore, the response to PW deflection appears to be predominantly mediated by inputs from VPM, whereas multi-whisker responses arise through the combined action of inputs from POm and intracortical connections (Bruno and Simons 2002; Fox et al. 2003; Kwegyir-Afful 2005; Lavallée et al.

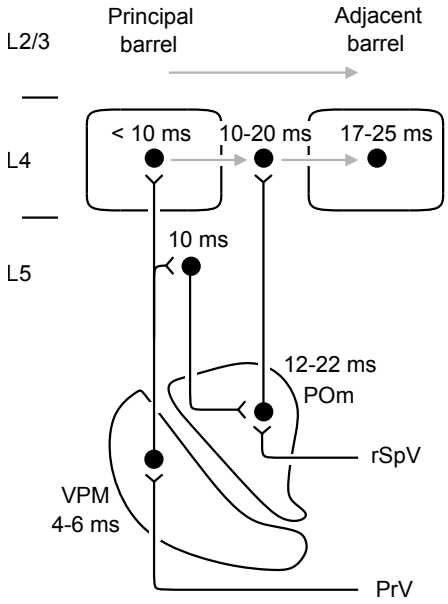


**Figure 1.3: Multi-whisker responses are influenced by thalamic input and lateral cortical connectivity.** Activity is first relayed to the cortex by short latency input from VPM to the principal barrel in the first 10 ms following whisker deflection. Activity then spreads to adjacent barrels via recurrent excitatory inputs from POm and lateral connections within the cortex. Notably, POm must integrate information from descending transthalamic inputs and numerous subcortical projections, including those from the periphery. Figure adapted from (Diamond et al. 1992), with latency data from (Armstrong-James and Callahan 1991; Armstrong-James et al. 1992).

2005).

Interestingly, the extent to which individual neurons in S1 are selective for the PW over an AW can vary considerably even between neighbouring neurons within the same barrel column (Kerr et al. 2007; Sato et al. 2007). This suggests that a degree of fine-scale organisation exists beyond that of barrels and septa that influences the way in which L4 excitatory neurons sample thalamic inputs. Consistent with this idea, sequential studies demonstrated that whilst VPM represents the major input to L4, individual neurons differ in the degree to which they receive input from POm (Audette et al. 2018; Viaene et al. 2011a; Viaene et al. 2011b; Viaene et al. 2011c). The L4 population is therefore heterogeneous in terms of its integration of thalamic input, with some neurons receiving more higher-order information than others. However, the mechanisms that determine how individual neurons sample thalamic inputs are not fully understood.

In part, the thalamic input received by a L4 excitatory neuron is thought to reflect

its morphology and how this relates to the organisation of barrels and septa. As discussed, the response properties of neurons are known to vary as a function of their soma position (Fox et al. 2003). However, a proportion of L4 excitatory neurons are also known to target barrels with their dendrites (Guillamon-Vivancos et al. 2019; Simons and Woolsey 1984; Staiger 2004), presenting an additional strategy for the sampling of specific thalamic inputs. These properties are best understood in relation to their establishment and refinement during critical periods of development in the first postnatal weeks. This is the focus of the next section and relates to the experimental work in this thesis.

### 1.2.2 The establishment of somatosensory circuitry

Thalamocortical development is a largely sequential process that involves the co-ordinated action of neuronal-intrinsic factors and activity-dependent mechanisms. For example, the specification of functional areas, and the production of the correct number and types of neurons are thought to reflect genetic programs during embryonic development (López-Bendito and Molnár 2003; Molnár et al. 2003; Vitali and Jabaudon 2014). Other features, such as the patterning of thalamic axons and refinement of cortical circuitry, occur later, and are heavily influenced by the sensory periphery during critical periods of postnatal development (Erzurumlu and Gaspar 2012; Li and Crair 2011; Vitali and Jabaudon 2014; Wu et al. 2011). This section will present a brief account of S1 development, discussing the growth of thalamic inputs, and the factors governing the postnatal refinement of circuitry in L4.

As with other cortical areas, the specification of S1 is determined by the action of diffusible morphogens, such as fibroblast growth factors (FGFs) secreted from the commissural plate. Of particular importance is FGF8, which determines the spatial extent of S1 and the putative location of the barrel field within the developing neuroepithelium by regulating the expression of various transcription factors in embryonic progenitor cells within the ventricular proliferative zones (Fukuchi-Shimogori and Grove 2001). Examples include paired box 6 (Pax6), empty spirals

homeobox 2 (Emx2), and LIM homeobox 2 (Lhx2). Pax6 and Emx2 are expressed in opposing gradients in the ventricular zone, and specify rostral (i.e., somatosensory, motor) and caudal (i.e., visual) cortical identity, respectively (Bishop et al. 2000). Lhx2 shows similar patterns of expression to Emx2, but promotes specification of the cortex as a whole through the suppression of alternative fates, including palaeocortex and the cortical hem (Bulchand et al. 2003; Chou et al. 2009).

The route from the thalamus to the cortex is complex, requiring the traversal of several developing boundary zones (e.g., between the diencephalon and telencephalon) characterised by sharp changes in gene expression (López-Bendito and Molnár 2003; Molnár et al. 1998; Molnár and Butler 2002; Puelles et al. 2000; Stoykova and Gruss 1994). As such, developing thalamocortical axons are subject to the influence of numerous attractive and repulsive factors, and are highly dependent upon guidance molecules, including those from cortex (Barbe and Levitt 1992; Donoghue and Rakic 1999; Gao et al. 1998; Suzuki et al. 1997). Indeed, the same factors involved in the specification of cortical areas have been demonstrated to act as indirect regulators of thalamic axon growth, likely by providing positional information on cortical guidance cues. For example, ectopic expression of FGF8 results in the development of duplicate, areal-shifted barrel fields that are nonetheless fully innervated by the thalamus (Fukuchi-Shimogori and Grove 2001). Their importance is emphasised further by knockdown studies where thalamic axons fail to reach the cortex entirely (Bishop et al. 2000). Incidentally, loss of thalamic input does not appear to affect the general distribution of morphogenetic expression in the ventricular zone (Miyashita-Lin et al. 1999; Nakagawa et al. 1999), reinforcing the idea that the specification of cortical areas is largely the result of intrinsic mechanisms.

In contrast, the appropriate development of barrels in S1 is critically dependent upon activity. VPM axons reach the cortical plate at around E15, which is before their target neurons assume position in L4 (Auladell et al. 2000; Kanold and Luhmann 2010; Lund and Mustari 1977). Instead of proceeding to invade the cortex prematurely, axons aggregate in the subplate and participate in a process of

activity-dependent refinement which is necessary for the appropriate targeting of L4 (Pal et al. 2021). This waiting period ends around birth, or postnatal day 0 (P0), after which VPM axons ascend radially (Agmon et al. 1993; Rebsam et al. 2002; Senft and Woolsey 1991), using transient projections from the subplate to L4 as a scaffold (Piñon et al. 2009).

The characteristic somatotopic representation of the whiskers develops over the course of the first postnatal week in a series of well-defined stages (Erzurumlu and Gaspar 2012; Li and Crair 2011; Wu et al. 2011). VPM axons first form rows within L4 at around P2, before segregating into whisker-specific clusters by P3 (Lee and Erzurumlu 2005; Rebsam et al. 2002). Interestingly, ablation of whisker follicles prevents formation of the corresponding barrel if performed prior to P4, but not after (Datwani et al. 2002; Durham and Woolsey 1984; Rebsam et al. 2005). Thus, the period from P0-P4 appears to represent a critical period for structural plasticity, where the formation of somatotopy is particularly sensitive to perturbation. Between P5-P7, barrels emerge as visible aggregates of neurons within L4 (Rice et al. 1985). From P6, L4 excitatory neurons begin to orient their dendrites with respect to incoming thalamic inputs, often targeting the nearest barrel (Espinosa et al. 2009). All stages of this process are dependent upon activity. Comprehensive genetic knockout studies have demonstrated that perturbing glutamatergic transmission produces defective phenotypes characterised by poorly defined or absent barrels, aberrant dendritic morphology, and abnormal response properties in L4 (discussed in Erzurumlu and Gaspar 2012; Erzurumlu and Kind 2001; Inan and Crair 2007).

The targeted orientation of dendrites represents a strategy by which L4 excitatory neurons can sample specific thalamic inputs. Despite being a well-recognised feature of S1 L4 neurons, relatively little is known about how targeted dendrites are established, other than the involvement of an activity-dependent period of dendritic remodelling. Moreover, it is not clear why some L4 excitatory neurons target barrels with dendrites and others do not (Simons and Woolsey 1984; Staiger 2004). One study aimed to identify the source of excitatory inputs responsible for this

process, using genetic deletions in either the cortex or thalamus, targeting proteins involved in presynaptic vesicle exocytosis (Narboux-Nême et al. 2012). Whilst cortical deletion had little discernible effect, thalamic deletion resulted in a lack of dendritic targeting by L4 neurons, and the absence of barrels. Subsequent work investigated possible mechanisms intrinsic to L4 excitatory neurons that might mediate the ability of L4 excitatory neurons to respond to incoming thalamic inputs (Matsui et al. 2013). The Broad complex, Tramtrack and Bric-a-brac (BTB) proteins, are a family of transcription factors that have been implicated in a wide array of processes throughout cortical development (Siggs and Beutler 2012). BTB domain-containing 3 (Btbd3) was found to be exclusively expressed by L4 excitatory neurons in S1 during barrel formation, and knockdown of Btbd3 was observed to reduce the proportion of L4 excitatory neurons exhibiting targeted dendritic morphology (Matsui et al. 2013). Notably, in NMDAR knockout animals, Btbd3 could not be translocated to the nucleus, indicating that it is unable to contribute to transcriptional programs in the absence of excitatory activity. Taken together, these observations suggest that the activity dependent recruitment of Btbd3 is responsible for the targeted dendritic growth exhibited by L4 neurons.

Interestingly, one of the upstream regulators of Btbd3 expression is Lhx2 (Wang et al. 2017). As discussed, Lhx2 plays a prominent role in the specification of cortical fate, however it is also expressed in postmitotic neurons in the first postnatal weeks (Bulchand et al. 2003). Sequential studies have investigated the role of Lhx2 in barrel development using a series of targeted manipulations in progenitors and postmitotic neurons. These have observed that the formation of barrels in S1 is impaired when the expression of Lhx2 is reduced in cortical progenitors (Shetty et al. 2013). The development of thalamic inputs in this manipulation is impaired, characterised by the premature invasion of S1 by VPM axons before birth (Pal et al. 2021), and thus the absence of activity-dependent refinement in the subplate. Meanwhile, reduced Lhx2 expression in cortical neurons results in the loss of dendritic morphologies that are targeted towards barrels in L4 (a phenotype that could be rescued by induced expression of Btbd3; Wang et al. 2017). These

observations implicate Lhx2 as a master regulator of the activity-dependent development of somatotopy in S1 (Chou and Tole 2019). Additionally, recent work has shown that postnatal expression of Lhx2 can be used to distinguish a specific population of excitatory cortical neurons that reside in upper cortical layers, including L4 (Huilgol et al. 2022; Matho et al. 2021). This suggest that Lhx2 expression is heterogenous, and is consistent with a model whereby neurons with higher levels of Lhx2 are more likely to target barrels with their dendrites.

The second postnatal week is characterised by multiple interacting phases of structural plasticity that are coordinated across sensory and motor regions, culminating in eye-opening and the onset of active whisker exploration around P14 (Landers and Philip Zeigler 2006; Lendvai et al. 2000; Maravall et al. 2004; Shoykhet et al. 2005; Stern et al. 2001; Wen and Barth 2011). These structural developments are accompanied by profound changes in the sensory response properties of individual neurons. For example, responses to whisker deflection are initially restricted to L4 neurons within the principal barrel, with multi-whisker responses emerging from P10 (Borgdorff et al. 2007). Moreover, the degree to which cortical activity is subject to modulation by non-sensory, contextual input increases dramatically (Borgdorff et al. 2007; Bureau et al. 2006; Luhmann and Khazipov 2018; Mizuno et al. 2018). This time course corresponds to the development of lateral connectivity in the cortex (Wen and Barth 2011), and the innervation of septa by POm axons (Kichula and Huntley 2008), which occur over several days following the emergence of barrels. P16 is generally considered to mark the conclusion of the critical period for plasticity in S1. However, it is clear that the response properties of individual neurons, and the somatotopic representation of L4 more broadly, continue to be influenced by sensory experience (Feldman and Brecht 2005; Glazewski et al. 1998). Indeed, pivotal studies have explored the origins of sensory-evoked plasticity in S1, with emerging roles for higher-order thalamic inputs from POm.

### 1.2.3 Higher-order thalamic inputs act as an instructive cue for sensory-evoked plasticity

Representations of the sensory environment are established early in cortical development, as discussed in **Section 1.2.2**. Despite this, there is substantial evidence that sensory experience and perceptual learning continue to drive changes in the response properties of neurons and remodel the topography of cortical areas into adulthood. This process, generally referred to as sensory-evoked plasticity, is achieved through the strengthening and weakening of synapses by long-term potentiation (LTP) and depression (LTD), respectively. The mechanisms of LTP and LTD have been well characterised at the level of single synapses in isolated preparations of brain tissue, yet their implementation across populations of neurons in the intact brain is not fully understood. At some level, sensory-evoked plasticity must require an instructive cue, both to highlight salient events that justify learning, and to prevent the aberrant or pathological strengthening or weakening of synapses. A number of recent studies in S1 have implicated inputs from the higher-order thalamic nuclei, POm, as critical regulators of sensory-evoked plasticity in vivo (Audette et al. 2019; Gambino et al. 2014; Williams and Holtmaat 2019). This is thought to reflect the fact that POm integrates sensory information from the periphery with numerous other inputs, as discussed in **Section 1.2.1**, and is therefore well-placed to deliver contextual information to cortical circuits.

L2/3 of S1 has become a popular model in which to study the induction of sensory-evoked long-term potentiation (sLTP), as the excitatory connection between L4 and L2/3 can be readily potentiated by a number of methods (Aroniadou-Anderjaska and Keller 1995; Castro-Alamancos et al. 1995; Feldman 2000; Gambino et al. 2014; Glazewski et al. 1998; Mégevand et al. 2009). Additionally, excitatory neurons in L2/3 receive direct inputs from both L4 and POm (Bureau et al. 2006; Jouhanneau et al. 2014; Petreanu et al. 2009), presenting the means to explore how plasticity of ascending sensory information is influenced by contextual modulation (**Figure 1.4**). In contrast to those in L4, L2/3 excitatory neurons exhibit pyramidal morphology, characterised by an elaborate apical dendrite that extends to the cortical

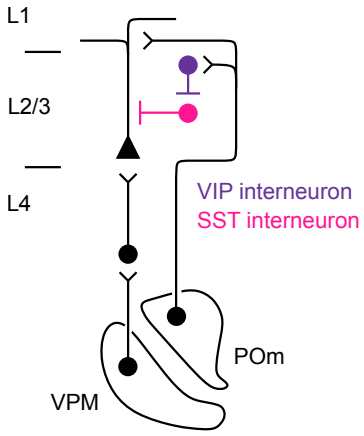


**Figure 1.4: Putative circuits for sensory-evoked plasticity in S1 L2/3.** L2/3 pyramidal neurons receive proximal input from L4, and distal inputs from POm. This convergence of first-order and higher-order information has been proposed to form the basis of a mechanism that regulates the induction of sensory-evoked plasticity in L2/3. Importantly, VIP interneurons also receive input from POm, and are thought to facilitate active dendritic processes in L2/3 pyramidal neurons via a disinhibitory circuit involving SST interneurons (Williams and Holtmaat 2019).

surface with extensive arborisations in L1. This structure allows for the anatomical compartmentalisation of inputs and is thought to increase the complexity of stimulus representations that can be achieved by individual neurons (London and Häusser 2005; Spruston 2008). Consistent with this idea, inputs to L2/3 pyramidal neurons from L4 typically target proximal regions close to the soma, whereas those from POm predominantly target distal regions in L1 (Feldmeyer 2012; Harris and Shepherd 2015).

The responses of S1 L2/3 pyramidal neurons to whisker deflection can be potentiated by short periods (i.e., one minute) of rhythmic whisker stimulation (RWS) in vivo (Gambino et al. 2014; Mégevand et al. 2009). Furthermore, this process is dependent upon the presence of long-lasting depolarisations in the apical dendrite that are mediated by NMDARs (Gambino et al. 2014). These depolarisations are driven by the influx of calcium and are reminiscent of dendritic events, called plateau potentials, which are typically associated with long-range inputs to L2/3 from surrounding cortical areas and/or higher-order thalamic nuclei (Antic et al. 2010; Lavzin et al. 2012; Major et al. 2013; Palmer et al. 2014; Xu et al. 2012). Indeed, additional experiments found that the inhibition of POm activity prevents the generation of plateau potentials during RWS and disrupts the induction of

sLTP in L2/3 (Gambino et al. 2014).

Notably, optogenetic activation of POm axons alone is not sufficient to induce sLTP (Gambino et al. 2014). In keeping with this, subsequent work in vitro has shown that simultaneous activation of L4 and POm are required to induce LTP in L2/3 (Williams and Holtmaat 2019). Further investigation of the underlying mechanisms found that this is dependent upon the recruitment of specific populations of inhibitory interneurons by POm inputs. Martinotti cells represent a subtype of somatostatin-expressing (SST) interneurons that inhibit the apical dendrites of L2/3 pyramidal neurons (Silberberg and Markram 2007; Wang et al. 2004). In turn, Martinotti cells are inhibited by vasoactive intestinal peptide-positive (VIP) interneurons, thus forming a disinhibitory circuit that is able to modulate activity within the apical dendrites of L2/3 pyramidal neurons (Lee et al. 2013; Letzkus et al. 2015; Pi et al. 2013). Interestingly, VIP interneurons in S1 receive input from POm (Audette et al. 2018), and are known to be activated by non-sensory, contextual variables such as arousal and active movement of the whiskers (Garcia-Junco-Clemente et al. 2017; Yu et al. 2019). As such, disinhibitory circuits represent a possible mechanism by which plasticity is regulated within L2/3. This is reinforced by experiments showing that chemogenetic inhibition of VIP interneuron activity disrupts the induction of LTP in L2/3 *in vitro* (Williams and Holtmaat 2019). Taken together, these observations suggest that the coincident arrival of sensory information via L4 and contextual information from POm is required for the induction of sensory-evoked plasticity in L2/3. The disinhibition of the apical dendrite by POm inputs represents a potential mechanism by which L2/3 neurons are instructed to undergo sLTP in response to salient sensory experiences. It is important to acknowledge that this model characterises ascending inputs from L4 to L2/3 as being purely sensory, however excitatory neurons in both of these layers receive convergent inputs from VPM and POm, as discussed in **Section 1.2.1**. It is possible therefore, that higher-order input to L4 also plays an important role in the regulation of sensory-evoked plasticity, though this has not been explicitly tested.

Interestingly, connections from POm to the cortex have also been shown to exhibit plasticity. Mice that have undergone training in an automated sensory association task (SAT) exhibit significant potentiation of POm inputs to L2/3 after around 48 h (Audette et al. 2019). Interestingly, this time point was observed to coincide with the emergence of behavioural task success, suggesting a direct link between the potentiation of POm inputs and perceptual learning. In addition to the findings discussed above, these data indicate that POm is involved in two separate mechanisms that represent sequential stages of sensory-evoked plasticity. For example, intracortical plasticity (i.e. between L4 and L2/3) might involve forming new associations between sensory stimuli and the context in which they occur. Subsequently, if these associations are rewarded (e.g., during behavioural training) this could lead to the potentiation of thalamic inputs and learning (Buchan et al. 2021). This process is broadly analogous to the synaptic tagging and capture hypothesis that has been popularised in hippocampal circuits (Frey and Morris 1997; Redondo and Morris 2011), whereby the weak potentiation of synapses primes, or tags, them for LTP in response to subsequent plasticity-inducing experiences.

As discussed in **Section 1.2.1**, neighbouring neurons in L4 differ in the degree to which they receive input from POm, which is also reflected in the heterogeneity of their multi-whisker response properties. This has also been observed in L2/3, with some pyramidal neurons responding more strongly than others to optogenetic stimulation of POm axons (Audette et al. 2018). Notably, those that receive greater input from POm, also exhibit multi-whisker responses (Jouhanneau et al. 2014). Given the proposed role of POm inputs in the regulation of sLTP, this suggests that some L2/3 pyramidal neurons may be more sensitive to plasticity than others. Indeed, theoretical work has shown that neurons in recurrent networks that are less selective than their neighbours, are more likely to exhibit synaptic plasticity in response to sensory inputs (Sweeney and Clopath 2020).

## 1.3 The emerging role of lineage in the establishment of fine-scale thalamocortical connectivity

**Section 1.2** gave an account of the rodent somatosensory system and described a number of roles for higher-order thalamic inputs during sensory processing. As discussed, neighbouring neurons within L4 exhibit fine-scale differences in terms of their sampling of thalamic inputs and dendritic morphologies, with profound consequences for their sensory response properties (Audette et al. 2018; Jouhanneau et al. 2014; Kerr et al. 2007; Sato et al. 2007; Sermet et al. 2019; Viaene et al. 2011a). Interestingly, this appears to be a general feature of primary sensory areas in rodents. For example, the organisation of primary visual cortex (V1) is often referred to as being a salt-and-pepper distribution, as nearby neurons exhibit heterogeneous orientation selectivity (Hooser et al. 2006; Ohki et al. 2005). However, we lack a framework through which to relate the heterogeneous response properties of individual neurons to other established features of diversity within the cortex, such as neuronal cell types. One emerging idea is that the fine-scale organisation of synaptic connectivity reflects the developmental history, or lineage, of individual neurons. This section will discuss the notion of fine-scale organisation within cortical circuits more broadly, before outlining ways in which lineage might influence the connections formed by cortical neurons, including those with the thalamus.

### 1.3.1 Fine-scale connectivity is a general feature of cortical circuitry

Despite the high density of neurons within the cortex ($10^5$ per 1 $mm^3$; Braitenberg and Schüz 1998; Oberlaender et al. 2012), the connection probability between nearby ($< 100$ $\mu$m) pairs of excitatory neurons is surprisingly low, at around 10-20 %, and decays with distance (Ko et al. 2011; Perin et al. 2011; Stepanyants et al. 2009). This gives rise to a sparse network, consistent with a model in which the connections between pairs of neurons are largely probabilistic, developing independently of the rest of the network (Binzegger et al. 2004; Braitenberg and Schüz 1998; Hellwig et al. 1994; Hellwig 2000). However, several studies have identified

instances of non-random connectivity within otherwise homogeneous populations of neurons (Markram 1997; Song et al. 2005). For example, L2/3 pyramidal neurons in V1 are more likely to be connected if they share common input from L4 (Yoshimura et al. 2005). Similarly, the probability of a L2/3 pyramidal neuron making connections with a pair of L5 excitatory neurons in S1 is considerably higher if they are interconnected (Kampa et al. 2006). Given that the inputs received by a neuron determine its response properties (Harris and Mrsic-Flogel 2013), it could be predicted that non-random connectivity forms between functionally similar neurons, serving to process or amplify specific types of information. This idea is reinforced by experiments demonstrating that the connection probability between L2/3 pyramidal neurons in V1 is higher if they exhibit similar orientation tuning (Ko et al. 2011). Importantly, these relationships are neither restricted to input connectivity, nor to local cortical circuitry. For example, the connection probability between L5 excitatory neurons in V1 varies as a function of their long-range outputs (Brown and Hestrin 2009). Taken together, these observations suggest that an additional level of fine-scale organisation exists within cortical circuits, which instructs the formation of functional subnetworks that are defined by specific patterns of local and long-range connectivity. Notably, a given neuron may participate in several subnetworks, thus providing a mechanism through which neighbouring neurons can either process information independently or integrate several streams of information across a larger population.

As discussed in **Section 1.2.2**, the establishment of synaptic connectivity involves a combination of neuronal-intrinsic (i.e., genetic) factors and activity-dependent processes. Broadly, it is thought that genetic mechanisms establish a scaffold of neuronal connectivity that is subsequently refined by activity. However, it is unclear whether activity-dependent processes are given carte blanche to arbitrarily change connections between cortical neurons, or whether they are constrained by a set of rules that are specified earlier in development (discussed in Zador 2019). The fact that subnetworks are often defined by patterns of input connectivity encouraged the view that they arise through Hebbian plasticity mechanisms, whereby

neurons that receive shared inputs develop bistable connections (Clopath et al. 2010; Hebb 2002). However, sequential studies in S1 demonstrated that patterns of non-random connectivity between L5 excitatory neurons are present early in postnatal development (Markram 1997; Perin et al. 2011; Song et al. 2005), and common across experimental animals, suggesting that they are established independently of sensory experience. Rather, these findings argue that the rules governing fine-scale connectivity are genetically prescribed, and active during development.

### 1.3.2 Excitatory cortical neurons derive from a heterogeneous population of progenitors

One emerging theory is that fine-scale connectivity between cortical neurons is influenced by their developmental history, or lineage. This is largely inspired by Rakic's radial unit hypothesis (discussed in **Section 1.3.3**) which proposes that the organisation of the cortex ultimately reflects the clonal relationships between neurons derived from single progenitor cells (Rakic 1988). This is reinforced by an increasing body of work that suggests the functional properties of adult neurons can be understood as a function of the progenitor type from which they derive.

Excitatory cortical neurons are born between E10-E18 from progenitor cells in the ventricular proliferative zones of the dorsal pallium (Franco and Müller 2013). Neuroepithelial cells give rise to a common type of neurogenic progenitor, called radial glial cells (RGCs; **Figure 1.5**), that reside in the ventricular zone (Anthony et al. 2004; Malatesta et al. 2000; Noctor et al. 2001; Noctor et al. 2002; Tamamaki et al. 2001). RGCs undergo rounds of self-renewing, asymmetric division that typically generate one RGC and one non-RGC daughter cell (Miyata et al. 2001; Noctor et al. 2001; Noctor et al. 2004). Whilst some of these daughter cells are postmitotic neurons, the majority of RGC divisions give rise to a further class of progenitor cells known as intermediate progenitors (IPs). Generally, IPs undergo one symmetric division to produce two postmitotic neurons, thus amplifying the output of RGCs (Haubensak et al. 2004; Miyata et al. 2004; Noctor et al. 2004;

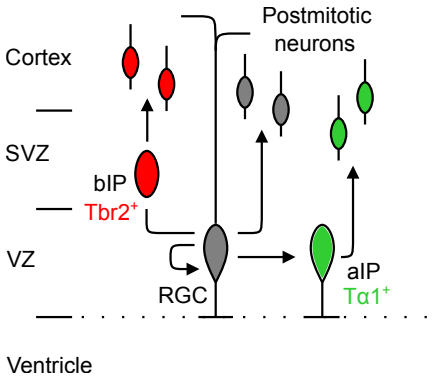


**Figure 1.5: Cortical neurons are generated contemporaneously from a diverse pool of progenitors.** Neuroepithelial cells give rise to RGCs that reside in the VZ. RGCs undergo sequential rounds of self-renewing division that typically generate one RGC, and one non-RGC daughter cell. These non-RGC daughter cells are predominantly IPs, which ultimately produce postmitotic neurons. The IP population is heterogeneous, including aIPs residing in the VZ, and bIPs that migrate to the SVZ. It is important to acknowledge that RGCs can give rise to postmitotic neurons directly, and that IPs can undergo self-renewing division. There are also several other varieties of cortical progenitor, which have been omitted for visualisation purposes (discussed in Franco and Müller 2013).

Wu et al. 2005). Whilst individual RGCs are typically thought to produce approximately ten neurons in the mouse cortex (Gao et al. 2014; Yu et al. 2009), the experimentally observed output of a RGC will reflect how early in development it has been labelled and how many self-renewing divisions it then exhibits. Indeed, labelling very young RGCs, and particularly neuroepithelial cells earlier in development, can result in the labelling of tens or even hundreds of cortical neurons from the same individual progenitor.

It is now recognised that IPs comprise a heterogeneous population of different progenitor types, whose neurogenic potential is regulated through the action of dynamic transcriptional programmes (Llorca et al. 2019; Oberst et al. 2019; Telley et al. 2016; Telley et al. 2019). Broadly, IPs can be distinguished by features such as the expression of specific genetic markers, their morphology, and laminar position within the proliferative zones (discussed in Franco and Müller 2013). For example, basal intermediate progenitors (bIPs) express the transcription factor T-box brain protein 2 (Tbr2; also known as EOMES), exhibit multipolar morphology, and migrate to the subventricular zone (SVZ) soon after they are born (Englund et al. 2005; Miyata et al. 2004; Noctor et al. 2004). Meanwhile, apical intermediate

progenitors (aIPs) can be identified by the expression of the tubulin alpha 1 (T$\alpha$1) promoter, their short apical processes, and the fact that their soma remain within the VZ throughout neurogenesis (Gal 2006; Stancik et al. 2010). Several other progenitor types have been described, including basal radial glial cells (bRGCs). bRGCs are rare in rodents in comparison to gyrencephalic mammals (Wang et al. 2011), where they are thought to have contributed to expansion of the upper cortical layers throughout evolution (Hansen et al. 2010).

The heterogeneity of cortical progenitors raises the question: how do progenitors contribute to the diversity of cell types within the adult cortex? It is generally accepted that increased numbers of progenitors are responsible for the enlargement of the cortex throughout evolution (Florio and Huttner 2014; Kriegstein et al. 2006; Martínez-Cerdeño et al. 2006). Therefore, one possibility is that different types of progenitor have emerged solely to increase overall neurogenic capacity within the developing cortex. However, recent studies have begun to identify features of adult neurons that appear to vary as a function of lineage (Ellender et al. 2019; Guillamon-Vivancos et al. 2019; Tyler et al. 2015). This suggests that progenitors might contribute to the diversity of cortical circuits by conferring specific functional properties to their progeny, for example through prescribed transcriptional programs.

### 1.3.3 Clonal relationships give rise to fine-scale excitatory subnetworks

Newly born postmitotic excitatory neurons migrate radially into the developing cortex, using the apical processes of RGCs as a scaffold (Noctor et al. 2001). This process occurs in an inside-out manner, with deep layer neurons generally being born before those in upper layers (Angevine and Sidman 1961; Donoghue and Rakic 1999; Noctor et al. 2004; Qian et al. 2000). For example, progenitors dividing at E12 versus E15 predominantly give rise to neurons in L5 and L2/3, respectively (Telley et al. 2016). These observations inspired the radial unit hypothesis, which proposes that the migration of clonally-related neurons gives rise to

radially-organised ontogenetic columns that exhibit shared connectivity and functional specificity (Rakic 1988). The first direct evidence for this came from a collection of elegant studies from the lab of Song Hai Shi. These studies used a retroviral lineage tracing method between E12-13 to visualise clonally-related neurons in the adult brain that are derived from a single RGC (Yu et al. 2009). By performing simultaneous recordings from multiple pairs of neurons across cortical layers, it was observed that clonally-related pairs are considerably more likely to be connected to each other than pairs that include unrelated neurons. Interestingly, this is dependent on the formation of preferential electrical connections between clonally-related neurons, via gap junctions, in early postnatal development (Yu et al. 2012). Thus, clonal relationships appear to give rise to subnetworks of excitatory neurons within the cortex, similar to those discussed in **Section 1.3.1**.

The fact that these observations are dependent upon gap junctions suggests a scenario whereby lineage-dependent transcriptional programs first establish preferential electrical coupling, which is subsequently reinforced by the potentiation of synaptic connections by Hebbian mechanisms. In keeping with this idea, two-photon calcium imaging experiments demonstrated that clonally-related neurons in L2/3 of V1 exhibit orientation preferences that are more similar than expected by chance (Li et al. 2012), suggesting that lineage-dependent subnetworks show functional specificity. Remarkably, similar observations have been made in the optic tectum of Xenopus laevis tadpoles (Muldal et al. 2014), suggesting that clonal relationships represent an evolutionarily conserved mechanism for the establishment of fine-scale connectivity across different brain areas, and vertebrate species.

Notably, labelling single RGCs at this stage of development typically results in clones of fewer than ten neurons (Gao et al. 2014; Li et al. 2012; Yu et al. 2009). Given that cortical neurons typically receive thousands of inputs, it is difficult to imagine a small number of clonally related neurons having a substantial impact upon spiking activity. However, it has been demonstrated that stimulation of single neurons is sufficient to impact perceptual decision making (Buchan and Rowland 2018; Tanke et al. 2018). Additionally, recent theoretical work has predicted that

the orientation selectivity of V1 pyramidal neurons is predominantly determined by the strongest 1 % of the inputs that they receive (Goetz et al. 2021). Therefore, it is possible that the response properties of cortical neurons are influenced by a small number of clonally-related connections.

Similarly, it is unclear whether lineage relationships observed in small clones can account for the functional organisation of larger populations of cortical neurons. As discussed in **Section 1.3.2**, the size of a clone will vary as a function of the time that the mitotically active progenitor cell is labelled. Thus, larger clones can be visualised by labelling progenitors at an earlier point in cortical development. For example, one study used a genetically-modified mouse model to label cortical progenitors at significantly earlier stages of embryonic development, which yielded clones of up to 800 neurons that span the cortical layers (Ohtsuki et al. 2012). Subsequent imaging experiments found that clonally-related neurons in V1 continue to exhibit similar orientation selectivity. However, the variance within the clonally-related population was considerably larger than that observed in smaller clones (Li et al. 2012). A second study, using a similar labelling strategy at E10, assessed whether preferential patterns of connectivity are preserved within large clones (Cadwell et al. 2020). By performing simultaneous recordings from multiple pairs of clonally-related and unrelated neurons, this study observed that the probability of interlaminar connections remains considerably higher between clonally-related neurons in both S1 and V1, similar to observations in smaller clones (Cadwell et al. 2020; Yu et al. 2012). Notably, intralaminar connections did not appear to be influenced by clonal relationships. An inherent feature of clonal relationships is that the average degree of relatedness between pairs of neurons within a clone is inversely proportional to its size. Therefore, it is possible that the degree of relatedness between two neurons may serve to instruct the weight ascribed to ontogenetic mechanisms responsible for shaping their functional properties. This is consistent with the observation that the likelihood of observing similar orientation selectivity between clonally-related pairs decreases with increasing clone size (Ohtsuki et al. 2012). Taken together, this indicates that clonal relationships represent a general

principle of cortical organisation that acts to shape the functional properties of large populations of neurons.

### 1.3.4 Clonal relationships reflect the action of multiple lineage-dependent mechanisms

These studies demonstrate that both the fine-scale connectivity and the large-scale functional organisation of cortical circuits in the adult brain, can be related back to the developmental history of individual neurons. However, it remains to be established how these observations relate to the heterogeneous pool of progenitor types discussed in **Section 1.3.2**. The large clones labelled early in cortical development by the above studies likely contain the progeny of multiple progenitors (Cadwell et al. 2020; Ohtsuki et al. 2012). However, it is not possible to distinguish clonally-related neurons as a function of progenitor type using the nonspecific labelling strategies described above. As such, recent work has used the expression of specific genetic markers to visualise neurons in the adult brain as a function of the progenitor type from which they derive. These studies adopt an experimental design whereby the neurons derived from a progenitor type of interest can be compared to those derived from other progenitors (OPs) at the same stage of cortical development. For example, recordings were performed in S1 to compare the properties of L2/3 pyramidal neurons derived from bIPs (bIP-derived) to nearby neurons derived from OPs (OP-derived; Tyler et al. 2015). This revealed substantial differences between the two populations across a number of measures, including fundamental characteristics such as resting membrane potential and input resistance. Subsequent work characterised the morphology of bIP-derived neurons in both L2/3 and L4 of S1 (Guillamon-Vivancos et al. 2019). Notably, bIP-derived L4 neurons were more likely to exhibit asymmetric dendritic morphologies, suggestive of the targeted sampling of thalamic inputs. Another study targeted excitatory neurons in S1 derived from aIPs (aIP-derived), and compared their fine-scale intralaminar connectivity with that of neighbouring OP-derived neurons (Ellender et al. 2019).

Interestingly, they found that aIP-derived neurons in L2/3 and L4 exhibit an out-of-class connectivity bias, such that they preferentially connect to OP-derived neurons over other aIP-derived neurons. In part, this may reflect biases in the neuronal output of certain progenitors. For example, within L2/3, aIPs exhibit some degree of fate restriction for transcriptomically-defined excitatory neuronal subtypes (Ellender et al. 2019). However, within L4, a neuron's progenitor of origin is still able to predict its connectivity, even though transcriptomic approaches have failed to identify subtypes within this layer (Ellender et al. 2019; Tasic et al. 2016; Tasic et al. 2018). These progenitor-type rules might also contribute to the observation that intralaminar connectivity biases are not present amongst clonally-related neurons (Cadwell et al. 2020). Taken together, these observations show that excitatory neurons can exhibit distinct electrophysiological properties, morphologies, and patterns of fine-scale connectivity as a function of the progenitor type from which they derive. Specifically, it indicates that neighbouring cortical neurons can sample differently from the available pre-synaptic inputs, and in a manner that reflects lineage.

## 1.4 Thesis aims

As discussed throughout this chapter, a growing body of evidence suggests that different cortical progenitor types convey distinct functional attributes to their progeny, including their morphology, intrinsic electrical properties, and local synaptic connectivity. This thesis aims to build upon these observations by investigating whether lineage also plays a role in establishing the cortical integration of long-range excitatory inputs from the thalamus, using aIP-derived L4 neurons as a model population. To achieve this, longitudinal studies will be performed that enable the properties of mature cortical neurons to be examined as a function of the progenitor type from which they were derived during embryonic development.

- **Chapter 3** will characterise the relationship between the lineage and the sensory response properties of excitatory neurons in S1 L4. An optogenetic strategy will be used to identify the activity of aIP-derived L4 neurons from extracellular recordings *in vivo*. Subsequently, their spiking activity in response to whisker deflection will be compared to that of OP-derived L4 neurons.

- **Chapter 4** will explore how the lineage of S1 L4 excitatory neurons relates to their morphology and sampling of thalamic inputs. Reconstructions of aIP-derived and OP-derived L4 neurons will be produced such that their soma position and dendritic morphology can be related to the location of barrels and septa. Paired recordings will then be performed *in vitro*, in order to compare the relative input that each population receives from VPM and POm.

- **Chapter 5** will investigate the expression of Lhx2 as a possible mechanism through which lineage-dependent properties of S1 L4 excitatory neurons are established. Quantitative immunohistochemistry will be used to compare the expression levels of Lhx2 in aIP-derived and OP-derived L4 neurons during early postnatal development. If differences are observed, Lhx2 expression will be manipulated such that its influence over the dendritic morphology,

thalamic inputs, and sensory response properties of L4 excitatory neurons can be assessed.

- **Chapter 6** will explore the functional contribution of aIP-derived L4 neurons to sensory processing by investigating their role in sensory-evoked cortical plasticity. To achieve this, a paradigm will be established for the induction of sLTP in S1 L2/3 *in vivo*.

# Chapter 2

# Materials and methods

## 2.1 Experimental animals

Experiments were performed using both male and female C57/BL6 wildtype mice, which were bred, housed, and used in accordance with the UK animals (Scientific Procedures) Act (1986). Breeding females were checked for plugs daily and the day of plugging was considered embryonic day (E) 0.5.

## 2.2 *In utero* electroporation

*In utero* electroporation (IUE) was performed using standard procedures at E14 consistent with previous studies targeting S1 L4 (Langevin et al. 2007; Telley et al. 2016). Briefly, pregnant females were anaesthetised using isofluorane (Zoetis). Buprenorphine (Vetergesic; 0.1 mg/kg) and meloxicam (Metacam; 5mg/kg) were administered subcutaneously. The uterine horns were exposed by midline laparotomy. A mixture of plasmid DNA (~2 µg/µl) and 0.03 % fast green dye (Sigma Aldrich) was injected intraventricularly using micropipettes pulled from borosilicate glass capillaries (1.5 mm outer diameter, Warner Instruments), through the uterine wall and amniotic sac. Plasmid DNA included: T$\alpha$1-Cre (Stancik et al. 2010), in which Cre recombinase is under the control of a portion of the Tubulin alpha-1 (T$\alpha$1) promoter; CAG-tdTomato/GFP (Franco et al. 2012), which uses the chicken $\beta$-actin (CAG) promoter to control a flexible excision (FLEx) cassette, whereby Cre recombination permanently switches expression from tdTomato

to enhanced green fluorescent protein (GFP); EF1$\alpha$-ChR2-YFP (pAAV-EF1$\alpha$-double-floxed-hChR2(H134R)-EYFP-WPRE-HGHpA; Addgene #20298; http://n2t.net/addgene:20298; RRID: Addgene_20298; a gift from Karl Deisseroth), in which Cre recombination turns on the expression of channelrhodopsin-2 fused to enhanced yellow fluorescent protein (ChR2-EYFP) under the control of the human elongation factor-1a promoter; CAG-TdTom (pAAV-CAG TdTom-WPRE; Addgene #83029; http://n2t.net/addgene:83029; RRID:Addgene_83029; a gift from Angelique Brodey), in which the gene for expression of tdTomato is under the control of the CAG promoter; CAG-Lhx2 (pAAV-CAG-Lhx2), in which mouse Lhx2 is under the control of the CAG promoter. To generate CAG-Lhx2, mouse Lhx2 cDNA was amplified from TetO-FUW-Lhx2 (Addgene #61537; http://n2t.net/addgene:61537; RRID:Addgene_61537; a gift from Rudolf Jaenisch) and cloned into the AAV backbone derived from pAAVCAG-iCre (Addgene #51904; http://n2t.net/addgene:51904; RRID:Addgene_51904; a gift from Jinhyun Kim); and a floxed version of CAG-Lhx2 (pAAV-CAG-Flex-Lhx2-WPRE), in which Cre recombination turns on the expression of mouse Lhx2 under the control of the CAG promoter. To generate floxed CAG-Lhx2, mouse Lhx2 cDNA was amplified from TetO-FUW-Lhx2 (Addgene #61537; http://n2t.net/addgene:61537; RRID:Addgene_61537; a gift from Rudolf Jaenisch) and cloned into the AAV backbone derived from pAAV-Flex-GFP (Addgene #28304; http://n2t.net/addgene:28304; RRID:Addgene_28304; a gift from Edward Boyden). Plasmids were injected as a 1:1 ratio and the total volume injected per embryo was ~2 µl. The anode of a 5 mm Platinum Tweezertrode (BTX) was placed over the dorsal telencephalon outside the uterine muscle. Five pulses (50 ms duration separated by 950 ms) at 36 V were delivered with an ECM 830 pulse generator (BTX). The uterine horns were placed back inside the abdomen, the cavity filled with warm physiological saline, and the abdominal muscle and skin incisions were closed with Vicryl (Ethicon) and Prolene (Ethicon) sutures, respectively. Dams were monitored until the birth of the pups and further analgesia was provided, as appropriate.

## 2.3 Optimisation of IUE

IUE in mice is known to have variable transfection success and survival rates (Baumgart and Grebe 2015; Bitzenhofer et al. 2017; Martínez-Garay et al. 2016). This is thought to reflect multiple factors, including surgical technique, the proportion of embryos that are electroporated, the mouse strain, embryonic age, targeted brain area, and electroporation settings. As the majority of embryos that underwent IUE in this thesis were subsequently prepared for *in vivo* electrophysiological experiments, it was particularly important to have confidence in the success of the electroporation. To increase this confidence and increase the number of animals that could be used for *in vivo* recordings, I made two refinements to the IUE pipeline. First, rather than avoiding embryos that were closest to the cervix (as has been done previously; Nixon 2017), I electroporated all accessible embryos. Second, a CAG-tdTomato plasmid was introduced to facilitate a postnatal screening step that would confirm transfection success (**Figure 2.1A**; Bitzenhofer et al., 2017) and make it possible to guide electrode placement in adult mice.

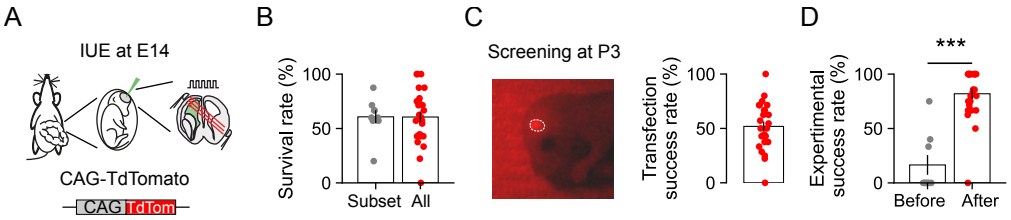


**Figure 2.1: IUE refinements increase experimental success rate.**
**(A)** Animals underwent IUE at E14 using a combination of plasmids that included CAG-tdTomato. **(B)** The survival rate was not affected by targeting all accessible embryos, rather than a subset of embryos (n = 9 and 25 surgeries; p = 0.986, t test). **(C)** tdTomato$^+$ fluorescence could be observed through the skull at P3, making it possible to screen for successful transfection. **(D)** These refinements resulted in a significant increase in success rate in terms of the proportion of animals that could be used for *in vivo* electrophysiological recording experiments (n = 9 and 25 surgeries; p $<$ 0.001, Mann Whitney U). All data are presented as mean ± SEM.

Injecting and electroporating all available embryos had no detectable effect on the survival rate (**Figure 2.1B**; survival when targeting a subset of embryos was 60.72 ± 5.99 %, survival when targeting all embryos was 60.56 ± 5.01 %). Screening pups at P3 allowed the transfection success rate to be estimated by distinguishing

tdTomato$^+$ pups from tdTomato$^-$ littermates (**Figure 2.1C**). Surgical dams were removed from the home cage for the duration of screening and placed in a clean cage out of view. Bedding material from the home cage was rubbed over double gloved hands prior to handling in order to reduce the risk of introducing foreign scents to the pups. Care was taken to cause as little disruption to the nest area as possible. Pups were illuminated using a custom-built LED (525 nm, 30W). In the case of successful transfection, tdTomato$^+$ fluorescence could be clearly observed through the skull (**Figure 2.1C**; transfection success at P3 was 51.86 ± 4.36 %). Generally, it was not possible to screen pups after P4 due to the fur. Animals that did not pass screening were used for other experiments where possible, or culled. Overall, these refinements significantly increased experimental success rate (**Figure 2.1D**; experimental success before was 16.48 ± 9.05 %, experimental success after was 81.95 ± 4.59 %), ultimately reducing the number of animals required to generate the data necessary for this thesis. This represents a considerable improvement in line with the strategy of the National Centre for the Replacement, Reduction and Refinement of Animals in Research.

## 2.4 Postnatal intrathalamic viral injections

Animals that had undergone IUE were used for targeted intracerebral injections at P21. Mice were anaesthetised using isofluorane and placed in a stereotaxic frame (Kopf Instruments). Vetergesic (0.1 mg/kg) was administered subcutaneously, and EMLA cream (Aspen) was applied to the scalp. An incision was made to expose the skull. Bregma and lamda were located and a small craniotomy ($< 1$ mm$^2$) was performed using a H.MH-170 pneumatic dental drill (Foredom) to expose the pial surface. Injections were targeted to either the ventral posteromedial nucleus (VPM) (in mm: 1.8 lateral, 1.4 posterior with respect to bregma and 3.1 deep from pia), or the posterior medial nucleus (POm) (in mm: 1.4 lateral, 2.1 posterior to bregma and 3 deep from pia) of the thalamus. 120-240 nl of an adeno-associated virus (AAV) carrying CAG-ChR2-GFP, in which ChR2-GFP was under the control of the CAG promoter (Boyden, UNC Vector Core), was injected over a period of 8 minutes

using a pulled glass micropipette (Blaubrand intraMARK). The craniotomy was covered, and the skin closed with Vicryl sutures. Further analgesia was provided, as appropriate. Post hoc histological analysis was used to confirm correct location of the thalamic injections.

## 2.5 *In vitro* preparation and recording conditions

Acute slices were prepared from postnatal animals from P21 (range P21-28), or from P60 (range P60-75) where a postnatal intracerebral injection had been performed. Animals were anaesthetised using isofluorane and decapitated. Thalamocortical 350-400 µm slices (55 ° with respect to midline) were cut using a vibrating microtome (Microm). Slices were prepared in artificial cerebrospinal fluid (aCSF) containing (in mM): 65 sucrose, 85 NaCl, 2.5 KCl, 1.25 $NaH_2PO_4$, 7 $MgCl_2$, 0.5 $CaCl_2$, 25 $NaHCO_3$ and 10 glucose, pH 7.2-7.4, bubbled with carbogen gas (95 % O2 / 5 % CO2). Slices were immediately transferred to a storage chamber containing aCSF (in mM): 130 NaCl, 3.5 KCl, 1.2 $NaH_2PO_4$, 2 $MgCl_2$, 2 $CaCl_2$, 24 $NaHCO_3$ and 10 glucose, pH 7.2 - 7.4, at 32 °C, and bubbled with carbogen gas. When required, slices were transferred to a recording chamber and continuously superfused with aCSF bubbled with carbogen gas with the same composition as the storage solution (32 °C and perfusion speed of 2 ml/min). Whole-cell current-clamp recordings were performed using glass pipettes, pulled from borosilicate glass capillaries (1.2 mm outer diameter, Warner Instruments), containing (in mM): 110 potassium gluconate, 40 HEPES, 2 ATP-Mg, 0.3 Na-GTP, 4 NaCl and 4 mg/ml biocytin (pH 7.2-7.3; osmolarity 290-300 mosmol/l).

## 2.6 *In vitro* stimulus protocols and data analysis

Recordings were made using a Multiclamp 700B (Molecular Devices) amplifier and acquired using WinWCP (University of Strathclyde, UK) or pClamp (Molecular Devices) software. All recordings were low pass filtered at 2 kHz and digitized at a sampling frequency of 10 kHz. Slices were placed into a recording chamber and

barrels were visualised in layer 4 (L4) under brightfield illumination. The distribution of cells labelled by IUE meant that the intrinsic electrophysiological properties and morphology of neurons were sampled across the extent of S1. Single L4 excitatory neurons within barrels were identified and targeted using video assisted Dodt contrast imaging. Progenitor identity was confirmed using fluorescent light. The intrinsic properties of the recorded neurons were assessed using a variety of protocols consisting of hyperpolarising and depolarising current steps (from -300 to +600 pA, 100 pA steps) in current clamp. Measurements included resting membrane potential, spike threshold, spike frequency, spike amplitude and inter-spike interval. The resting membrane potential was calculated from a pre-stimulus period of 0 pA current injection, averaged over 10 sweeps. The values of spike threshold voltage were calculated manually from the recorded traces. All other measures were calculated using custom scripts written in python. Spontaneous excitatory postsynaptic currents (sEPSCs) were recorded in voltage clamp whilst holding the cell at -70 mV. Each sEPSC recording was 10 minutes long. The pClamp event detection tool was used to create a standardised template by manually selecting ~200 spontaneous events. This template was then used to automatically detect sEPCSs. The amplitude and frequency of the sEPCSs were calculated using custom scripts written in MATLAB. Monosynaptic thalamic inputs to layer 4 (L4) neurons were studied by stimulating ChR2-GFP expressing axons in L4, which originated from either POm or VPM. Photoactivation of ChR2 was achieved using 1 ms light pulses via an LED (473 nm; 3.8-21.6 $mW/mm^2$, LedEngin) and the amplitude of short-latency, time-locked, light-evoked excitatory postsynaptic potentials (EPSPs) were measured from pairs of simultaneously recorded L4 neurons from the average of 10-40 sweeps. Light intensity was adjusted to produce low amplitude monosynaptic EPSPs (mean peak $< 3$ mV), to minimize the chance of recruiting polysynaptic activity.

## 2.7 *In vivo* preparation and recording conditions

Extracellular recordings were performed from P60 (range P60 – 75) for quantifying response properties, and from P28 (range P28 – 35) for plasticity experiments. Animals were anaesthetised with 25 % urethane (1 g/kg; Sigma) in phosphate-buffered saline (PBS; Thermo Fisher), then mounted in a stereotaxic frame (Stoelting) and continuously supplied with oxygen (0.3 ml/min) throughout the recording. Glycopyrronium Bromide (Glycopyrrolate; 0.01 mg/kg) was administered subcutaneously, and Marcaine (Aspen) was applied to the scalp. A heat mat controlled by a direct current temperature regulation system (FHC inc.) was used to maintain body temperature at 37 °C. A single incision was made to remove the skin from the skull and a craniotomy of ~ 2 mm diameter was performed using a pneumatic dental drill (Foredom). A 32-channel single-shank electrode (Neuronexus) was repeatedly submerged in 1,1'-Dioctadecyl-3,3,3',3'-Tetramethylindocarbocyanine Perchlorate (DiI) lipophilic dye (2.5 mg/ml, in 70 % ethanol, Thermo Fisher) and then slowly inserted into the cortex at an angle of 20 ° from the vertical (in mm: 3 lateral, 1.2 posterior to bregma; 0.9 deep from pia). In all experiments, baseline activity was recorded for between 30 min and 1 hr following electrode insertion.

## 2.8 *In vivo* stimulation and recording protocols

The electrode was connected to an acquisition board (OpenEphys) using a NPD36 connector (Omnetics) and a RHD2132 amplifier (Intan). In order to deflect two single whiskers independently, borosilicate capillaries (1.5 mm outer diameter, Warner Instruments) were attached to two piezoelectric bending actuators (Piezo Technics). Deflection was achieved using a single 100 Hz sinusoidal waveform controlled by a Piezo Controller (Piezo Technics). Photoactivation of ChR2 was achieved using 10 ms light pulses via an LED (473 nm, 45 mW/mm$^2$, LedEngin) positioned above the cortical surface. All stimulus protocols were generated using custom scripts written in MATLAB and delivered via a PulsePal pulse train generator (OpenEphys). The principal whisker (PW) relative to the electrode insertion site

was manually identified online by the presence of a robust, short-latency spiking response following whisker deflection and a characteristic current source density profile (CSD), calculated as the second spatial derivative of the local field potential (LFP). The adjacent whisker (AW) was defined as the whisker immediately rostral to the principal whisker. If this whisker was missing or did not evoke a response, the whisker immediately caudal was used. The identities of the PW and AW were confirmed offline using the population spike rate and response latency (time to first spike) of all L4 excitatory neurons from a given animal.

To study sensory long-term potentiation (sLTP), a rhythmic whisker stimulation (RWS) protocol was performed as has been described previously (Gambino et al., 2014). Before (pre) and after (post) RWS, responses were measured by deflecting multiple whiskers (~10) with a single piezoelectric bending actuator at 0.1 Hz for 100 trials. During RWS, the whiskers were deflected for 1 min at 8 Hz (i.e., 100 Hz waveform every 125 ms). Electrodes were immersed in 1 % Tergazyme (Sigma Aldrich) for 2 hr between recording sessions. Data was acquired at 30 kHz. To obtain multiunit activity (MUA), data was bandpass filtered between 300-6000 Hz. MUA was detected using the median absolute deviation of the filtered signal (Rey et al. 2015). To obtain the LFP, data was lowpass filtered under 300 Hz and a 50 Hz notch filter was applied. To obtain single unit activity, data was spike sorted using Kilosort (Pachitariu et al. 2016), and curated in Phy (Rossant et al. 2016).

## 2.9 *In vivo* analysis

Cortical layers were defined using the PW CSD. The shortest latency CSD sink evoked upon stimulation of the principal whisker was defined as L4. Electrode channels above L4 were assigned as L2/3. Regular spiking (primarily excitatory) neurons were separated from fast-spiking (putative interneurons) neurons using a spike waveform trough-to-peak time of 0.5 ms as the separation criterion. To identify neurons that were directly activated by ChR2, repeated light pulses were delivered to the probe insertion site. Optotagged neurons were defined by a mean

response latency $< 5$ ms. To control for the recruitment of polysynaptic light-evoked activity, the AMPA receptor blocker DNQX (10 mM, Tocris) was applied to the cortical surface in a subset of experiments, as reported previously (Lima et al., 2009). The stimulus-evoked response window for single whisker deflection was defined as 50 ms (e.g., **Figure 3.2**). In all experiments, spontaneous activity was calculated on a trial-by-trial basis as the average spike rate of a given unit or channel and subtracted from stimulus-evoked responses. Time to first spike was calculated as the 1 ms time bin containing the first spike 5–20 ms following whisker deflection in each trial. Peak spike latency was calculated as the 1 ms time bin containing the maximum number of spikes on average across all trials. The selectivity index for individual neurons was calculated as:

$$R_{PW}/R_{PW} + R_{AW}$$

where $R_{PW}$ and $R_{AW}$ were the cumulative spontaneous subtracted spike count in the 50 ms following deflection of the PW or AW, respectively (e.g., **Figure 3.2B**). For train deflection $R_{PW}$ and $R_{AW}$ were the total sum of the spontaneous subtracted spike counts in four separate 50 ms windows following each deflection (e.g., **Figure 3.2C**). The stimulus-evoked response window for the deflection of multiple whiskers was defined as 250 ms (e.g., **Figure 6.1**). Population coupling was quantified as the spike-triggered MUA (stMUA) at zero lag as described previously (Okun et al. 2015). To compare across recordings, MUA was normalised by the median absolute deviation.

## 2.10 Histological analysis

Following whole-cell patch-clamp recording, acute brain slices were fixed in 4 % paraformaldehyde (PFA, Sigma Aldrich) in 0.1 M PBS (pH 7.4). Biocytin-filled cells were visualised using repeated incubation with streptavidin alexa fluor 680 (1:1000, Thermo Fisher), boosted using anti-streptavidin (1:1000, goat, Vector Laboratories). For whole-brain histology, brains were fixed by cardiac perfusion of

PBS followed by 4 % PFA. Brains were stored in 4 % PFA for an additional 24 hr, after which they were washed and stored in PBS. Tissue was sectioned at 50 µm on a vibrating microtome (Microm).

The standard immunohistochemistry protocol was as follows. Sections were washed three times in PBS for 5 min, then blocked in 20 % normal goat serum (NGS; Sigma Aldrich) in 0.1 % Triton-X (Thermo Fisher) in PBS (PBST) for 2 h at RT. Sections were washed in PBS and incubated overnight with primary antibody diluted in 0.1 % PBST at 4 °C. Primary antibodies included: anti-VGlut2 (1:250, rabbit, Synaptic Systems), anti-GFP (1:1000, chicken, Aves Lab), anti-RFP (1:1000, rat, Chromotek), and anti-Lhx2 (1:500, rabbit, Abcam). VGLUT2 staining was facilitated using heated antigen retrieval at 92 °C in 10 mM fresh sodium citrate (pH 6.0) for 30 min prior to primary antibody incubation. Slices were washed in PBS and were incubated for 2 hr with secondary antibodies diluted in 0.1 % PBST at RT. Secondary antibodies included: anti-chicken alexa fluor 488 (1:1000, goat, Thermo Fisher), anti-rat alexa fluor 568 (1:1000, goat; Thermo Fisher), and anti-rabbit alexa fluor 635 (1:1000, goat, Thermo Fisher). Sections were counter-stained with 4',6-Diamidino-2-Phenylindole, Dihydrochloride (DAPI, 1:10000, Thermo Fisher) and mounted on slides with VectaShield (Vectorlabs). Fluorescent images were acquired with a LSM 880 confocal microscope (Zeiss) equipped with 488 nm, 561 nm, and 633 nm lasers and a 20x water-immersion objective (W Plan-Apochromat) using ZEN software (Zeiss). All cell counting, localisation and fluorescence analysis was performed using FIJI (ImageJ).

Soma position was analysed with custom scripts written in MATLAB. Soma coordinates were labelled manually, and a reference line drawn along the L4/L5 boundary based on VGLUT2 fluorescence. The image and soma coordinates were then transformed with respect to the reference line, thereby straightening the cortical layers whilst maintaining relative soma position. Barrel boundaries were detected automatically based on VGLUT2 fluorescence in L4. All soma were assigned a barrel index score with 1 indicating a soma located in the middle of a barrel, and 0 indicating a soma located at the midpoint between two barrel boundaries.

Biocytin-filled neurons were reconstructed using Neurolucida and Neuroexplorer software (MBF Bioscience) and co-registered to immunofluorescence images of the barrel field. The identity of the principal barrel was defined anatomically as the barrel with which the majority of dendrites overlapped. The adjacent barrel was defined as the next closest barrel. Dendritic overlap was quantified as a percentage of total dendritic length. Neurons with $< 5$ % total dendritic length within any barrel were excluded from further analyses. Lhx2 expression levels were quantified as a ratio of the mean pixel intensity (MPI) of the cell body of an aIP-derived L4 neuron over the mean MPI of three neighbouring OP-derived L4 neurons within the same z-plane and within a 100 x 100 µm region of interest.

## 2.11 Statistical analysis

All data are presented as mean ± standard error unless otherwise stated. All statistical analysis was performed in Python using SciPy. Continuous data were assessed for normality and appropriate parametric or non-parametric statistical tests were applied (* $p<0.05$, ** $p<0.01$, *** $p<0.001$).

## 2.12 Code

All code used to acquire and analyse data that contributed to this thesis can be accessed at https://github.com/mjbuchan.

# Chapter 3

# The sensory response properties of S1 L4 excitatory neurons are lineage-dependent

## 3.1 Introduction

The functional contribution of a neuron to sensory processing is intimately related to its selectivity for specific features of the sensory environment (Harris and Mrsic-Flogel 2013). As such, understanding how different types of information are integrated during sensory processing requires knowledge of the mechanisms that shape the sensory response properties of individual neurons.

The response properties of cortical neurons reflect the thalamic inputs that they receive (Bruno and Simons 2002; Hubel and Wiesel 1962; Kwegyir-Afful 2005; Reid and Alonso 1995). First-order thalamic nuclei are driven by subcortical input (e.g., the retina) and are considered the primary relay from the sensory periphery to cortex, transferring sensory information via neurons with simple response properties (Sherman and Guillery 1998). In contrast, higher-order thalamic nuclei receive input from multiple sources that can be of a cortical or subcortical origin (Diamond et al. 1992; Groh et al. 2014; Lavallée et al. 2005; Usrey and Sherman 2019). Consequently, neurons of higher-order nuclei display more complex response properties,

reflecting the encoding of both sensory and contextual information (Diamond et al. 1992; Roth et al. 2016). In addition to facilitating the transfer of sensory information through an ascending hierarchy of transthalamic pathways (Mo and Sherman 2019; Theyel et al. 2010), higher-order thalamic nuclei also send feedback projections to lower cortical areas, where they are thought to influence the processing and plasticity of first-order input (Castejon et al. 2016; Gambino et al. 2014; Mease et al. 2016; Williams and Holtmaat 2019)

The initial discovery of the isomorphic relationship between whiskers in the mystacial pad and barrels in L4 of the S1 (Woolsey and Van der Loos 1970), encouraged a view of the somatosensory system as a collection of parallel circuits, or labelled lines, with the deflection of a single whisker eliciting topographically restricted responses in a given barrelette, barreloid, and barrel (Welker 1971). However, whilst individual neurons in S1 L4 are typically highly responsive to a single, PW, they also respond to the deflection of up to around ten surrounding, or AWs (Armstrong-James et al. 1992; Armstrong-James and Fox 1987; Chapin 1986; Ito 1988; Simons 1978). Interestingly, the extent to which neurons are selective in their response to the PW over an AW can vary considerably even between neighbouring neurons within a single barrel column (Kerr et al. 2007; Sato et al. 2007), reminiscent of the 'salt and pepper' distribution of stimulus representation in rodent primary visual cortex (Hooser et al. 2006; Ohki et al. 2005). This suggests that a degree of fine-scale organisation exists beyond that of the somatotopic arrangement of S1, that influences the response properties of individual neurons in L4. However, the mechanism through which this is established is unknown.

One potential explanation is that the response properties of a neuron are influenced by its developmental history, or lineage. All excitatory cortical neurons are born from a heterogeneous pool of progenitor cells, which reside in the ventricular proliferative zones during embryonic development (Franco and Müller 2013; Gal 2006; Greig et al. 2013; Noctor et al. 2001; Stancik et al. 2010; Tyler and Haydar 2013). Previous work has shown that the local synaptic connectivity of excitatory cortical neurons reflects the progenitor type from which they derive, suggesting

that neighbouring neurons sample inputs differently, and in a manner that reflects their lineage (Cadwell et al. 2020; Ellender et al. 2019; Yu et al. 2009).

This chapter will characterise the response properties of S1 L4 excitatory neurons as a function of the progenitor type from which they derive. Specifically, the aims of this chapter are as follows:

- To characterise the *in vivo* response properties of S1 L4 excitatory neurons
- To identify S1 L4 excitatory neurons as a function of lineage *in vivo*
- To assess whether the response properties of S1 L4 excitatory neurons are lineage-dependent

## 3.2 Results

### 3.2.1 S1 L4 response properties are heterogeneous

In order to characterise the response properties of S1 L4 excitatory neurons, it was first necessary to establish a method to record and identify their activity *in vivo*. Extracellular recordings were performed from postnatal day 60 (P60) using a linear 32 channel electrode in urethane anaesthetised C57/Bl6 mice (**Figure 3.1A**, see **Section 2.7**). The electrode was inserted orthogonally to the pial surface of S1 at standard stereotaxic coordinates used to target the barrel field (in mm: -3.0 lateral, 1.4 posterior with respect to bregma; 0.9 deep from pia) at a 20 ° angle.

Deflection of individual whiskers was achieved using glass micropipettes attached to piezoelectric bending actuators. The PW was identified online by the presence of a robust, short latency whisker-evoked spiking response that gave rise to a characteristic CSD profile, calculated as the second spatial derivative of the LFP (**Figure 3.1B**). The electrode channel corresponding to the minimum value of the infragranular CSD sink was taken to be the centre of L4 (see **Section 2.9**). Prior to recordings, the electrode was coated in DiI lipophylic dye to allow for the post hoc confirmation of electrode position in S1 (**Figure 3.1B**). Regular-spiking (RS, primarily excitatory) neurons were distinguished from fast-spiking (FS, primarily interneurons) neurons based on the waveform properties of single units isolated using Kilosort (**Figure 3.1C**; Pachitariu et al. 2016). A trough-to-peak time of 0.5 ms was used as the separation criterion (FS trough-to-peak was 0.31 ± 0.01 ms and RS trough-to-peak was 1.01 ± 0.02 ms) in keeping with previous studies in rodent cortex (Barthó et al. 2004; Niell and Stryker 2008; Okun et al. 2015). Thus, the activity of putative L4 excitatory neurons could be observed in addition to simultaneously recorded multi-unit activity (MUA) and the LFP (**Figure 3.1D**). Consistent with previous studies, the spontaneous activity of L4 excitatory neurons varied coherently in the absence of sensory stimulation and followed a characteristic lognormal distribution (**Figure 3.1D-E**; Buzsáki and Mizuseki 2014; Luczak et al. 2013; Okun et al. 2010).

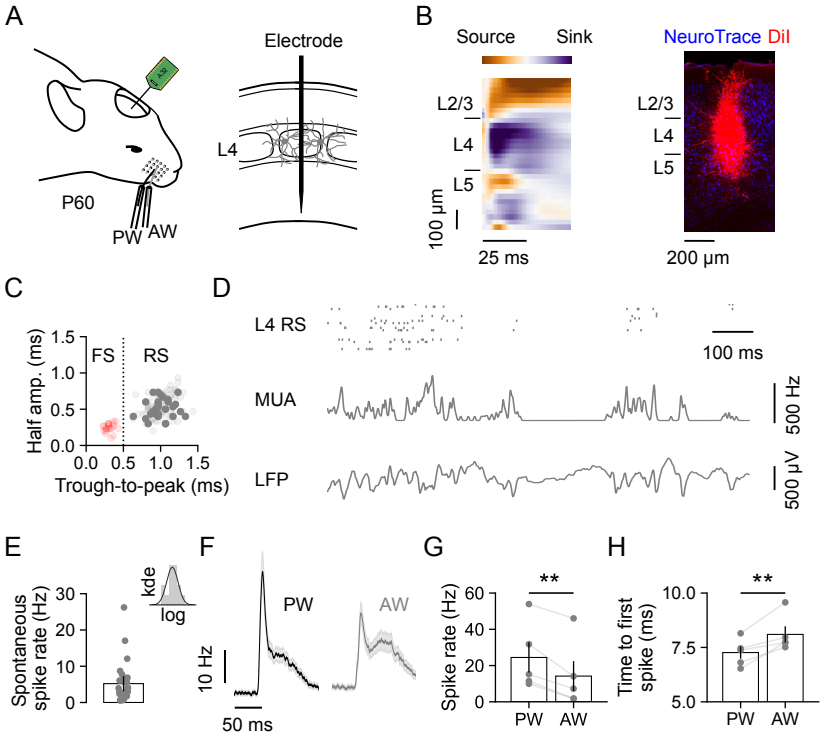


**Figure 3.1: Identification of S1 L4 excitatory neurons from extracellular recordings.** **(A)** The activity of individual S1 L4 neurons was recorded in response to deflection of the PW or AW from P60 using a linear 32 channel electrode in urethane anaesthetised mice. **(B)** L4 was identified using the LFP CSD profile following PW deflection (left). Histological analysis confirmed electrode position in S1 (right). **(C)** RS (primarily excitatory) neurons were distinguished from FS (primarily interneurons) neurons based on the waveform properties of single units. A trough-to-peak time of 0.5 ms was used as the separation criterion. Filled circles correspond to excitatory neurons included in **Figures 3.1, 3.2, and 3.6**. **(D)** Population raster of spontaneous activity from 10 excitatory neurons (top), MUA (middle) and mean LFP (bottom) recorded from a single animal across five adjacent electrode channels centred on the L4 current sink. **(E)** Spontaneous spike rate of identified L4 neurons. Inset represents the log distribution of spontaneous spike rates, black line indicates gaussian fit (n = 28 neurons). **(F)** Mean L4 neuronal responses from an individual animal following a single deflection of the PW (left) or AW (right). Shading indicates SEM around the mean. **(G)** PW deflection elicited a higher spike rate compared to AW deflection (n = 5 animals; p = 0.006, paired t-test). **(H)** Peak responses were faster following PW deflection than AW deflection (n = 5 animals; p = 0.009, paired t-test). Data represented as mean ± SEM.

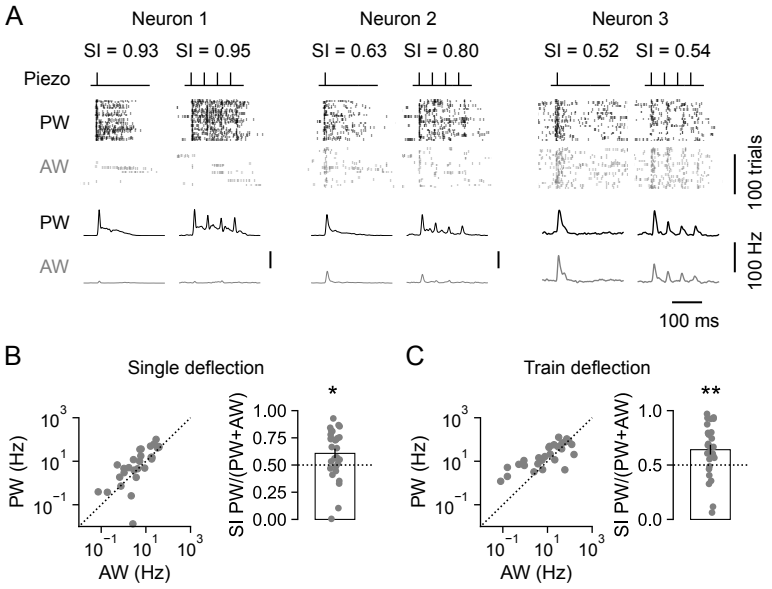


**Figure 3.2: S1 L4 excitatory neurons exhibit heterogeneous receptive field properties. (A)** Three L4 neurons with different SI, as defined by relative response to the PW and AW. Raster plots and corresponding PSTHs show spiking activity over 100 trials of either single deflections (inner left) or trains of deflections (inner right) of the PW (black) or AW (grey). **(B)** Responses of individual neurons to single deflections of the PW and AW (left), and the distribution of corresponding SI values (right). L4 neurons were selective for the PW (n = 28 neurons; p = 0.019, one sample t-test). **(C)** Responses of individual neurons to trains of deflections of the PW and AW (left), and the corresponding SI values (right). L4 neurons were selective for the PW (n = 28 neurons; p = 0.004, one sample t-test). Data represented as mean ± SEM.

Where possible, the AW was defined as the whisker immediately rostral to the PW. If this whisker was missing, barbered, or did not evoke a response, the whisker immediately caudal was used. The identities of the PW and AW were confirmed post hoc using the spike rate and response latency following whisker deflection of all RS neurons recorded from an individual animal (see **Section 2.8**; discussed in Estebanez et al. 2018). As expected, both PW and AW deflection evoked responses in L4 excitatory neurons (**Figure 3.1F**), with PW deflection exhibiting a significantly higher spike rate (**Figure 3.1G**; PW spike rate was 24.46 ± 8.33 Hz, AW spike rate was 14.19 ± 8.28 Hz) and shorter latency (**Figure 3.1H**; PW latency was 7.26 ± 0.28 ms, AW latency was 8.10 ± 0.37 ms) compared to AW deflection, consistent with previous observations (Armstrong-James et al. 1992; Armstrong-James and Fox 1987; Chapin 1986; Ito 1988; Simons 1978).

To quantify the response properties of L4 neurons, a selectivity index (SI) was

defined, where values closer to 1 indicated neurons that responded mainly to the PW, and SI values closer to 0.5 indicated similar levels of response to the PW and AW (El-Boustani et al. 2020; Sato et al. 2007). The SI was assessed in the 50 ms following either single whisker deflections or trains of whisker deflections (four deflections at 10 Hz; **Section 2.8**). Some L4 excitatory neurons displayed very high SI values, but others displayed SI values close to 0.5 (**Figure 3.2A**). Consequently, whilst L4 excitatory neurons as a population were selective for deflections of the PW (**Figure 3.2B-C**; single deflection mean SI was 0.61 ± 0.04; train deflection mean SI was 0.64 ± 0.04), the range of SI values confirmed that individual L4 excitatory neurons exhibit considerable heterogeneity in terms of their selectivity for the PW (single deflection IQR was 0.48 to 0.76; train deflection IQR was 0.53 to 0.79).

### 3.2.2 S1 L4 response properties are lineage-dependent

To investigate whether the heterogeneous response properties of L4 excitatory neurons are associated with lineage, *in utero* electroporation (IUE; see **Section 2.2**) was used to pulse-label a population of dividing progenitor cells in C57/Bl6 embryos at embryonic gestation day 14 (E14), when L4 excitatory neurons are being born (**Figure 3.3A**; Costa and Müller 2015; Langevin et al. 2007; Telley et al. 2016). The tubulin alpha1 (T$\alpha$1) promoter can be used to label apical intermediate progenitors (aIPs) within the VZ (Ellender et al. 2019; Gal 2006; Stancik et al. 2010). Based on their morphology and cell cycle characteristics, aIPs can be distinguished from OPs (Gal 2006; Stancik et al. 2010), which are thought to include radial glial cells within the VZ, and outer radial glia and basal intermediate progenitor cells within the subventricular zone (Franco and Müller 2013; Kowalczyk et al. 2009; Noctor et al. 2001; Noctor et al. 2004; Taverna et al. 2014; Wang et al. 2011).

To characterise the response properties of aIP-derived and OP-derived L4 neurons, they were first distinguished by optotagging, an established method for the identification of opsin-expressing cell types *in vivo* (**Figure 3.3E**; Estebanez et al.

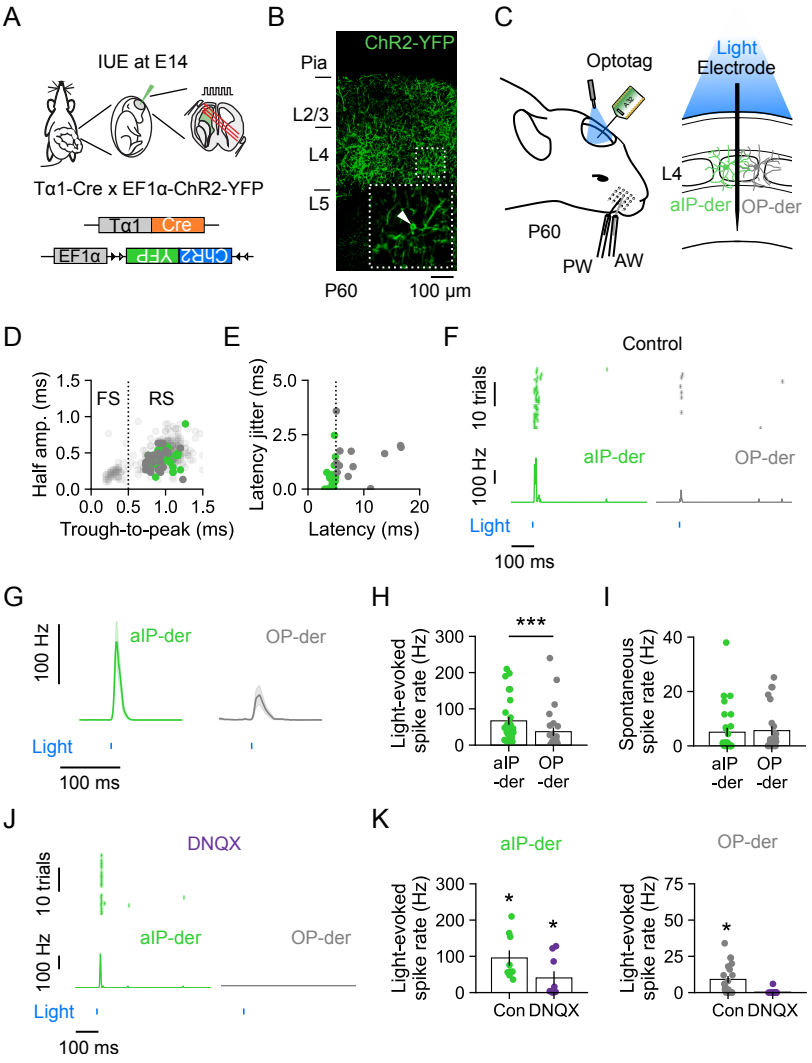


**Figure 3.3: Identification of aIP-derived L4 neurons from extracellular recordings. (A)** Animals underwent IUE of a T$\alpha$1-Cre and a floxed ChR2-YFP plasmid at E14. **(B)** ChR2-YFP$^+$ aIP-derived L4 neurons could be observed at P60. **(C)** The spiking activity of optotagged aIP-derived L4 neurons and neighbouring (non-optotagged) OP-derived L4 neurons was recorded in response to deflection of the PW or AW. **(D)** Regular-spiking (RS, primarily excitatory) neurons were distinguished from fast-spiking (FS, primarily interneurons) neurons based on the waveform properties of single units. A trough-to-peak time of 0.5 ms was used as the separation criterion. Filled circles correspond to excitatory neurons included in **Figures 3.3, 3.4, 3.5, and 3.6**. **(E)** aIP-derived (ChR2-YFP$^+$) L4 neurons were distinguished from OP-derived L4 neurons based on spike times in response to repeated light pulses. A mean light-evoked spike latency of 5 ms was used as the separation criterion. **(F)** Light-evoked spiking of an individual aIP-derived L4 neuron (left) and OP-derived L4 neuron (right). **(G)** Mean light-evoked spiking response of a population of aIP-derived and OP-derived L4 neurons (n = 29 and 26 neurons). Shading indicates SEM around the mean. **(H)** Light-evoked spiking was higher in aIP-derived L4 neurons (n = 29 and 26 neurons; $p < 0.001$, Mann Whitney U test). **(I)** Spontaneous spike rates did not differ between aIP-derived and OP-derived L4 neurons (n = 29 and 26 neurons; p = 0.24, Mann Whitney U test). **(J)** Example recordings show that after blocking synaptic transmission with the glutamate receptor blocker, DNQX, light-evoked spiking was still evident in an optotagged aIP-derived neuron but was abolished in a nearby OP-derived neuron. **(K)** Population data revealed that DNQX reduced, but did not abolish, light-evoked responses in aIP-derived neurons (n = 9 neurons; p = 0.004 and p = 0.012, one sample Wilcoxon signed-rank test against a median of zero). Whereas DNQX abolished light-evoked responses in OP-derived neurons (n = 20 neurons; p = 0.001, p = 0.317, one sample Wilcoxon signed-rank test against a median of zero; axis re-scaled to aid visualisation). Data represented as mean ± SEM.

2018; Lima et al. 2009; Nieh et al. 2015). This involved the electroporation of two DNA constructs: a T$\alpha$1-Cre construct in which Cre recombinase is under the control of a portion of the T$\alpha$1 promoter, and a ChR2-YFP reporter construct that expresses channelrhodopsin 2 (ChR2) fused to yellow fluorescent protein (YFP) following Cre recombination. Thus, ChR2-YFP was expressed in aIPs and not in concurrently dividing OPs, in line with previous work (Ellender et al. 2019). IUE was targeted to the region of the VZ that gives rise to S1 excitatory neurons, such that when animals were allowed to survive postnatally, aIP-derived (ChR2-YFP$^+$) neurons could be observed in S1 L4 (**Figure 3.3B**). As above, extracellular recordings were performed from excitatory S1 L4 neurons (**Figure 3.3C**). Light pulses (10 ms, 473 nm) were delivered to the recording site to selectively activate and identify aIP-derived L4 neurons, and responses to deflections of the PW or AW were investigated.

Again, RS and FS neurons were separated based on the waveform properties of single units using a trough-to-peak time of 0.5 ms as the separation criterion (**Figure 3.3D**; FS trough-to-peak was 0.31 $\pm$ 0.01 ms, RS trough-to-peak was 0.99 $\pm$ 0.01 ms). Neurons that exhibited reliable, short latency ($<$ 5 ms) light-evoked responses were considered to be directly activated by ChR2 and classed as aIP-derived (**Figure 3.3E-F**). Those that exhibited a longer latency, or no, light-evoked response, were classed as OP-derived. As expected, the light-evoked spiking response of aIP-derived L4 neurons was greater than that of OP-derived L4 neurons (**Figure 3.3G-H**; aIP-derived spike rate was 66.97 $\pm$ 11.02 Hz, OP-derived was 37.08 $\pm$ 11.56 Hz). However, the spike rate of aIP-derived and OP-derived L4 neurons was similar in the absence of sensory stimuli (**Figure 3.3I**; aIP-derived spontaneous spike rate was 5.03 Hz $\pm$ 1.60, OP-derived spontaneous spike rate was 5.62 Hz $\pm$ 1.57), indicating that the expression of ChR2 does not result in increased excitability. To control for the recruitment of polysnaptic light-evoked activity, the AMPA receptor blocker DNQX was administered topically to the cortical surface in a subset of animals (**Figure 3.3J**). DNQX reduced the light-evoked response in aIP-derived neurons, but it remained significantly above spontaneous

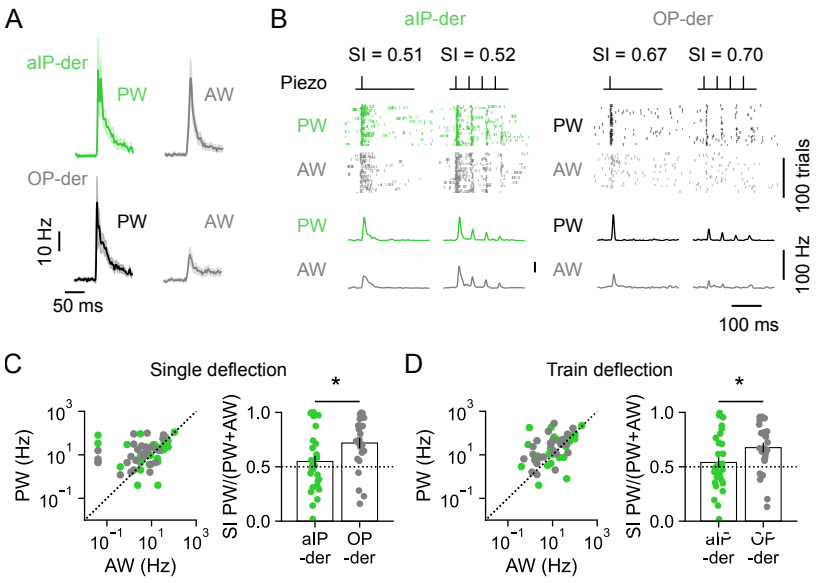


**Figure 3.4: aIP-derived L4 neurons exhibit multi-whisker response properties.** **(A)** Mean L4 spiking responses from an individual animal following a single deflection of the PW (left) or AW (right). Shading indicates SEM around the mean. **(B)** Spiking of an individual aIP-derived (left; green) and OP-derived L4 neuron (right; black) over 100 trials of either a single deflection (inner left) or train deflection (inner right) of the PW or AW. **(C)** Responses of individual aIP-derived and OP-derived L4 neurons to single deflection of the PW and AW (left), and the distribution of corresponding SI values (right). aIP-derived L4 neurons were less selective to the PW, and relatively more responsive to the AW, when compared to OP-derived neurons (n = 29 and 26 neurons; p = 0.019, Mann Whitney U test). **(D)** Responses to train deflection of the PW and AW (left), and corresponding SI values (right). aIP-derived L4 neurons were less selective to the PW, and therefore relatively more responsive to the AW (n = 29 and 26 neurons; p = 0.040, t-test). Data represented as mean ± SEM.

levels (**Figure 3.3K**; control spike rate was 95.56 ± 21.01 Hz, DNQX spike rate was 40.44 ± 18.35 Hz), suggesting that direct light-evoked activation of ChR2 was preserved. However, the response of OP-derived neurons was completely abolished (**Figure 3.3K**; control spike rate was 9.10 ± 2.32 Hz, DNQX spike rate was 0.30 ± 0.30 Hz).

As above, deflections of the PW and AW evoked responses in both the aIP-derived and OP-derived L4 neurons (**Figure 3.4A**). However, compared to OP-derived L4 neurons, aIP-derived neurons showed stronger relative responses to the AW. This was reflected in lower SI values for the aIP-derived L4 neurons to both single and trains of deflections of the whiskers (**Figure 3.4B-D**; single deflection mean SI was 0.55 ± 0.05 for aIP-derived and 0.71 ± 0.05 for OP-derived; train deflection

mean SI was 0.54 ± 0.05 for aIP-derived and 0.67 ± 0.04 for OP-derived). These data reveal that aIP-derived neurons exhibit greater multi-whisker responsivity than neighbouring OP-derived neurons, suggesting that the response properties of L4 excitatory neurons reflect the progenitor type from which they derive.

### 3.2.3 Temporal properties of whisker-evoked responses

It is possible that temporal differences in the whisker-evoked responses could contribute to the differences observed in the SI of aIP-derived and OP-derived L4 neurons. To investigate this possibility, a series of measures were calculated to characterise the temporal response profile of aIP-derived and OP-derived L4 neurons following whisker deflection (see **Section 2.9**). Response latency, estimated as the time to first spike, was shorter following PW deflection compared to AW deflection for both aIP-derived and OP-derived neurons (**Figure 3.5A**; aIP-derived PW latency was 8.58 ± 0.58 ms, and AW latency was 10.80 ± 0.87 ms; OP-derived PW latency was 8.72 ± 0.55 ms, and AW latency was 12.27 ± 1.03 ms), consistent with previous work and data in **Figure 3.1**. The delay between PW and AW first spike was not different between the two populations (**Figure 3.5B**; aIP-derived delay was 2.29 ± 1.03 ms, OP-derived delay was 3.58 ± 1.29 ms). Similarly, the peak response latency was shorter following PW deflection compared to AW deflection for both aIP-derived and OP-derived neurons (**Figure 3.5C**; aIP-derived PW peak latency was 13.63 ± 0.74 ms, and AW peak latency was 15.22 ± 0.47 ms; OP-derived PW peak latency was 13.76 ± 0.78 ms, and AW peak latency was 16.46 ± 0.52 ms). The delay between PW and AW peak response latency was indistinguishable between the two populations (**Figure 3.5D**; aIP-derived peak delay was 2.04 ± 0.64 ms, OP-derived peak delay was 2.69 ± 0.88 ms). Therefore, the temporal response properties following whisker deflection are comparable for aIP-derived and OP-derived L4 neurons, with AW responses exhibiting a consistent delay relative to PW responses, in keeping with previous work (Armstrong-James et al. 1992; Armstrong-James and Fox 1987; Diamond et al. 1992).

To further characterise the differences in SI between aIP-derived and OP-derived L4

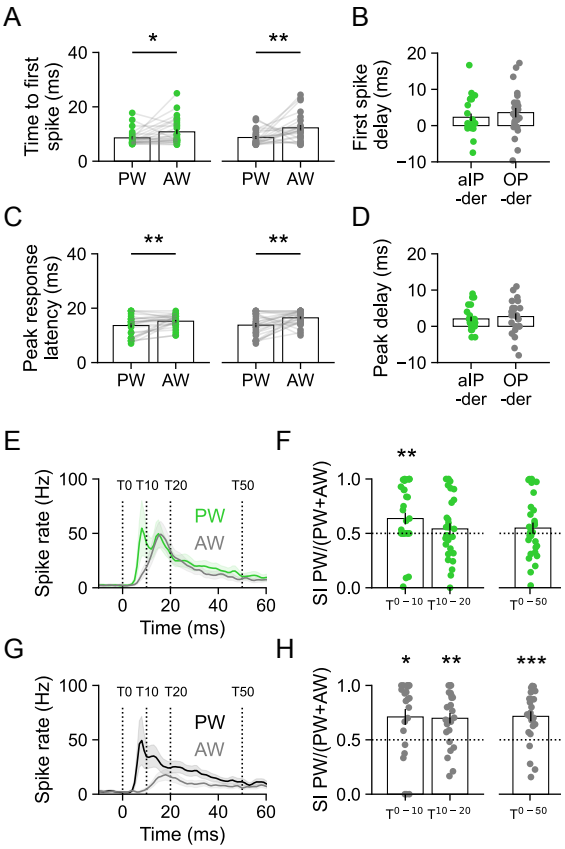


**Figure 3.5: Temporal response properties do not account for differences in selectivity. (A)** Time to first spike was faster following PW deflection than AW deflection for both aIP-derived (left; n = 29 neurons; p = 0.049, Wilcoxon signed-rank test) and OP-derived L4 neurons (right; n = 26 neurons; p = 0.008, Wilcoxon signed-rank test). **(B)** The relative delay between PW and AW time to first spike was similar for aIP-derived and OP-derived L4 neurons (n = 29 and 26 neurons; p = 0.443, t-test). **(C)** Peak response latency was faster following PW deflection than AW deflection for both aIP-derived (left; n = 29 neurons; p = 0.004, Wilcoxon signed-rank test) and OP-derived L4 neurons (right; n = 26 neurons; p = 0.008, Wilcoxon signed-rank test). **(D)** The relative delay between PW and AW peak latency was similar for aIP-derived and OP-derived L4 neurons (n = 29 and 26 neurons; p = 0.553, t-test). **(E)** Mean spiking responses of aIP-derived L4 neurons following single PW and AW deflection. $T^{0-50}$ indicate different windows for SI calculation. Shading indicates SEM around the mean. **(F)** aIP-derived L4 neurons were selective for the PW between $T^{0-10}$ (n = 29 neurons; p = 0.008, Wilcoxon signed-rank against a median of 0.5), but not between $T^{10-20}$ (n = 29 neurons; p = 0.424, Wilcoxon signed-rank against a median of 0.5), consistent with SI calculated between $T^{0-50}$ (data from **Figure 3.4**; n = 29 neurons; p = 0.343, one-sample t-test). **(G)** Mean spiking responses of OP-derived L4 neurons following single PW and AW deflection. $T^{0-50}$ indicate windows for SI calculation. Shading indicates SEM around the mean. **(H)** OP-derived L4 neurons were selective for the PW between $T^{0-10}$ (n = 26 neurons; p = 0.025, Wilcoxon signed-rank against a median of 0.5), and remained selective for $T^{10-20}$ (n = 26 neurons; p = 0.001, Wilcoxon signed-rank against a median of 0.5), and $T^{0-50}$ (n = 29 neurons; $p < 0.001$ , one-sample t-test). Data represented as mean ± SEM.

neurons, the SI was recalculated at different time windows following single whisker deflections (**Figure 3.5E-H**). In the 0-10 ms immediately following whisker deflection, aIP-derived neurons were selective for the PW (**Figure 3.5F**; aIP-derived $T^{0-10}$ mean SI was 0.66 ± 0.05), consistent with the delayed onset of the AW response. However, at 10–20 ms following whisker deflection, aIP-derived neurons were no longer selective for the PW (**Figure 3.5F**; aIP-derived $T^{10-20}$ mean SI was 0.55 ± 0.05), which was consistent with the SI calculated over the full 50 ms response window ($T^{0-50}$; **Figure 3.5F**; aIP-derived $T^{0-50}$ mean SI was 0.55 ± 0.05). In contrast, OP-derived neurons were selective for the PW in the $^{0-10}$ ms following whisker deflection (**Figure 3.5H**; OP-derived $T^{0-10}$ mean SI was 0.71 ± 0.07), they remained selective for the PW at 10–20 ms (**Figure 3.5H**; OP-derived $T^{10-20}$ mean SI was 0.70 ± 0.05), and over the full 50 ms response window (**Figure 3.5H**; OP-derived $T^{0-50}$ mean SI was 0.71 ± 0.05).

Taken together, these data suggest that the temporal properties of whisker-evoked responses do not differ between aIP-derived and OP-derived L4 neurons. Rather, the data support the conclusion that the differences in SI reflect the relative strength of inputs to the two neuronal populations. The timescale over which the SI differences emerge is consistent with differences in recurrent excitatory inputs to the two neuronal populations, including those routed via higher-order thalamus (Armstrong-James et al. 1992; Armstrong-James and Fox 1987; Diamond et al. 1992).

### 3.2.4 S1 L4 population coupling is lineage-dependent

To investigate whether the degree of recurrent excitatory connectivity could contribute to the differences in response size following AW deflection, an established measure of population coupling was calculated for aIP-derived and OP-derived L4 neurons (Okun et al. 2015). Population coupling quantifies the correlation between the activity of individual neurons, and that of the local population. It is known to inversely correlate with stimulus selectivity, and is predictive of a number of functional attributes, including the probability of receiving recurrent excitatory

inputs, and the sensitivity of neurons to feedback from higher brain areas (Okun et al. 2015; Sweeney and Clopath 2020).

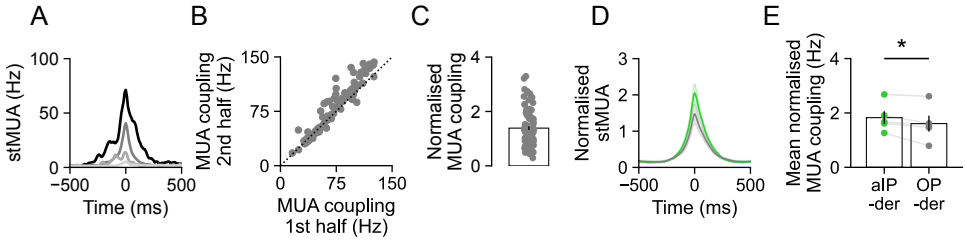


**Figure 3.6: aIP-derived L4 neurons are strongly coupled to population activity.** **(A)** stMUA of four example unlabelled L4 excitatory neurons. MUA coupling corresponds to the height of stMUA at zero time lag. **(B)** MUA coupling is highly consistent over time (n = 100 neurons; $p < 0.001$, Pearson's R). **(C)** Normalised MUA coupling of identified RS neurons (n = 100 neurons). **(D)** Mean normalised stMUA of aIP-derived and OP-derived L4 neurons. Shading indicates SEM around the mean. **(E)** aIP-derived L4 neurons were more strongly coupled to population MUA compared to OP-derived L4 neurons (n = 5 animals; $p = 0.041$, t-test). Data represented as mean ± SEM.

The coupling of L4 excitatory neurons to population activity was calculated as the spike-triggered MUA (stMUA) at zero time lag, as reported previously (**Figure 3.6A**; see **Section 2.9**; Okun et al. 2015). MUA coupling was consistent over time (**Figure 3.6B**; R = 0.92) and varied continuously across the recorded population (**Figure 3.6C**; mean normalised MUA coupling was 1.38 ± 0.06), similar to observations in visual and auditory cortex (Okun et al. 2015). This suggests that there exists considerable diversity amongst L4 excitatory neurons in terms of their relationship to the activity of the local network. Indeed, lineage proved to be an effective discriminator of population coupling, with aIP-derived L4 neurons found to be more strongly coupled to population MUA than OP-derived L4 neurons (**Figure 3.6D-E**; aIP-derived MUA coupling was 1.83 ± 0.24, and OP-derived MUA coupling was 1.61 ± 0.29). These data show that population coupling is a lineage-dependent property of S1 L4 excitatory neurons, and suggest that aIP-derived L4 neurons receive greater recurrent excitatory inputs than OP-derived L4 neurons.

## 3.3 Discussion

In this chapter, a combination of *in utero* labelling and *in vivo* electrophysiology were used to characterise the relationship between the sensory response properties and the lineage of excitatory neurons in S1 L4. The data support the conclusion that response properties are lineage-dependent, with aIP-derived L4 neurons being more likely to exhibit multi-whisker responses compared to OP-derived L4 neurons.

In agreement with earlier work in S1, L4 neurons exhibited heterogeneity in their spiking response properties following deflection of the PW and AW (Armstrong-James et al. 1992; Armstrong-James and Fox 1987; Chapin 1986; Ito 1988; Kerr et al. 2007; Sato et al. 2007; Simons et al. 1992; Simons 1978). By identifying L4 excitatory cortical neurons as a function of the embryonic progenitor type from which they derive, it was possible to demonstrate that one source of this heterogeneity is the neuron's lineage. Previous evidence has shown that clonally-related excitatory neurons derived from the same individual progenitor cell can exhibit similar stimulus selectivity in the visual system (Li et al. 2012; Muldal et al. 2014; Ohtsuki et al. 2012). The current findings advance this observation by revealing that shared response properties are not just a feature of an individual clone, but can be a general feature of the neurons derived from particular types of excitatory embryonic progenitors.

Ultimately, a neuron's spiking activity reflects the inputs that it receives (Harris and Mrsic-Flogel 2013). Responses to AW deflection are known to incorporate inputs from a number of distinct sources, both cortical and subcortical (Armstrong-James et al. 1992; Diamond et al. 1992). One possibility is that the greater AW-evoked spiking responses exhibited by aIP-derived L4 neurons are the result of directly sampling inputs from first-order thalamus in adjacent barrels. However, the observation that AW responses are delayed relative to PW responses in both aIP-derived and OP-derived L4 neurons suggest that this is not the case. Rather, the temporal response properties following AW deflection are more likely to reflect

recurrent excitatory inputs originating in higher-order thalamus or from within local cortical circuits (Armstrong-James et al. 1992; Armstrong-James and Fox 1987; Diamond et al. 1992). This is reinforced by the observation that aIP-derived L4 neurons are more strongly coupled to population activity than OP-derived L4 neurons. Population coupling has been generally thought to reflect local connectivity with nearby excitatory neurons (Okun et al. 2015), although correlated activity between cortical neurons could feasibly reflect participation within excitatory subnetworks characterised by shared long-range connectivity (Brown and Hestrin 2009; Kampa et al. 2006; Yoshimura et al. 2005), including with the higher-order thalamus. Indeed, the fact that aIP-derived L4 neurons have been shown to receive less intralaminar input, particularly from other aIP-derived L4 neurons (Ellender et al. 2019), suggests that lineage-dependent differences in coupling are more likely to result from long-range inputs. Whilst the data presented here cannot distinguish between thalamic and cortical recurrent excitatory inputs, the timescale of response following AW deflection is consistent with that associated with the higher-order thalamus (Armstrong-James et al. 1992; Armstrong-James and Fox 1987; Diamond et al. 1992). In keeping with this idea, the response properties of S1 neurons are known to differ depending on the degree of input that they receive from higher-order thalamus (Castejon et al. 2016; Mease et al. 2016; Zhang and Bruno 2019). Notably, neurons that receive greater input are more likely to exhibit multi-whisker response properties when compared to neighbouring neurons (Jouhanneau et al. 2014).

In summary, this chapter has demonstrated that the sensory response properties of S1 L4 excitatory neurons are lineage-dependent. One potential explanation is that aIP-derived neurons receive greater input from higher-order thalamus. This possibility will be explored in **Chapter 4**.

# Chapter 4

# The sampling of thalamic inputs by S1 L4 excitatory neurons is lineage-dependent

## 4.1 Introduction

L4 of S1 receives direct input from two thalamic nuclei via anatomically segregated thalamocortical projections that convey distinct information about sensory stimuli (**Figure 4.1A**). Tactile information from single whiskers is conveyed via neurons in the first-order, ventral posterior medial nucleus (VPM) of the thalamus. VPM neurons project to discrete anatomical structures within L4, called barrels, forming a somatotopic map of the mystacial pad (Simons 1978; Woolsey and Van der Loos 1970). Meanwhile, information from multiple whiskers is conveyed via neurons in the higher-order, posterior medial nucleus (POm), which receives inputs of both a cortical and subcortical origin (Diamond et al. 1992; Lavallée et al. 2005). POm projections to S1 target the inter-barrel regions within L4, called septa, as well as L1 and L5a (Bureau et al. 2006; Koralek et al. 1988; Lu and Lin 1993; Meyer et al. 2010; Wimmer et al. 2010).

Despite the anatomical organisation of thalamic inputs to S1 being well characterised, the way that they are sampled by L4 excitatory neurons is less well understood. Previous work, using both electrical and optical stimulation methods, has shown that whilst VPM represents the major input to L4, individual neurons differ in the degree to which they receive higher-order input from POm (Audette et al. 2018; Viaene et al. 2011a; Viaene et al. 2011b; Viaene et al. 2011c). The L4 population is therefore heterogeneous in terms of its integration of thalamic input, with some neurons receiving more higher-order information than others. However, the mechanisms that determine how individual neurons sample thalamic inputs are unknown.

In part, the thalamic input received by a L4 excitatory neuron is thought to reflect its morphology and how this relates to the organisation of barrels and septa. For example, L4 excitatory neurons with soma located in septa are more likely to exhibit multi-whisker receptive fields than those within the barrel core, consistent with the sampling of POm inputs (Fox et al. 2003). Additionally, a proportion of L4 excitatory neurons are known to target barrels with their dendrites (Egger et al. 2008; Simons and Woolsey 1984; Staiger 2004), consistent with the sampling of VPM inputs. As such, soma position and dendritic morphology have become established measures to infer the extent to which L4 excitatory neurons are sampling inputs from either barrels or septa, and thus VPM or POm, respectively.

**Chapter 3** demonstrated that the response properties of S1 L4 excitatory neurons are lineage-dependent, and predicted that multi-whisker response properties exhibited by aIP-derived L4 neurons could be the result of receiving greater input from the higher-order thalamic nuclei, POm. This chapter will first explore the relationship between lineage and the morphology of S1 L4 excitatory neurons, before quantifying the relative thalamic inputs received by aIP-derived and OP-derived L4 neurons. Specifically, the aims of this chapter are as follows:

- To determine whether the soma position or dendritic morphology of S1 L4 excitatory neurons are lineage-dependent

- To investigate whether the thalamic inputs received by S1 L4 excitatory neurons are lineage-dependent

## 4.2 Results

### 4.2.1 aIP-derived L4 neurons do not preferentially localise to barrels or septa

In order to visualise S1 L4 excitatory neurons as a function of lineage, a second IUE strategy was used (**Figure 4.1B**). Animals underwent IUE at E14 with two DNA constructs: T$\alpha$1-Cre and a CAG-FLEx two-colour reporter plasmid, where Cre recombination permanently switches expression from tdTomato to enhanced green fluorescent protein (GFP) under the control of the CAG promoter (see **Section 2.2** Franco et al. 2012). Once again, IUE was targeted to the region of VZ that gives rise to S1 excitatory neurons. When animals were allowed to survive postnatally, GFP$^+$ (aIP-derived) and tdTomato$^+$ (OP-derived) neurons could be observed in S1 L4, consistent with previous work (Ellender et al. 2019).

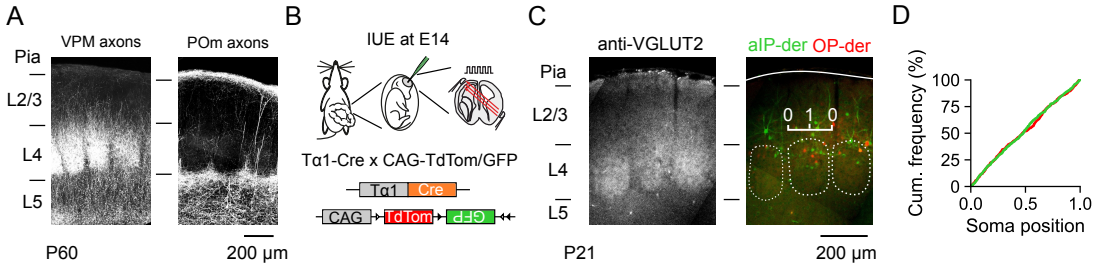


**Figure 4.1: aIP-derived and OP-derived L4 neurons do not differ in terms of soma location. (A)** Thalamic axonal input to S1 from VPM (left) and POm (right), visualised with ChR2-GFP. **(B)** IUE of a T$\alpha$1-Cre and two-colour CAG-FLEx reporter plasmid was used to label aIP-derived (GFP$^+$, green) and OP-derived (tdTomato$^+$, red) L4 neurons in S1. **(C)** VGLUT2 immunohistochemistry at P21 (left) was used to relate the position of labelled soma to the organisation of barrels and septa. A soma position index was defined, with a value of 1 indicating a soma located in the centre of a barrel, and a value of 0 indicating a soma located at the centre point between two barrel boundaries (right). **(D)** There was no significant difference in the distribution of aIP-derived or OP-derived L4 neurons (n = 537 and 351 neurons; p = 0.800, t-test). Data represented as mean ± SEM.

To quantify the soma position of L4 excitatory neurons with respect to barrels and septa, a soma position index was defined, where a value of 1 indicates a soma located at the centre of a barrel, and 0 indicates the midpoint between two barrel boundaries (**Figure 4.1C**; see **Section 2.10**). This index revealed that there was no significant difference in the distribution of soma position between aIP-derived and OP-derived L4 neurons at P21 (**Figure 4.1D**; mean soma position index was

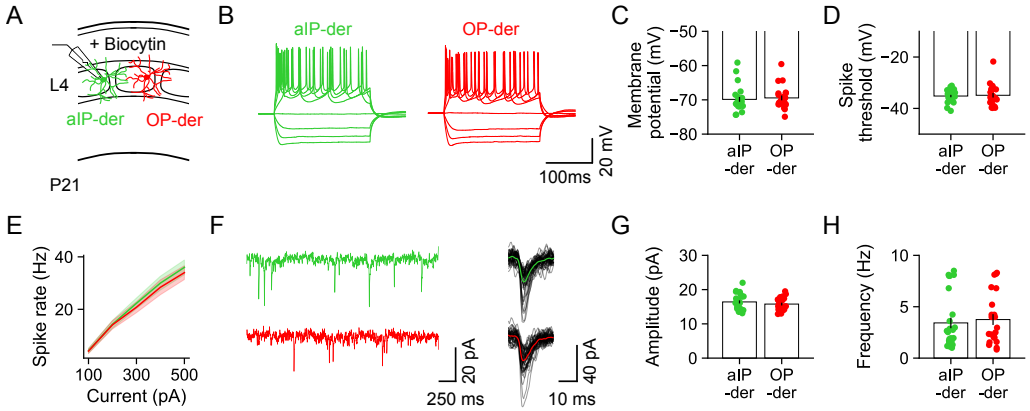


**Figure 4.2: aIP-derived L4 neurons do not exhibit distinct intrinsic electrical or synaptic properties. (A)** *In vitro* patch-clamp recordings were performed in acute brain slices from an aIP-derived and OP-derived L4 neurons. **(B)** Example current clamp recordings from an aIP-derived and an OP-derived L4 neurons in response to current steps. **(C)** Resting membrane potential did not differ between the aIP-derived and OP-derived L4 neurons (n = 25 and 22 neurons; p = 0.241, Mann Whitney U test). **(D)** Spike threshold did not differ between the aIP-derived and OP-derived L4 neurons (n = 25 and 22 neurons; p = 0.440, Mann Whitney U test). **(E)** Spike rate in response to injected current did not differ between the aIP-derived and OP-derived L4 neurons (100, 200, 300, 400 and 500 pA steps; n = 25 and 22 neurons; p = 0.260, Mixed ANOVA). **(F)** Voltage clamp recordings of spontaneous excitatory synaptic currents in an aIP-derived and OP-derived L4 neuron. Composite traces represent the mean of 50 spontaneous events. **(G)** The amplitude of spontaneous excitatory synaptic currents did not differ between aIP-derived and OP-derived L4 neurons (n = 26 and 22 neurons; p = 0.311, t-test). **(H)** The frequency of spontaneous excitatory synaptic currents did not differ between aIP-derived and OP-derived L4 neurons (n=26 and 22 neurons; p = 0.225, Mann Whitney U test). Data represented as mean ± SEM.

0.48 ± 0.01 for aIP-derived and 0.48 ± 0.02 for OP-derived). This suggests that soma position is not lineage-dependent with respect to the progenitor types studied here.

### 4.2.2 aIP-derived L4 neurons do not target the principal barrel with their dendrites

To characterise dendritic morphology, targeted *in vitro* whole-cell patch clamp recordings were made from neighbouring aIP-derived and OP-derived L4 neurons from P21 using a biocytin internal solution (**Figure 4.2A-B**). As reported previously (Ellender et al. 2019), there were no differences in intrinsic electrophysiological properties between aIP-derived and OP-derived L4 neurons including resting membrane potential (**Figure 4.2C**; aIP-derived was -67.74 ± 1.16 mV, OP-derived

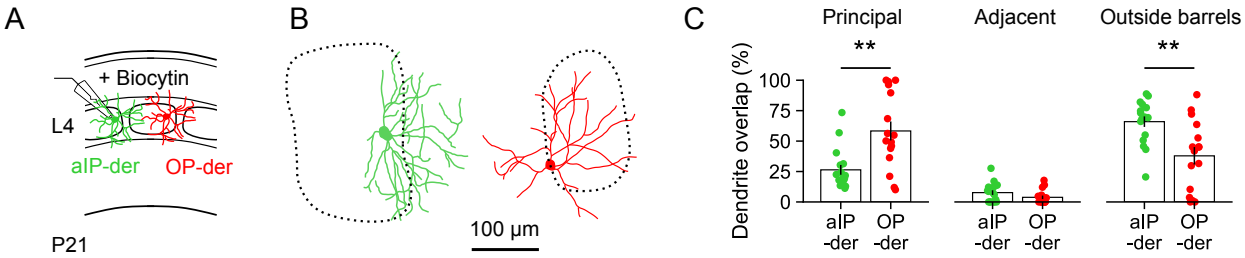


**Figure 4.3: aIP-derived and OP-derived L4 neurons differ in their dendritic morphology. (A)** Biocytin fills from P21 were used to reconstruct the dendritic morphology of aIP-derived and OP-derived L4 neurons. **(B)** Example reconstructions of an aIP-derived (left) and OP-derived (right) L4 neuron. **(C)** Dendrites of OP-derived L4 neurons were more likely to target the principal barrel than aIP-derived L4 neurons (left; n = 17 and 16 neurons; p = 0.005, Mann-Whitney U test). Dendrites of both populations exhibited a similar degree of overlap with the adjacent barrel (middle; n = 17 and 16 neurons; p = 0.145, Mann-Whitney U test). Dendrites of aIP-derived L4 neurons were more likely to target the area outside of barrels, including septa (right; n = 17 and 16 neurons; p = 0.004, Mann-Whitney U test). Data represented as mean ± SEM.

was -70.76 ± 0.99 mV), spike threshold (**Figure 4.2D**; aIP-derived was -35.18 ± 0.46 mV, OP-derived was -34.89 ± 0.88 mV), and spike rate in response to injected current (**Figure 4.2E**; 100, 200, 300, 400 and 500 pA steps; aIP-derived was 4.20 ± 0.98 Hz, 14.30 ± 1.49 Hz, 22.30 ± 2.01 Hz, 30.00 ± 2.65 Hz, and 36.00 ± 2.80 Hz; OP-derived was 4.09 ± 0.90 Hz, 14.09 ± 1.58 Hz, 20.79 ± 2.08 Hz, 28.41 ± 2.85 Hz, 33.98 ± 2.62 Hz), or in the amplitude (**Figure 4.2F-G**; aIP-derived was 16.40 ± 0.45 pA, OP-derived was 15.77 ± 0.40 pA) and frequency (**Figure 4.2H**; aIP-derived was 3.55 ± 0.49 Hz, OP-derived was 3.79 ± 0.39 Hz) of their spontaneous excitatory synaptic inputs.

Biocytin-filled neurons were visualised using Streptavidin, reconstructed, and co-registered to immunofluorescent images of the barrel field (**Figure 4.3A-B**). The overlap of the dendrites with the principal barrel was quantified as a percentage of total dendritic length (see **Section 2.10**). The dendrites of OP-derived L4 neurons tended to target the principal barrel (**Figure 4.3C**; OP-derived overlap with principal barrel was 58.32 ± 7.78 %, adjacent barrel was 3.80 ± 1.44 %, and area outside barrels was 37.88 ± 7.19 %). In contrast, the dendrites of aIP-derived L4 neurons tended to overlap with areas outside of the principal barrel, including septa (**Figure 4.3C**, aIP-derived overlap with principal barrel was 26.38 ± 4.03 %, adjacent barrel was 7.67 ± 1.91 %, and area outside barrels was 65.96

± 4.31 %). Thus, although the distribution of neuronal soma is comparable for the progenitor populations characterised here, a L4 neuron's dendritic morphology appears to reflect the neuron's lineage. One prediction is that the morphology of L4 neurons could influence their integration of inputs from different sources, including the thalamus (Fox et al. 2003; Koralek et al. 1988; Lu and Lin 1993; Wimmer et al. 2010).

### 4.2.3 aIP-derived L4 neurons preferentially sample inputs from higher-order thalamus

In order to test this prediction directly, the same IUE strategy was used at E14 to label aIP-derived and OP-derived neurons with GFP and tdTomato, respectively (**Figure 4.4A**). Once the animal had reached P21, a thalamic injection of an AAV expressing ChR2-GFP was stereotaxically targeted to either VPM or POm (**Figure 4.4A-C**; see **Section 2.4**). This experimental design enabled the preparation of acute brain slices from P60, having allowed sufficient time for the expression of ChR2-GFP, and record from neuronal pairs comprising a $GFP^+$ (aIP-derived) and a $tdTomato^+$ (OP-derived) L4 neuron, whilst using light pulses (1 ms, 473 nm) to selectively activate ChR2-expressing thalamic axons in S1 (see **Section 2.6**).

Activation of VPM axons (**Figure 4.4D**) elicited excitatory postsynaptic potentials (EPSPs) with short onset latencies, consistent with monosynaptic inputs to both populations of L4 neurons (response delay 3.78 ± 0.33 ms in aIP-derived neurons and 3.87 ± 0.40 ms in OP-derived neurons). However, the amplitude of the EPSP in the OP-derived neuron was consistently larger than in the paired aIP-derived neuron (**Figure 4.4E**), such that an index capturing the relative VPM input strength to aIP-derived neurons was significantly below 0.5 (**Figure 4.4F**; 0.32 ± 0.02). Meanwhile, activation of POm axons (**Figure 4.4G**) also elicited EPSPs with short onset latencies, consistent with monosynaptic inputs to both L4 populations (response delay 3.24 ± 0.44 ms in aIP-derived neurons and 3.45 ± 0.51 ms in OP-derived neurons). In contrast to the VPM input however, POm input revealed an amplitude bias in the reverse direction, such that EPSPs were

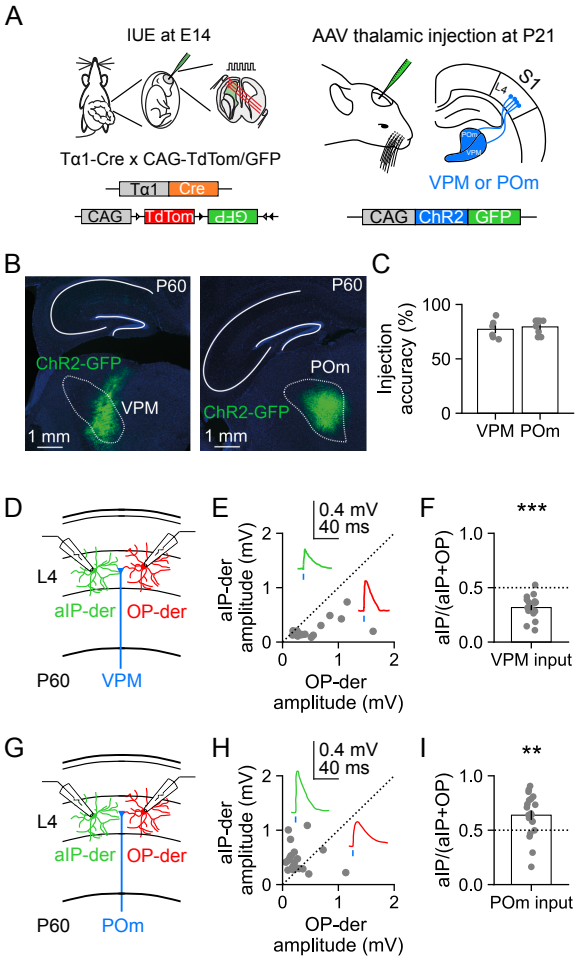


**Figure 4.4: aIP-derived and OP-derived L4 neurons sample thalamic inputs differently.** **(A)** Experimental design for studying thalamic input to lineage-defined L4 neurons. IUE of a T$\alpha$1-Cre and two-colour reporter plasmid was used to label aIP-derived (GFP$^+$, green) and OP-derived (tdTomato$^+$, red) L4 neurons in S1 (left). At P21, the mice received a thalamic injection of an AAV encoding CAG-ChR2-GFP, into either VPM or POm (right). **(B)** Histological analysis at P60 confirmed ChR2-GFP expression in the target thalamic nucleus. **(C)** Injection accuracy was defined as percentage ChR2-GFP expression restricted to the target nucleus. **(D)** To measure VPM input, simultaneous whole-cell recordings were performed from neuronal pairs comprising an aIP-derived and an OP-derived L4 neuron in acute slices from P60, whilst ChR2-GFP$^+$ VPM axons were stimulated with light pulses. **(E)** EPSP peak amplitudes for pairs of aIP-derived and OP-derived neurons in response to light stimulation of VPM axons. **(F)** aIP-derived neurons received weaker VPM input than OP-derived neurons (n = 18 neuron pairs; $p < 0.001$, one sample t-test). **(G)** To measure POm input, simultaneous whole-cell recordings were performed from neuronal pairs comprising an aIP-derived and an OP-derived L4 neuron in acute slices from P60, whilst ChR2-GFP$^+$ POm axons were stimulated. **(H)** EPSP peak amplitudes for pairs of aIP-derived and OP-derived neurons in response to light stimulation of POm axons. **(I)** POm input was biased towards aIP-derived neurons, which received stronger POm input than OP-derived neurons (n = 21 neuron pairs; $p = 0.002$, one sample t-test). Data represented as mean ± SEM.

consistently larger in the aIP-derived neuron than in the paired OP-derived neuron (**Figure 4.4H**), and an index of the relative POm input strength to aIP-derived neurons was significantly above 0.5 (**Figure 4.4I**; 0.64 ± 0.04).

## 4.3 Discussion

In this chapter, a combination of *in utero* labelling, functional anatomy and histological analysis was used to explore how the lineage of S1 L4 excitatory neurons relates to their morphology and sampling of thalamic inputs. The data support the conclusion that the dendritic morphology of L4 excitatory neurons is lineage-dependent, with aIP-derived L4 neurons more likely to target areas outside of barrels with their dendrites compared to OP-derived L4 neurons. Moreover, aIP-derived L4 neurons receive greater input from the higher-order thalamic nucleus, POm, relative to OP-derived L4 neurons.

Morphological studies provided a potential basis for the differential sampling of thalamic inputs in S1, whose anatomical organisation has been well characterised. Reconstructions of progenitor-defined L4 neurons revealed that whilst their soma positions were comparable, the dendrites of individual aIP-derived neurons were more likely to project outside of the principal barrel, when compared to OP-derived L4 neurons. This compliments previous evidence that L4 neurons vary in the degree to which their dendrites target barrels, and that neuronal morphology may be a mechanism through which progenitor-related properties are expressed (Guillamon-Vivancos et al. 2019). It will be interesting to explore whether morphological diversity represents a general mechanism through which progenitors influence the synaptic connectivity of their progeny. This could include future investigations into the relationship between the fine-scale morphology and functional connectivity of neurons derived from other progenitor types, and also how morphology relates to differences in intracortical connectivity, which may also contribute to lineage-dependent response properties (Ellender et al. 2019).

Subsequent experiments combining optogenetic thalamic circuit mapping with paired recordings in L4 confirmed that aIP-derived neurons receive greater levels of input from POm and lower levels of input from VPM, consistent with the idea that the multi-whisker responses of aIP-derived neurons reflect a greater targeting by higher-order thalamus (Fox et al. 2003; Jouhanneau et al. 2014; Kwegyir-Afful

2005). These data reinforce the notion that thalamic inputs from POm to S1 show heterogeneity at a cellular level (Audette et al. 2018; Viaene et al. 2011a; Viaene et al. 2011b; Viaene et al. 2011c) and reveal that lineage is a critical determinant of how individual cortical neurons sample inputs from thalamus.

In summary, this chapter has shown that the dendritic morphology of S1 L4 excitatory neurons is lineage-dependent, and has confirmed that aIP-derived L4 neurons receive greater input from the higher-order thalamic nucleus, POm, relative to OP-derived L4 neurons. **Chapter 5** will investigate a potential mechanism responsible for the establishment of lineage-dependent dendritic morphology, and thus the preferential sampling of higher-order thalamic inputs by aIP-derived L4 neurons.

# Chapter 5

# Lhx2 forms part of a lineage-based mechanism through which the sampling of thalamic inputs is established

## 5.1 Introduction

In S1, the characteristic somatotopic representation of the mystacial pad develops in the first postnatal week (Erzurumlu and Gaspar 2012; Li and Crair 2011; Vitali and Jabaudon 2014; Wu et al. 2011). By the time that mice reach P7, barrels can be identified, and L4 excitatory neurons have begun to orient their dendrites with respect to the organisation of incoming thalamic inputs (Espinosa et al. 2009; Rebsam et al. 2002). This process is known to depend upon the transmission of sensory-evoked activity (Iwasato et al. 2000), which has led to the reported involvement of numerous activity-dependent genes (Ince-Dunn et al. 2006; Kashani et al. 2006; Matsui et al. 2013). However, the mechanisms responsible for coordinating their action are poorly understood. For example, it is not clear how L4 excitatory neurons develop the ability to respond to incoming thalamic inputs, nor why such considerable heterogeneity exists in terms of their dendritic morphology with respect to the organisation of barrels and septa (Egger et al. 2008;

Guillamon-Vivancos et al. 2019; Simons and Woolsey 1984; Staiger 2004).

The transcription factor Lhx2 is predominantly associated with its role as a cortical selector gene (Bulchand et al. 2003; Mangale et al. 2008; Monuki et al. 2001), however it has also been implicated in the development of S1 (Chou and Tole 2019; Pal et al. 2021; Shetty et al. 2013; Wang et al. 2017). Lhx2 is highly expressed in excitatory cortical progenitors during embryonic development, and in postmitotic neurons in the first postnatal weeks (Bulchand et al. 2003; Chou and O'Leary 2013; Hsu et al. 2015; Nakagawa et al. 1999). Notably, the formation of barrels in S1 is impaired when the expression of Lhx2 is reduced in cortical progenitors (Shetty et al. 2013), whereas reduced Lhx2 expression in postmitotic neurons results in an increased proportion of L4 excitatory neurons with dendrites that do not target their principal barrel (Wang et al. 2017). Moreover, recent work has shown that early postnatal expression of Lhx2 can be used to distinguish a specific population of excitatory cortical neurons residing in upper layers, including L4 (Huilgol et al. 2022; Matho et al. 2021). This suggests that Lhx2 expression in L4 is heterogeneous and is consistent with a model in which developing neurons with higher levels of Lhx2 are more likely to target barrels with their dendrites.

**Chapter 4** demonstrated that the dendritic morphology of S1 L4 excitatory neurons is lineage-dependent, and confirmed that aIP-derived L4 neurons receive greater input from the higher-order thalamic nucleus, POm, when compared to OP-derived L4 neurons. This chapter will investigate whether Lhx2 is a key component of this lineage-dependent developmental process. Specifically, the aims of this chapter are as follows:

- To determine whether the expression of Lhx2 is lineage-dependent during postnatal S1 development.
- To develop a strategy for the manipulation of Lhx2 expression.
- To explore the relationship between Lhx2 expression and the higher-order properties of aIP-derived L4 neurons.

## 5.2 Results

### 5.2.1 Expression of Lhx2 in S1 L4 excitatory neurons is lineage-dependent

In order to compare Lhx2 expression between L4 excitatory neuronal populations, animals underwent IUE at E14 with T$\alpha$1-Cre and CAG-FLEx to label aIP-derived and OP-derived neurons with GFP and tdTomato (**Figure 5.1A**), as in **Chapter 4**. Immunohistochemical analysis was then performed at P7, a time point at which L4 circuitry is being established (Erzurumlu and Gaspar 2012; Li and Crair 2011; Vitali and Jabaudon 2014; Wu et al. 2011). Lhx2 expression was quantified as a ratio of the mean pixel intensity (MPI) of the cell body of an aIP-derived L4 neuron over the mean MPI of three neighbouring OP-derived L4 neurons within the same z-plane and within a 100 x 100 µm region of interest (see **Section 2.10**). Lhx2 was found to be differentially expressed by L4 neurons at this age, such that aIP-derived neurons exhibited significantly lower levels of Lhx2 than neighbouring OP-derived neurons (**Figure 5.1B-C**; relative expression was 0.35 ± 0.03). This level of endogenous Lhx2 expression in aIP-derived L4 neurons is consistent with evidence that low Lhx2 levels favour dendrites that do not target a specific barrel, and branch into septal regions outside barrels (Staiger 2004; Wang et al. 2017).

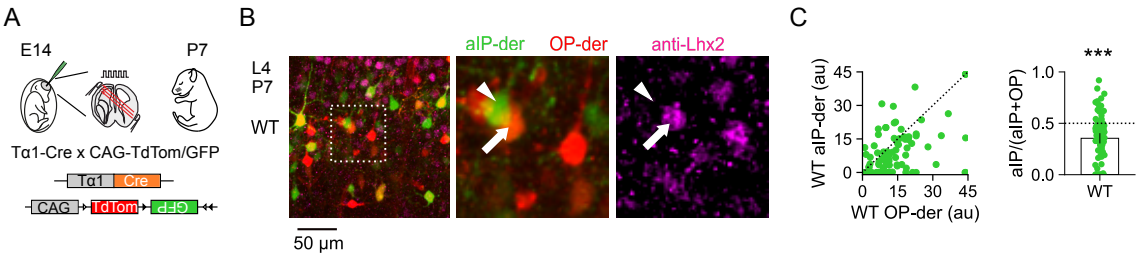


**Figure 5.1: aIP-derived L4 neurons exhibit low levels of Lhx2 expression during postnatal development. (A)** At E14, animals underwent IUE of a T$\alpha$1-Cre and two-colour reporter plasmid to label aIP-derived (GFP$^+$, green) and OP-derived (tdTomato$^+$, red) L4 neurons in S1. **(B)** Immunohistochemistry at P7 revealed lower levels of Lhx2 expression in aIP-derived neurons, compared to higher levels in OP-derived neurons. **(C)** Lhx2 expression levels were quantified (see Methods) in aIP-derived neurons and neighbouring OP-derived neurons within the same field of view (left; au, arbitrary units; values above 45 au have been set to 45 to aid visualisation). Normalized Lhx2 expression was significantly lower in aIP-derived neurons than OP-derived L4 neurons (right; n = 88 neurons, $p < 0.001$, one sample t-test). Data represented as mean ± SEM.

Given that Lhx2 is predominantly associated with circuit development and cell type specification in the first postnatal week (Bulchand et al. 2003; Nakagawa et al. 1999), the quantification of Lhx2 expression levels was repeated at P21, after the completion of barrel formation (**Figure 5.2A**). Interestingly, Lhx2 expression levels had markedly decreased (mean aIP-derived expression at P7 was 10.18 ± 1.16 au, mean aIP-derived expression at P21 was 4.37 ± 1.00 au; mean OP-derived expression at P7 was 14.99 ± 1.23 au, mean OP-derived expression at P21 was 4.47 ± 0.79 au) and statistically significant differences in Lhx2 expression were no longer observed between aIP-derived and OP-derived L4 neurons (**Figure 5.2B-C**; relative expression was 0.40 ± 0.06). This suggests that Lhx2 plays a transient, lineage-dependent, role during the formation of barrel cortex.

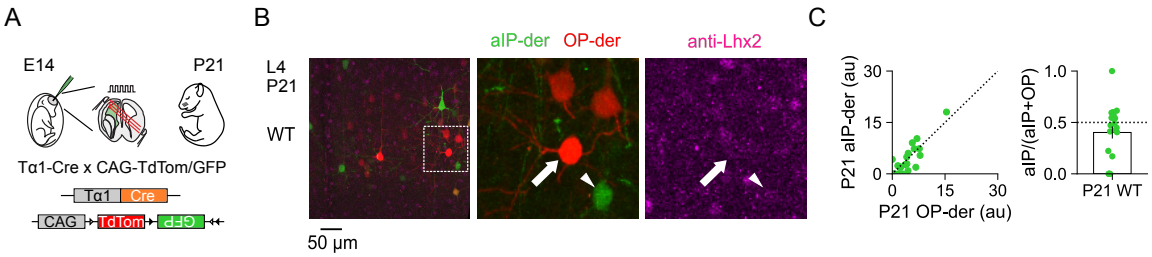


**Figure 5.2: Lhx2 expression has decreased and does not show lineage-dependent differences by P21.** **(A)** At E14, animals underwent IUE of a T$\alpha$1-Cre and two-colour reporter plasmid to label aIP-derived (GFP$^+$, green) and OP-derived (tdTomato$^+$, red) L4 neurons in S1. **(B)** Immunohistochemistry at P21 revealed low levels of Lhx2 expression in both aIP-derived and OP-derived neurons (contrast levels enhanced to aid visualisation). **(C)** Lhx2 expression levels were quantified in aIP-derived neurons and neighbouring OP-derived neurons within the same field of view (left; au, arbitrary units). Normalized Lhx2 expression was not different in aIP-derived and OP-derived L4 neurons at P21 (right; 0.40 ± 0.06; n = 20 neurons; p = 0.230, one sample Wilcoxon test against a median of 0.5). Data represented as mean ± SEM.

### 5.2.2 A tool to increase the expression of Lhx2 in electroporated L4 neurons

To test whether Lhx2 expression forms part of a lineage-based mechanism that determines how L4 neurons receive thalamic inputs, it was first necessary to develop a tool to manipulate the expression of Lhx2. A CAG-Lhx2 construct was developed, where the expression of Lhx2 is under the control of the CAG promoter (**Figure 5.3A**, see **Section 2.2**). IUE at E14 with CAG-Lhx2, in addition to T$\alpha$1-Cre and

CAG-FLEx, allowed the efficacy of the Lhx2 manipulation to be assessed. Lhx2 expression levels in aIP-derived L4 neurons that had undergone IUE of CAG-Lhx2 (Lhx2 aIP-derived) were considerably higher than wild-type aIP-derived (WT aIP-derived) neurons at P7 (**Figure 5.3B-C**; mean WT expression was 10.18 ± 1.16 au, mean Lhx2 expression was 248.57 ± 19.51 au), and Lhx2 expression between the electroporated aIP-derived and OP-derived L4 neurons within the same tissue was normalised (**Figure 5.3B-C**; relative expression was 0.50 ± 0.02).

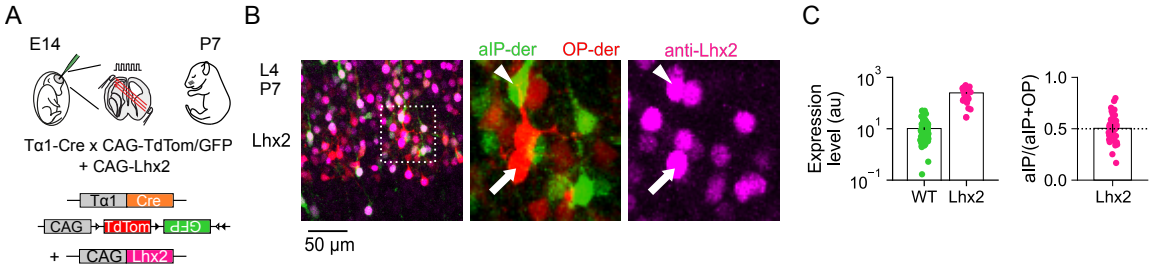


**Figure 5.3: An overexpression construct increases Lhx2 levels in electroporated L4 neurons.** **(A)** To raise Lhx2 levels in aIP-derived L4 neurons, a CAG-Lhx2 overexpression plasmid was delivered with T$\alpha$1-Cre and a two-colour reporter plasmid by IUE at E14. **(B)** Immunohistochemistry at P7 revealed similarly high levels of Lhx2 expression in aIP-derived neurons and OP-derived electroporated neurons. **(C)** Quantification confirmed increased levels in Lhx2-overexpressing (Lhx2) aIP-derived L4 neurons compared to WT aIP-derived L4 neurons (left; data from **Figure 5.1**). Within the Lhx2 electroporated tissue, expression levels were similar in the aIP-derived and OP-derived electroporated L4 neurons, such that there was no difference in relative expression (right; n = 40 neurons, p = 0.850, one sample t-test). Data represented as mean ± SEM, n = neurons.

Previous work has reported that reduced Lhx2 expression during embryonic development can cause impaired neuronal migration (Bulchand et al. 2003; Chou et al. 2009; Mangale et al. 2008; Monuki et al. 2001). To investigate any possible migratory effects associated with increased levels of Lhx2 expression, the soma location of WT aIP-derived and Lhx2 aIP-derived L4 neurons was compared at P21 (**Figure 5.4A**). The soma of WT aIP-derived and Lhx2 aIP-derived L4 neurons were located at similar distances from pia (**Figure 5.4B**; WT distance was 445.66 ± 16.04 $\mu$m, Lhx2 distance was 459.77 ± 32.80 $\mu$m) and occupied similar depths within L4 (**Figure 5.4C**; WT depth was 50.64 ± 2.14 %, Lhx2 depth was 43.32 ± 4.04 %). This suggests that there are no discernible effects of increased Lhx2 expression upon the migration of S1 L4 excitatory neurons.

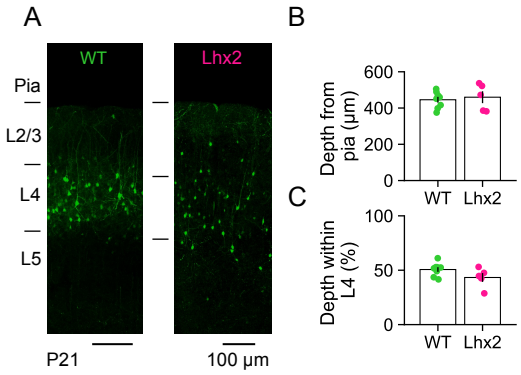


**Figure 5.4: Increased Lhx2 expression levels do not affect the migration of aIP-derived L4 neurons.** **(A)** WT aIP-derived neurons at P21, resulting from IUE of the T$\alpha$1-Cre plasmid and reporter plasmid at E14.5 (left). Lhx2 aIP-derived neurons at P21, resulting from IUE of the T$\alpha$1-Cre plasmid, reporter plasmid and a CAG-Lhx2 plasmid to increase Lhx2 expression levels (right). **(B)** The soma of WT and Lhx2 aIP-derived neurons were located at similar distances from pia (n= 8 and 5 animals; p = 0.670, t-test). **(C)** WT and Lhx2 neurons occupied similar depths within L4 (n = 8 and 5 animals; p = 0.110, t-test). Data represented as mean ± SEM.

### 5.2.3 Increased Lhx2 expression alters dendritic morphology

To characterise the dendritic morphology of Lhx2 aIP-derived L4 neurons, targeted *in vitro* whole-cell patch clamp recordings were performed from P21 using a biocytin internal solution (**Figure 5.5A-B**), as in **Chapter 4**. Lhx2 aIP-derived L4 neurons exhibited subtle differences in their intrinsic electrophysiological properties compared to WT aIP-derived L4 neurons, namely a slightly depolarised membrane potential (**Figure 5.5C**; WT was -69.86 ± 0.71 mV, Lhx2 was -67.74 ± 1.16 mV). However, there were no differences in spike threshold (**Figure 5.5D**; WT was -35.18 ± 0.46 mV, Lhx2 was -34.60 ± 0.84 mV), or spike rate in response to injected current (**Figure 5.5E**; 100, 200, 300, 400 and 500 pA steps; WT was 4.20 ± 0.98 Hz, 14.30 ± 1.49 Hz, 22.30 ± 2.01 Hz, 30.00 ± 2.65 Hz, 36.00 ± 2.80 Hz; Lhx2 was 7.89 ± 1.27 Hz, 19.73 ± 1.67 Hz, 29.47 ± 2.09 Hz, 37.37 ± 2.95 Hz, 37.50 ± 3.39 Hz). Moreover, the two populations exhibited comparable levels of spontaneous activity (**Figure 5.5F**), including the amplitude (**Figure 5.5G**; WT was 16.40 ± 0.45 pA, Lhx2 was 15.47 ± 0.25 pA), and frequency (**Figure 5.5H**; WT was 3.43 ± 0.52 Hz, Lhx2 was 3.55 ± 0.49 Hz) of excitatory synaptic inputs.

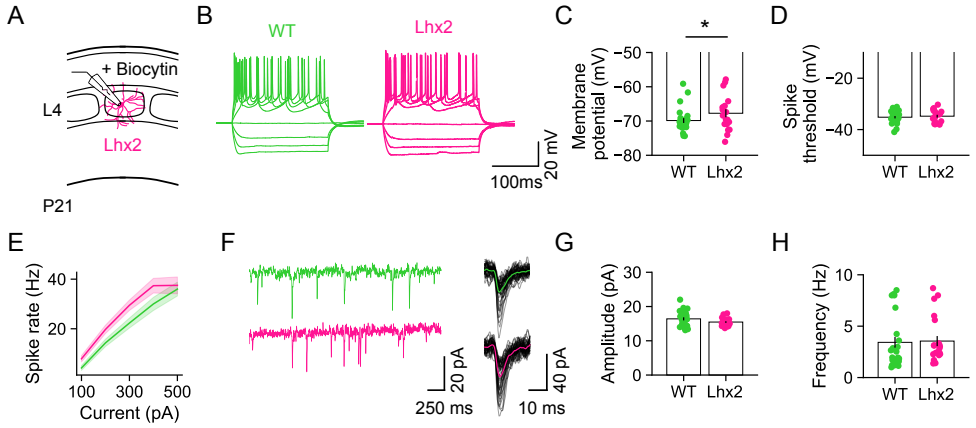


**Figure 5.5: Effects of increased Lhx2 levels on intrinsic electrical and synaptic properties of aIP-derived L4 neurons.** **(A)** *In vitro* patch-clamp recordings were performed in acute brain slices from Lhx2 aIP-derived neurons and compared to WT aIP-derived neurons (data from **Figure 4.2**). **(B)** Example current clamp recordings from a WT and Lhx2 aIP-derived L4 neuron in response to current steps. **(C)** Resting membrane potential was slightly more depolarised in Lhx2 aIP-derived neurons compared to WT (n = 25 and 19 neurons; p = 0.042, Mann Whitney U). **(D)** Spike threshold was not statistically different between WT and Lhx2 aIP-derived neurons (n = 25 and 14 neurons; p = 0.509, t-test). **(E)** Spike rate in response to injected current was not statistically different between WT and Lhx2 aIP-derived neurons (100, 200, 300, 400 and 500 pA steps; n = 25 and 19 neurons; p = 0.067, Mixed ANOVA). **(F)** Example voltage clamp recordings of spontaneous excitatory synaptic currents in a WT and an Lhx2 aIP-derived L4 neuron. **(G)** The amplitude of spontaneous excitatory synaptic currents was not statistically different between WT and Lhx2 aIP-derived neurons (n = 26 and 21 neurons; p = 0.094, t-test). **(H)** The frequency of spontaneous excitatory synaptic currents was not statistically different between WT and Lhx2 aIP-derived neurons (n = 26 and 21 neurons; p = 0.182, Mann Whitney U). Data represented as mean ± SEM.

Biocytin-filled neurons were visualised using Streptavidin, reconstructed and co-registered to immunofluorescence images of the barrel field (**Figure 5.6A-B**), as in **Chapter 4**. The overlap of the dendrites with the principal barrel was quantified as a percentage of total dendritic length (see **Section 2.10**). The dendrites of Lhx2 aIP-derived L4 neurons overlapped significantly more with the principal barrel, and significantly less with areas outside barrels compared to WT aIP-derived L4 neurons (**Figure 5.6C**; WT overlap with principal barrel was 26.38 ± 4.03 %, adjacent barrel was 7.67 ± 1.91 %, and area outside barrels was 65.96 ± 4.31 %; Lhx2 overlap with principal barrel was 55.63 ± 7.81 %, adjacent barrel was 9.10 ± 3.25 %, and area outside barrels was 47.98 ± 7.88 %). These data support the idea that Lhx2 is part of a lineage-based mechanism by which L4 neurons acquire different thalamic inputs through their dendritic morphologies.

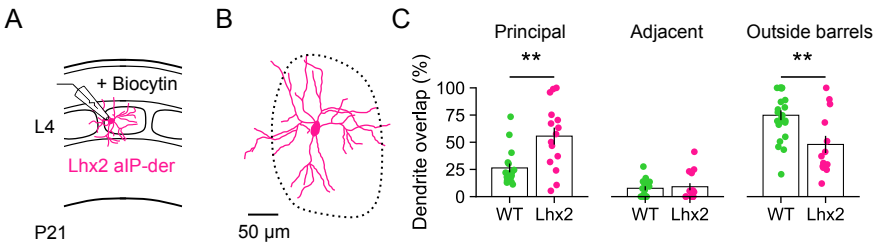


**Figure 5.6: Increased Lhx2 levels in aIP-derived neurons alters dendritic morphology.** **(A)** Biocytin fills from P21 were used to reconstruct the dendritic morphology of Lhx2 aIP-derived L4 neurons. **(B)** Example reconstruction of an Lhx2 aIP-derived L4 neuron. **(C)** Dendrites of Lhx2 aIP-derived L4 neurons were more likely to target the principal barrel compared to WT (left; WT data from **Figure 4.3**; n = 17 and 15 neurons; p = 0.005, Mann-Whitney U test). Dendrites of both populations exhibited a similar degree of overlap with the adjacent barrel (middle; n = 17 and 15 neurons; p = 0.727, Mann-Whitney U test). Dendrites of Lhx2 aIP-derived L4 neurons were less likely to target the area outside of barrels, including septa, compared to WT (right; n = 17 and 15 neurons; p = 0.009, Mann-Whitney U test). Data represented as mean ± SEM.

### 5.2.4 Increased Lhx2 expression abolishes lineage-dependent sampling of thalamic inputs

To test this prediction directly, the same IUE strategy was combined with the optogenetic circuit mapping of thalamic inputs used in **Chapter 4**. IUE was performed at E14 and once the animals had reached P21, they received a thalamic injection of an AAV expressing ChR2-GFP into either VPM or POm (**Figure 5.7A**). Whole cell patch clamp recordings from pairs of Lhx2 aIP-derived and Lhx2 OP-derived L4 neurons were then combined with light activation of ChR2-expressing thalamic axons in acute brain slices from P60. Activation of VPM or POm axons elicited EPSPs with short onset latencies (VPM response delay was 3.85 ± 0.35 ms and 3.4 ± 0.33 ms in Lhx2 aIP-derived and OP-derived, respectively; POm response delay was 3.75 ± 0.47 ms and 3.88 ± 0.46 ms in Lhx2 aIP-derived and OP-derived, respectively). However, unlike in the WT condition (see **Chapter 4**), EPSP amplitudes were comparable between Lhx2 aIP-derived L4 neurons and Lhx2 OP-derived L4 neurons, suggesting that the sampling of thalamic inputs was no longer biased under conditions of increased Lhx2 expression. VPM-evoked EPSP amplitudes were not different for paired Lhx2 aIP-derived and OP-derived L4 neurons (**Figure 5.7B-D**; bias index of 0.53 ± 0.04) and POm-evoked EPSP amplitudes were not

different for paired Lhx2 aIP-derived and OP-derived L4 neurons (**Figure 5.7E-G**; bias index of 0.52 ± 0.05). Taken together, these data suggest that increasing Lhx2 expression during development abolishes the lineage-dependent sampling of thalamic inputs by L4 neurons. For aIP-derived L4 neurons, this is characterised by a reduction in the relative levels of higher-order thalamic inputs from POm.

### 5.2.5 Identifying Lhx2-overexpressing aIP-derived L4 neurons *in vivo*

To establish the functional consequences of the relative reduction in higher-order POm input to Lhx2 aIP-derived L4 neurons, their response properties were characterised *in vivo*. Animals underwent IUE at E14 with T$\alpha$1-Cre, floxed ChR2-YFP and CAG-Lhx2, to enable individual Lhx2 aIP-derived L4 neurons to be identified by optotagging (**Figure 5.8A**, see **Section 2.2**). IUE was targeted to the region of the VZ that gives rise to S1 excitatory neurons such that when animals were allowed to survive postnatally, Lhx2 aIP-derived (ChR2-YFP$^+$) neurons could be observed in S1 L4 (**Figure 5.8B**). As in **Chapter 3**, *in vivo* extracellular recordings of excitatory S1 L4 neurons were performed from excitatory S1 L4 neurons (**Figure 5.8C**). Light pulses (10 ms, 473 nm) were delivered to the recording site to selectively activate and identify Lhx2 aIP-derived L4 neurons, and responses to deflections of the PW and AW were investigated. RS neurons were distinguished from FS neurons based on the waveform properties of single units (**Figure 5.8D**; FS trough-to-peak was 0.31 ms ± 0.01, RS trough-to-peak was 0.99 ms ± 0.01). Neurons that exhibited reliable, short latency (< 5 ms) light-evoked responses were considered to be directly activated by ChR2 and classed as Lhx2 aIP-derived (**Figure 5.8E-F**). Those that exhibited a longer latency, or no, light-evoked response, were classed as OP-derived in these recordings. As expected, the light-evoked spiking response of Lhx2 aIP-derived L4 neurons was greater than that of OP-derived L4 neurons recorded in the same animals (**Figure 5.8G-H**; Lhx2 aIP-derived spike rate was 141.89 Hz ± 41.09, OP-derived spike rate was 37.54 Hz

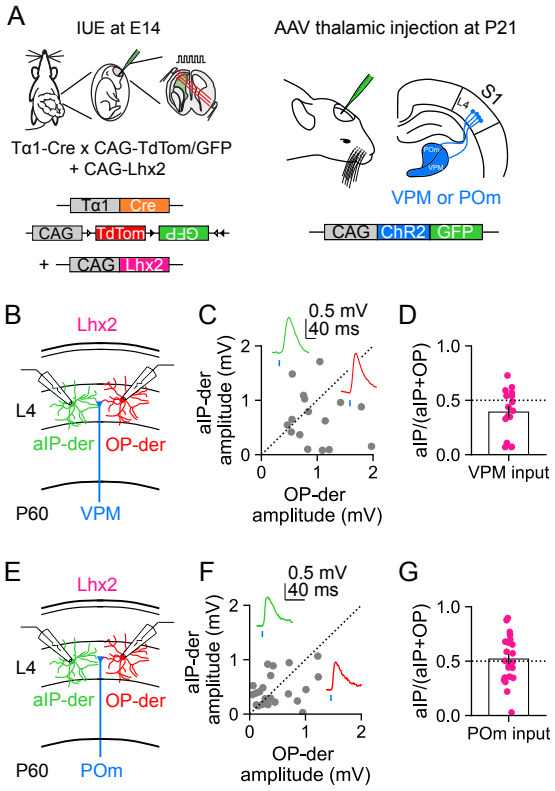


**Figure 5.7: Increased Lhx2 levels in aIP-derived L4 neurons disrupts higher-order thalamic inputs.** **(A)** IUE of a T$\alpha$1-Cre and reporter plasmid to label aIP-derived (GFP$^+$, green) and OP-derived (TdTom$^+$, red) L4 neurons, was combined with a CAG-Lhx2 plasmid to increase Lhx2 expression levels. At P21, the mice received a thalamic injection of an AAV encoding CAG-ChR2-GFP, into either VPM or POm. **(B)** To measure VPM input, simultaneous whole cell recordings were performed from Lhx2 aIP-derived and Lhx2 OP-derived L4 neuronal pairs in acute slices from P60, whilst ChR2-GFP$^+$ VPM axons were stimulated with light pulses. **(C)** EPSP peak amplitudes for pairs of Lhx2 aIP-derived and Lhx2 OP-derived L4 neurons in response to light stimulation of VPM axons. **(D)** No statistically significant bias was detected in the strength of VPM input (n = 18 neuron pairs; p = 0.060, one sample t-test). **(E)** To measure POm input, simultaneous whole cell recordings were performed from Lhx2 aIP-derived and Lhx2 OP-derived L4 neuronal pairs in acute slices from P60, whilst ChR2-GFP$^+$ POm axons were stimulated with light pulses. **(F)** EPSP peak amplitudes for pairs of Lhx2 aIP-derived and Lhx2 OP-derived L4 neurons in response to light stimulation of POm axons. **(G)** No statistically significant bias was detected in the strength of POm input (n = 22 neuron pairs; p = 0.687, one sample t-test). Data represented as mean ± SEM.

± 10.11). Interestingly, the spontaneous spike rate of Lhx2 aIP-derived L4 neurons was slightly higher than that of OP-derived L4 neurons (**Figure 5.8I**; Lhx2 aIP-derived was 20.73 Hz ± 5.24, OP-derived was 9.41 Hz ± 1.87), consistent with the somewhat more depolarised resting membrane potential of Lhx2 aIP-derived L4 neurons observed *in vitro* (**Figure 5.5C**).

### 5.2.6 Increased Lhx2 expression abolishes lineage-dependent sensory response properties *in vivo*

To examine the effect of increased Lhx2 expression, the whisker-evoked responses of the optotagged Lhx2 aIP-derived L4 neurons were compared with those of optotagged WT aIP-derived L4 neurons. The data from WT aIP-derived L4 neurons revealed that these neurons tend to exhibit multi-whisker responses, exhibiting similar levels of responsiveness to the PW and the AW (**Figure 5.9A**). In contrast, Lhx2 aIP-derived L4 neurons exhibited robust responses to the PW, but responses to AW deflection were greatly reduced (**Figure 5.9A**). As such, Lhx2 aIP-derived L4 neurons exhibited significantly higher SI values than WT aIP-derived L4 neurons in response to both single and train deflections of the whiskers (**Figure 5.9B-D**; single deflection mean SI was 0.55 ± 0.05 for WT and 0.76 ± 0.02 for Lhx2 aIP-derived neurons; train deflection mean SI was 0.55 ± 0.05 for WT and 0.78 ± 0.06 for Lhx2 aIP-derived neurons). Therefore, increased Lhx2 expression disrupts the multi-whisker response properties that are normally associated with aIP-derived L4 neurons, consistent with a reduction in how these neurons sample higher-order thalamic inputs.

To explore whether temporal differences in the whisker-evoked responses could contribute to the differences in the SI of Lhx2 aIP-derived and WT aIP-derived L4 neurons, a series of measures were calculated to characterise the temporal response profile Lhx2 aIP-derived L4 neurons following whisker deflection, as in **Chapter 3**. Response latency, estimated as the time to first spike, was shorter following PW deflection compared to AW deflection for both Lhx2 aIP-derived and WT aIP-derived L4 neurons (**Figure 5.10A**; WT aIP-derived PW latency was 8.58 ±

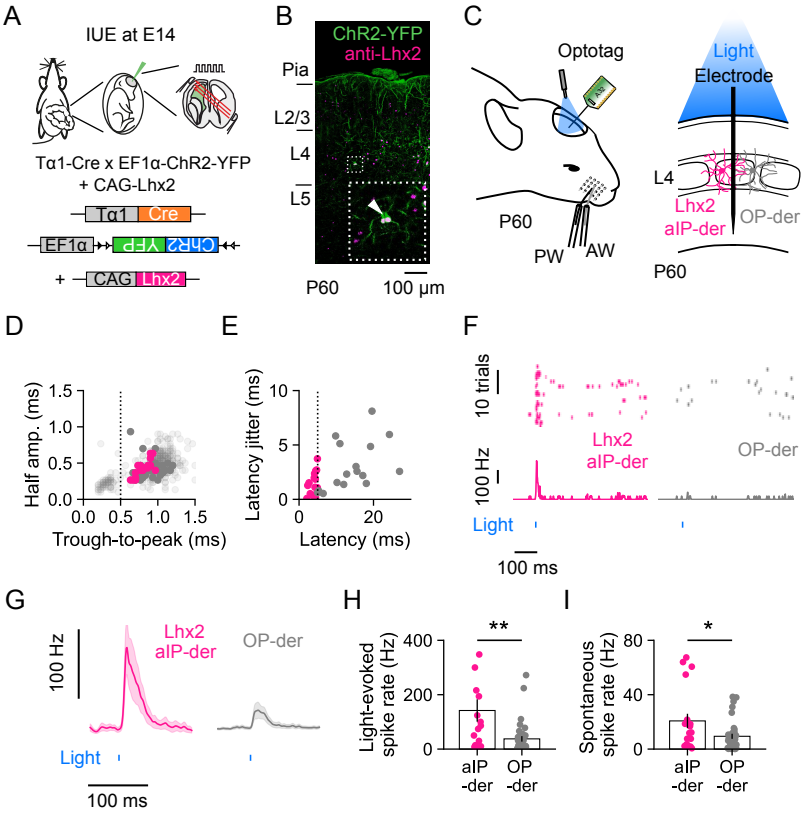


**Figure 5.8: Identification of Lhx2 aIP-derived L4 neurons from extracellular recordings.** **(A)** Animals underwent IUE of a T$\alpha$1-Cre, a floxed ChR2-YFP, and a CAG-Lhx2 plasmid at E14. **(B)** ChR2-YFP$^+$, Lhx2 aIP-derived L4 neurons could be observed at P60. **(C)** The spiking activity of optotagged Lhx2 aIP-derived L4 neurons and neighbouring (non-optotagged) OP-derived L4 neurons was recorded in response to deflection of the PW or AW. **(D)** RS neurons were distinguished from FS neurons based on the waveform properties of single units. A trough-to-peak time of 0.5 ms was used as the separation criterion. Filled circles correspond to excitatory neurons included in **Figures 5.8, 5.9, 5.10, and 5.11**. **(E)** Lhx2 aIP-derived (i.e., ChR2-YFP$^+$) L4 neurons were distinguished from OP-derived L4 neurons based on spike times in response to repeated light pulses. A mean light-evoked spike latency of 5 ms was used as the separation criterion. **(F)** Light-evoked spiking of an individual Lhx2 aIP-derived L4 neuron (left) and OP-derived L4 neuron (right). **(G)** Mean light-evoked spiking response of a population of Lhx2 aIP-derived and OP-derived L4 neurons. Shading indicates SEM around the mean. **(H)** Light-evoked spiking was higher in Lhx2 aIP-derived compared to OP-derived L4 neurons (n = 19 and 35 neurons; p = 0.004, Mann Whitney U test). **(I)** Spontaneous spike rates were higher in Lhx2 aIP-derived compared to OP-derived L4 neurons (n = 19 and 35 neurons; p = 0.025, Mann Whitney U test). Data represented as mean ± SEM.

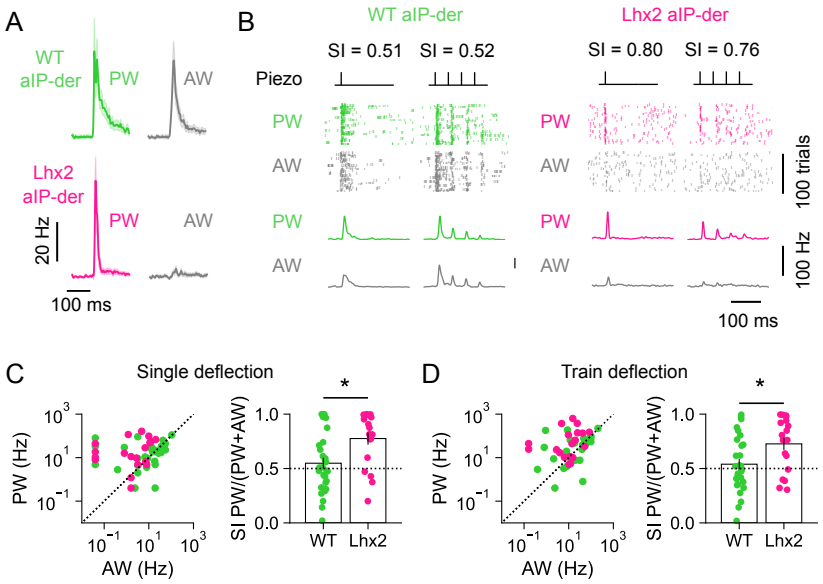


**Figure 5.9: Increased Lhx2 levels in aIP-derived L4 neurons disrupt multi-whisker response properties.** **(A)** Mean responses of WT aIP-derived L4 neurons (data from **Figure 3.3**) and Lhx2 aIP-derived L4 neurons following a single deflection of the PW (left) or AW (right). Shading indicates SEM around the mean. **(B)** Spiking of an individual WT aIP-derived neuron (left) and an Lhx2 aIP-derived neuron (right) over 100 trials of either a single deflection (inner left) or trains of deflection (inner right) of the PW or AW. **(C)** Responses of individual WT and Lhx2 aIP-derived L4 neurons to single deflection of the PW and AW (left), and the distribution of corresponding SI values (right). Compared to WT, Lhx2 aIP-derived L4 neurons showed greater selectivity for the PW and relatively less responsivity to the AW (n = 29, 19 neurons; p = 0.010, Mann Whitney U test). **(D)** Responses to train deflection of the PW and AW (left), and corresponding SI values (right). Compared to WT, Lhx2 aIP-derived L4 neurons showed greater selectivity for the PW and relatively less responsivity to the AW (n = 29, 19 neurons; p = 0.024, Mann Whitney U test). Data represented as mean ± SEM.

0.58 ms, and AW latency was 10.80 ± 0.87 ms; Lhx2 aIP-derived PW latency was 7.41 ± 0.28 ms, and AW latency was 10.19 ± 1.07 ms). The delay between PW and AW first spike was not different between the two populations (**Figure 5.10B**; WT aIP-derived delay was 2.29 ± 1.03 ms, Lhx2 aIP-derived delay was 1.03 ± 1.18 ms). Similarly, the peak response latency was shorter following PW deflection compared to AW deflection for both aIP-derived and OP-derived neurons (**Figure 5.10C**; WT aIP-derived PW peak latency was 13.63 ± 0.74 ms, and AW peak latency was 15.22 ± 0.47 ms; Lhx2 aIP-derived PW peak latency was 12.42 ± 0.62 ms, and AW peak latency was 15.47 ± 0.84 ms). The delay between PW and AW peak latency was indistinguishable between the two populations (**Figure 5.10D**; WT aIP-derived peak delay was 2.04 ± 0.64 ms, Lhx2 aIP-derived peak

delay was 3.05 ± 1.06 ms). Therefore, the temporal response properties following whisker deflection are comparable for Lhx2 aIP-derived and WT aIP-derived L4 neurons, with AW responses exhibiting a consistent delay relative to PW responses, in keeping with previous work (Armstrong-James et al. 1992; Armstrong-James and Fox 1987; Diamond et al. 1992), and data shown in **Chapter 3**.

To further characterise the differences in SI between Lhx2 aIP-derived and WT aIP-derived L4 neurons, the SI was recalculated at different time windows following single whisker deflections (**Figure 5.10E-H**). In the 0–10 ms immediately following whisker deflection, WT aIP-derived neurons were selective for the PW (**Figure 5.10F**; WT aIP-derived $T^{0-10}$ mean SI was 0.66 ± 0.05). However, at 10–20 ms following whisker deflection, WT aIP-derived neurons were no longer selective for the PW (**Figure 5.10F**; WT aIP-derived $T^{10-20}$ mean SI was 0.55 ± 0.05), which was consistent with the SI calculated over the full 50 ms response window (**Figure 5.10F**; WT aIP-derived $T^{0-50}$ mean SI was 0.55 ± 0.05). In contrast, Lhx2 aIP-derived L4 neurons were selective for the PW in 0-10 ms following whisker deflection (**Figure 5.10H**; Lhx2 aIP-derived $T^{0-10}$ mean SI was 0.65 ± 0.07), they remained selected for the PW at 10–20 ms (**Figure 5.10H**; Lhx2 aIP-derived $T^{10-20}$ mean SI was 0.77 ± 0.04), and over the full 50 ms response window (Figure 5.10H; Lhx2 aIP-derived $T^{0-50}$ mean SI was 0.76 ± 0.02).

Taken together, these data suggest that the temporal properties of whisker-evoked responses do not differ between Lhx2 aIP-derived and WT aIP-derived L4 neurons. Rather, the data support the conclusion that the differences in SI reflect the relative strength of inputs to the two neuronal populations, consistent with the observation that higher-order inputs are disrupted as a result of increased Lhx2 expression in aIP-derived L4 neurons.

### 5.2.7 Increased Lhx2 expression abolishes lineage-dependent population coupling

To investigate whether increased Lhx2 expression in aIP-derived neurons affects the degree of recurrent excitatory connectivity they receive relative to OP-derived

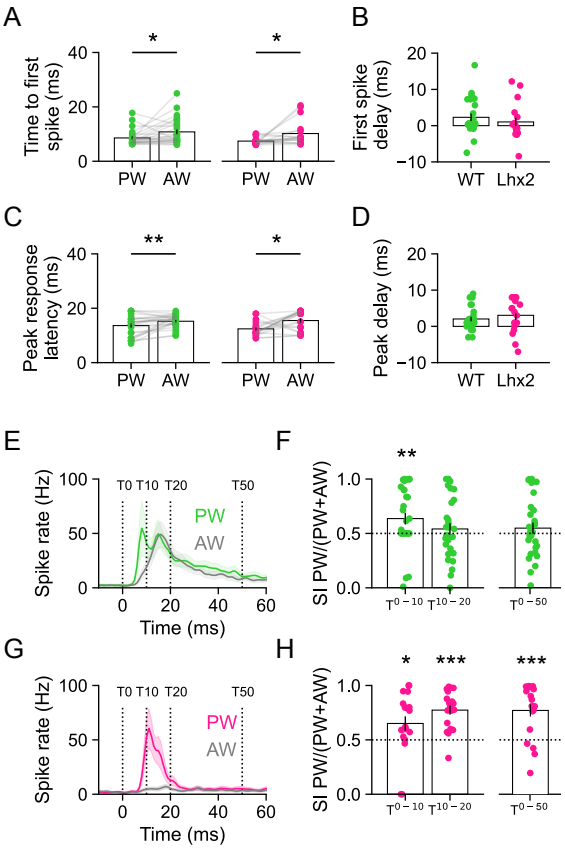


**Figure 5.10: Increased Lhx2 levels in aIP-derived L4 neurons does not affect temporal response properties.** **(A)** Time to first spike was faster following PW deflection than AW deflection for both WT aIP-derived (left; data from **Figure 3.5**; n = 29 neurons; p = 0.049, Wilcoxon signed-rank test) and Lhx2 aIP-derived L4 neurons (right; n = 19 neurons; p = 0.034, Wilcoxon signed-rank test). **(B)** The relative delay between PW and AW time to first spike was similar for WT aIP-derived and Lhx2 aIP-derived L4 neurons (n = 29 and 19 neurons; p = 0.423, t-test). **(C)** Peak response latency was faster following PW deflection than AW deflection for both aIP-derived (left; n = 29 neurons; p = 0.004, Wilcoxon signed-rank test) and OP-derived L4 neurons (right; n = 19 neurons; p = 0.008, Wilcoxon signed-rank test). **(D)** The relative delay between PW and AW peak latency was similar for aIP-derived and OP-derived L4 neurons (n = 29 and 19 neurons; p = 0.395, t-test). **(E)** Mean spiking responses of aIP-derived L4 neurons following single PW and AW deflection. $T^{0-50}$ indicate windows for SI calculation. Shading indicates SEM around the mean. **(F)** WT aIP-derived L4 neurons were selective for the PW between $T^{0-10}$ (n = 29 neurons; p = 0.008, Wilcoxon signed-rank against a median of 0.5), but not between $T^{10-20}$ (n = 29 neurons; p = 0.424, Wilcoxon signed-rank against a median of 0.5), consistent with SI calculated between $T^{0-50}$ (n = 29 neurons; p = 0.343, one-sample t-test). **(G)** Mean spiking responses of OP-derived L4 neurons following single PW and AW deflection. $T^{0-50}$ indicate windows for SI calculation. Shading indicates SEM around the mean. **(H)** OP-derived L4 neurons were selective for the PW between $T^{0-10}$ (n = 26 neurons; p = 0.025, Wilcoxon signed-rank against a median of 0.5), and $T^{10-20}$ (n = 26 neurons; p < 0.001, Wilcoxon signed-rank against a median of 0.5), consistent with SI calculated between $T^{0-50}$ (data from Figure 5.9; n = 29 neurons; p < 0.001 , one-sample t-test). Data represented as mean ± SEM.

neurons, their population coupling was calculated, as in **Chapter 3**. In contrast to WT, where aIP-derived L4 neurons were more strongly coupled to population MUA than OP-derived L4 neurons, the coupling of Lhx2 aIP-derived neurons was comparable to that of OP-derived neurons (**Figure 5.11A-B**; in WT animals aIP-derived coupling was 1.83 ± 0.24 Hz, and OP-derived coupling was 1.61 ± 0.29 Hz; in Lhx2 animals aIP-derived coupling was 1.69 ± 0.42 Hz, and OP-derived coupling was 1.69 ± 0.34 Hz). This suggests that increased Lhx2 expression abolishes lineage-dependent differences in population coupling and supports the idea that long-range excitatory inputs from the higher-order thalamus contribute to the population coupling of cortical neurons.

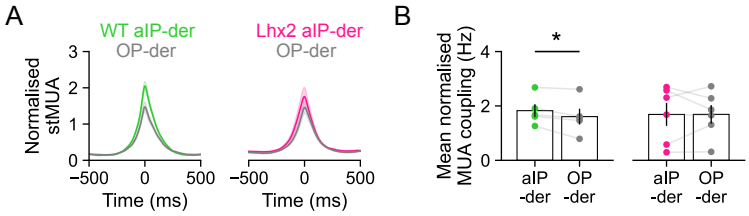


**Figure 5.11: Increased Lhx2 levels in aIP-derived L4 neurons alters population coupling.** **(A)** Mean normalised stMUA of WT (left) and Lhx2 (right) aIP-derived L4 neurons and OP-derived L4 neurons (data from **Figure 3.6**). MUA coupling corresponds to the height of the stMUA at zero time lag. Shading indicates SEM around the mean. **(B)** WT aIP-derived L4 neurons were more strongly coupled to population MUA compared to OP-derived L4 neurons (n = 5 animals; p = 0.041, t-test), whereas Lhx2 aIP-derived neurons were not (n = 5 animals; p = 0.993, t-test). Data represented as mean ± SEM.

## 5.3 Discussion

In this chapter, quantitative immunohistochemistry was used together with *in utero* labelling and *in vitro* and *in vivo* electrophysiology to investigate the expression of Lhx2 as a possible mechanism through which lineage-dependent properties of S1 L4 excitatory neurons are established. The data support the conclusion that Lhx2 forms part of a lineage-based mechanism that influences the dendritic morphology of L4 excitatory neurons, and thus the thalamic inputs that they receive.

Lhx2 is perhaps best known for its role in cortical fate specification early in embryonic development (Bulchand et al. 2003; Mangale et al. 2008; Monuki et al. 2001). However, it has also been shown to play an important role in the formation of barrels, and the development of targeted dendritic morphology in L4 of S1 (Chou and Tole 2019; Pal et al. 2021; Shetty et al. 2013; Wang et al. 2017). Here, Lhx2 expression in L4 was found to vary in a manner that reflects a cell's lineage. During the first week of postnatal cortical development, aIP-derived L4 neurons exhibited lower Lhx2 protein levels than OP-derived L4 neurons. This is consistent with a model in which low Lhx2 expression is associated with neurons that exhibit greater dendritic projections outside of the principal barrel (Wang et al. 2017). In agreement with previous work, Lhx2 expression had decreased by P21 (Bulchand et al. 2003; Chou and O'Leary 2013; Hsu et al. 2015; Nakagawa et al. 1999). Additionally, lineage-dependent differences were no longer observed, suggesting that the lineage-dependent expression of Lhx2 plays a transient role during the period of barrel formation in S1. The extent to which Lhx2 might interact with activity-dependent process that occur in the second postnatal week (e.g., the formation of lateral connectivity within the cortex; Wen and Barth 2011), remains to be established.

In order to investigate whether low levels of Lhx2 expression are responsible for establishing the higher-order properties of aIP-derived L4 neurons, a new construct was developed to experimentally increase the expression of Lhx2. Experimentally increasing Lhx2 in aIP-derived L4 neurons resulted in dendrites that no longer

projected outside of the principal barrel, abolished WT differences in how neurons sampled thalamic inputs, and resulted in aIP-derived neurons with reduced multi-whisker response properties. This reinforces the idea that these properties of L4 excitatory neurons are related, and that they are established through a common mechanism. These findings extend our understanding of how Lhx2 contributes to the coordination of fate specification and circuit assembly during the development of S1 (Chou et al. 2009; Chou and O'Leary 2013; Hsu et al. 2015; Shetty et al. 2013; Wang et al. 2017), and implicate Lhx2 as part of a lineage-based mechanism that establishes the lineage-dependent integration of thalamic inputs.

Complete knockdown of Lhx2 expression in cortical progenitors at E10 has previously been associated with a number of developmental malformations (Bulchand et al. 2003; Chou et al. 2009; Mangale et al. 2008; Monuki et al. 2001), often accompanied by the aberrant migration of cortical neurons, that prevent investigation of its loss of function in the cortex. However, this likely reflects disruption of the early role of Lhx2 as a cortical selector gene. In keeping with this, increasing Lhx2 expression at a later stage of embryonic development had no effect upon neuronal migration, with Lhx2 aIP-derived L4 neurons occupying a similar position within the cortex compared to WT. Similarly, given its role in coordinating a number of activity-dependent processes (Wang et al. 2017), it was important to verify that increased expression of Lhx2 did not give rise to neurons with abnormal intrinsic electrical or synaptic properties. *In vitro* electrophysiological recordings revealed that Lhx2 aIP-derived L4 neurons were largely indistinguishable from WT, aside from subtle differences in their resting membrane potential. Interestingly, this was mirrored by the observation that Lhx2 aIP-derived L4 neurons are more spontaneously active than OP-derived L4 neurons *in vivo*. Given that the excitability of neurons is controlled by the balance of excitatory and inhibitory activity, this raises the possibility that Lhx2 might also influence the inhibitory inputs received by L4 neurons.

Previous work has characterised L4 excitatory neurons as a relatively homogenous population in the mature brain (Ellender et al. 2019; Tasic et al. 2016; Tasic et al.

2018). However, the data presented here show that Lhx2 expression molecularly distinguishes L4 neurons, supporting the idea that Lhx2 can be used as a tool to distinguish cortical subpopulations (Huilgol et al. 2022; Matho et al. 2021). Interestingly, the fact that Lhx2 has also been linked to activity-dependent genes (Wang et al. 2017), suggests a potential point of convergence through which progenitor-based mechanisms could interact with activity-dependent processes during circuit formation.

In summary, this chapter has demonstrated that Lhx2 expression forms part of a lineage-based mechanism that determines how L4 neurons receive thalamic inputs. Specifically, aIP-derived L4 neurons exhibit low endogenous levels of Lhx2 expression relative to nearby OP-derived L4 neurons. When Lhx2 expression levels are increased, the higher-order properties of aIP-derived L4 neurons are abolished, including their sampling of higher-order inputs from POm. The functional consequences associated with increased Lhx2 expression will be explored further in **Chapter 6**.

# Chapter 6

# Higher-order inputs to aIP-derived neurons are required for sensory-evoked plasticity

## 6.1 Introduction

The role of higher-order thalamic nuclei during sensory processing is enigmatic. As discussed in **Chapter 1** and **Chapter 3**, they are known to facilitate the transfer of sensory information between cortical areas through an ascending hierarchy of transthalamic pathways (Mo and Sherman 2019; Sherman 2016; Theyel et al. 2010). However, higher-order thalamic nuclei also send feedback projections to primary cortical areas (e.g., S1), which have been implicated in a number of fundamental cognitive processes, including attention, arousal, nociception, and conscious perception (Frangeul et al. 2014; Masri et al. 2006; Nakajima and Halassa 2017; Petty et al. 2021; Suzuki and Larkum 2020). This apparent functional diversity reflects not only the variety of inputs received by higher-order nuclei (Chiaia et al. 1991; Diamond et al. 1992; Groh et al. 2014; Lavallée et al. 2005; Olsen and Witter 2016; Trageser and Keller 2004; Usrey and Sherman 2019), but also the heterogeneity of cortical circuits receiving higher-order inputs (Audette et al. 2018; Buchan et al. 2021; Sermet et al. 2019).

In the mouse somatosensory system, an emerging role for POm is as a regulator of sensory-evoked plasticity (Buchan et al. 2021; Chéreau et al. 2021; Roelfsema and Holtmaat 2018). In S1, sensory-evoked long-term potentiation (sLTP) can be induced in L2/3 by repetitive stimulation of the whiskers (Gambino et al. 2014; Mégevand et al. 2009). This process has been shown to require L4 activation and dendritic plateau potentials in L2/3 excitatory neurons, which are elicited by feedback projections from POm. The role of this higher-order feedback appears to be critical, as blocking POm activity prevents the induction of sLTP (Gambino et al. 2014; Williams and Holtmaat 2019). Notably, the role played by higher-order thalamic inputs to other cortical layers in sensory-evoked plasticity, including to L4 excitatory neurons, is unknown.

**Chapter 5** demonstrated that increased Lhx2 expression in aIP-derived L4 neurons abolished their higher-order properties, including a greater thalamic input from POm. This chapter will explore the functional consequences associated with reduced higher-order inputs to aIP-derived L4 neurons by investigating the induction of sensory-evoked cortical plasticity in L2/3 of S1. Specifically, the aims of this chapter are as follows:

- To establish a paradigm for the induction of sensory-evoked plasticity in S1
- To investigate the effects of disrupting higher-order inputs to aIP-derived L4 neurons upon sensory-evoked plasticity in L2/3

## 6.2 Results

### 6.2.1 RWS induces sensory-evoked plasticity

In order to investigate the functional contribution of higher-order inputs to aIP-derived L4 neurons, it was first necessary to establish a paradigm for the induction of sensory-evoked plasticity. WT animals underwent IUE with a T$\alpha$1-Cre and a floxed ChR2-YFP plasmid at E14 (**Figure 6.1A**) Once the animals had reached P28, extracellular recordings of MUA were performed in L2/3 of S1 under anaesthesia. The ChR2-YFP expression enabled robust light-evoked responses to be used as confirmation that each recording was targeting a region of S1 with high numbers of electroporated L4 neurons. This was also confirmed by histological analysis. A rhythmic whisker stimulation (RWS) protocol was adapted, and used to induce sensory-evoked long term potentiation (sLTP; **Figure 6.1B**; see **Section 2.6**; Gambino et al. 2014). This involved measuring responses to the simultaneous deflection of multiple whiskers during a pre-induction period (pre; 0.1 Hz deflections, 100 trials), an sLTP induction period consisting of RWS at 8 Hz for 1 min, and finally a post-induction period (post; 0.1 Hz deflections, 100 trials). Under these control conditions, RWS induced robust sLTP of whisker-evoked responses in L2/3 (**Figure 6.1C-D**; pre spike rate was 43.29 Hz $\pm$ 12.14 and post spike rate was 137.06 Hz $\pm$ 26.41), consistent with previous work (Gambino et al. 2014). To confirm that RWS was required to induce sLTP, subsequent control experiments were performed, where the RWS protocol was omitted (**Figure 6.1E**; delta spike rate in WT without RWS was 106.49 $\pm$ 11.64 % and in WT with RWS was 338.59 $\pm$ 46.23 %).

### 6.2.2 Increasing Lhx2 expression disrupts sensory-evoked plasticity

To investigate whether disrupting higher-order thalamic inputs to aIP-derived L4 neurons affects sensory-evoked plasticity, animals underwent IUE with a T$\alpha$1-Cre, floxed ChR2-YFP, and CAG-Lhx2 overexpression plasmid at E14 (**Figure 6.2A**).

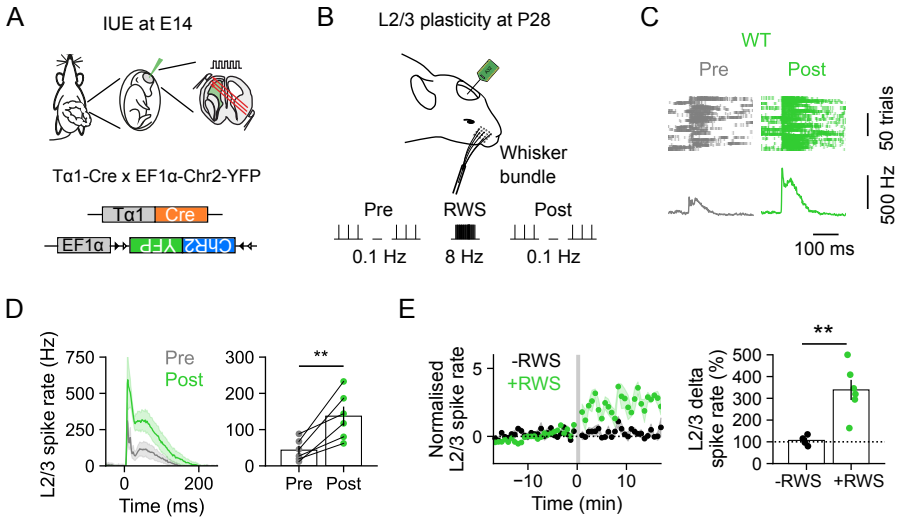


**Figure 6.1: RWS induces robust sensory-evoked plasticity in S1 L2/3. (A)** Animals underwent IUE of a T$\alpha$1-Cre and a floxed ChR2-YFP plasmid at E14, resulting in the labelling of WT aIP-derived L4 neurons. **(B)** Once the animals had reached P28, they were anaesthetised and sensory-evoked plasticity was examined in L2/3 of S1 using a RWS protocol (8 Hz for 60 s). The presence of electroporated L4 neurons at the recording site was confirmed by ChR2 stimulation and subsequent histology. **(C)** Raster plots and PSTHs show MUA in L2/3. Responses to whisker deflections (0.1 Hz) are shown before (pre) and after (post) RWS. **(D)** Mean (left) and separate (right) population data reveals that RWS potentiated L2/3 activity (n = 6 animals; p = 0.006, paired t-test). Shading indicates SEM around mean. **(E)** Normalised L2/3 MUA relative to the time of RWS (left; each data point is mean of five whisker deflections, 0.1 Hz). Shading indicates SEM around mean. Delta spike rate was significantly higher in animals that experienced RWS (n = 5, 6 animals; p = 0.004, t-test). Data represented as mean ± SEM.

This manipulation had been shown to disrupt the higher order properties of aIP-derived L4 neurons in S1 (See **Chapter 5**). Once these animals reached P28, they were subjected to the RWS protocol to investigate sensory-evoked plasticity. In contrast to WT animals, RWS failed to induce sLTP in L2/3 of Lhx2 animals (**Figure 6.2B-C**; Lhx2 pre spike rate was 73.88 Hz ± 30.10 and post spike rate was 78.01 Hz ± 31.73). These data support the conclusion that higher-order input to aIP-derived L4 neurons is required for sensory-evoked plasticity in L2/3.

### 6.2.3 Restricting Lhx2 expression to aIP-derived L4 neurons is sufficient to disrupt sensory-evoked plasticity

Whilst Lhx2 was only overexpressed in the electroporated neurons (**Figure 5.3**), the use of a CAG-Lhx2 construct meant that increased Lhx2 expression in OP-derived L4 neurons could contribute to the effects on sensory-evoked plasticity. To

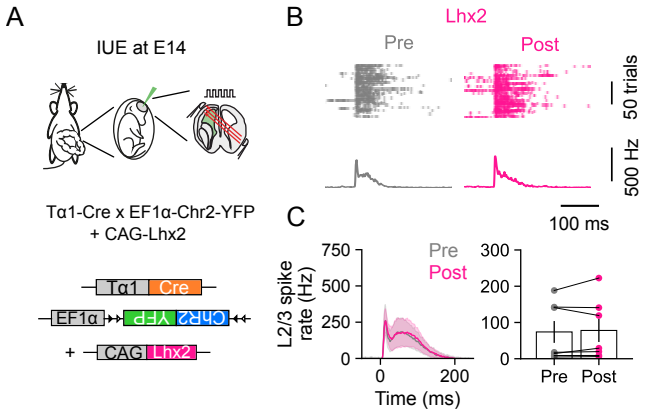


**Figure 6.2: Higher-order input to aIP-derived L4 neurons is required for sensory evoked plasticity in L2/3. (A)** Animals underwent IUE at E14 with a T$\alpha$1-Cre, floxed ChR2-YFP, and CAG-Lhx2 plasmid. **(B)** Once the animals reached P28, they were subjected to the RWS protocol. Raster plots and PSTHs show MUA in L2/3. Responses to whisker deflections (0.1 Hz) are shown before (pre) and after (post) RWS. **(C)** Mean (left) and separate (right) population data reveals that RWS failed to potentiate L2/3 activity (n = 7; p = 0.547, Wilcoxon signed-rank test). Shading indicates SEM around mean. Data represented as mean ± SEM.

control for this possibility, a floxed CAG-Lhx2 plasmid was generated that only expresses Lhx2 following Cre recombination (see **Section 2.2**). Thus, increased Lhx2 expression would be restricted to aIP-derived L4 neurons, which are referred to as fLhx2 aIP-derived neurons. As before, animals underwent IUE with a T$\alpha$1-Cre, floxed ChR2-YFP, and the floxed CAG-Lhx2 at E14 (**Figure 6.3A**) and once they had reached P28, they were subjected to the RWS protocol. Under these conditions, RWS again failed to induce sLTP in L2/3 (**Figure 6.3B-C**; fLhx2 pre spike rate was 61.49 ± 24.55 Hz, and post spike rate was 76.71 ± 24.18 Hz), suggesting that restricting increased Lhx2 expression to aIP-derived L4 neurons is sufficient to disrupt sensory-evoked plasticity in L2/3.

In summary therefore, considerable differences could be observed between the different conditions. Whilst electroporated animals with WT aIP-derived L4 neurons exhibited robust sLTP, both the Lhx2 and fLhx2 electroporated animals failed to show sLTP (**Figure 6.4A-B**; delta spike rate in WT was 338.59 ± 46.23 %, in Lhx2 was 120.71 ± 14.91 %, and in fLhx2 was 148.93 ± 31.79 %). Finally, to establish whether these effects were associated with differences in overall activity levels during the sLTP induction period, spiking during the RWS (8 Hz whisker

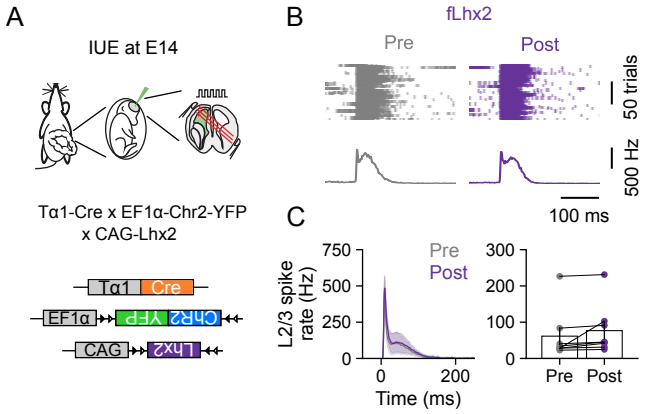


**Figure 6.3: Restricting increased Lhx2 levels to aIP-derived L4 neurons is sufficient to disrupt sensory-evoked plasticity.** **(A)** Animals underwent IUE of a T$\alpha$1-Cre, a floxed ChR2-YFP, and a floxed CAG-Lhx2 plasmid, such that increased Lhx2 expression would be restricted to aIP-derived L4 neurons (fLhx2). **(B)** Once the animals reached P28, they were subjected to the RWS protocol. Raster plots and PSTHs show MUA in L2/3. Responses to whisker deflections (0.1 Hz) are shown before (pre) and after (post) RWS. **(C)** Mean (left) and separate (right) population data reveals that RWS failed to potentiate L2/3 activity (n = 8; p = 0.122, Wilcoxon signed-rank test). Shading indicates SEM around mean. Data represented as mean ± SEM.

stimulation for 60 s) was compared and found to be comparable across the three experimental groups in both L4 (**Figure 6.4C**; WT mean L4 spike rate was 59.10 ± 9.43 Hz, Lhx2 mean L4 spike rate was 56.17 ± 12.66 Hz, fLhx2 mean L4 spike rate was 59.29 ± 8.01 Hz) and L2/3 (**Figure 6.4D**; WT mean L2/3 spike rate was 64.31 ± 12.00 Hz, Lhx2 mean L2/3 spike rate was 57.53 ± 14.42 Hz, fLhx2 mean L2/3 spike rate was 59.44 ± 8.15 Hz). Taken together, these data are consistent with a model in which higher-order thalamic inputs are required to elicit sensory-evoked plasticity in S1 (Gambino et al. 2014; Williams and Holtmaat 2019), and demonstrate the functional importance of a lineage-dependent mechanism through which thalamic inputs are integrated in cortex.

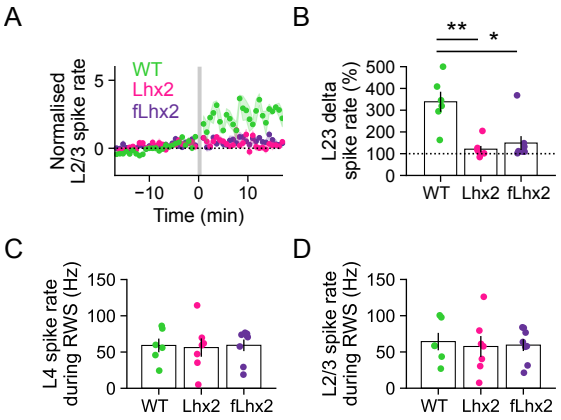


**Figure 6.4: Disruption of sensory-evoked plasticity cannot be attributed to spiking activity during the induction of RWS.** **(A)** Normalised L2/3 MUA relative to the time of RWS (data from **Figure 6.1**; each data point is mean of five whisker deflections, 0.1 Hz). Shading indicates SEM around mean. **(B)** Delta spike rate was significantly higher in WT animals compared to Lhx2, and fLhx2 animals (n = 6, 7 and 8 animals; p = 0.006, Kruskall Wallis test; WT vs. Lhx2, p = 0.006; WT vs. fLhx2, p = 0.040; Lhx2 vs. fLhx2, p = 1.000; Dunn's test). **(C)** Mean MUA during RWS (8 Hz for 60 s) was similar for WT, Lhx2 and fLhx2 animals in L4 (left; n = 6, 7, and 8 animals; p = 0.920, ANOVA). **(D)** Mean MUA during RWS was similar for WT, Lhx2 and fLhx2 animals in L2/3 (right; n = 6, 7 and 8 animals; p = 0.971, ANOVA). Data represented as mean ± SEM.

## 6.3 Discussion

In this chapter, a combination of *in utero* labelling and *in vivo* electrophysiology was used to assess the functional consequences associated with a reduction in higher-order thalamic inputs to aIP-derived L4 neurons. The data support the conclusion that higher-order thalamic inputs to aIP-derived L4 neurons are required for sensory-evoked cortical plasticity in S1, with increased Lhx2 expression restricted to aIP-derived L4 neurons being sufficient to disrupt the potentiation of whisker-evoked responses.

Higher-order inputs are known to play a number of diverse roles in sensory-evoked plasticity in S1 (Audette et al. 2019; Buchan et al. 2021; Chéreau et al. 2021; Gambino et al. 2014; Roelfsema and Holtmaat 2018; Williams and Holtmaat 2019). To explore how POm inputs to aIP-derived L4 neurons might contribute to this, it was first necessary to establish a paradigm for the induction of sensory-evoked plasticity *in vivo*. A RWS protocol, that has been reported to induce sLTP in urethane-anaesthetised mice (Gambino et al. 2014; Mégevand et al. 2009), was adapted to incorporate the simultaneous deflection of multiple whiskers. Consistent with previous work (Gambino et al. 2014), RWS reliably led to the potentiation of whisker-evoked responses in L2/3, thus providing a platform from which to explore the potential role of lineage-dependent circuits. Importantly, control experiments verified that sLTP was dependent on RWS, and the expression of ChR2-YFP enabled light-evoked responses to be used as confirmation that recordings were targeted to areas of S1 containing a substantial portion of electroporated neurons.

Subsequent experiments built on the observations of **Chapter 5**, which showed that manipulating the expression of Lhx2 disrupts the higher-order thalamic inputs received by aIP-derived L4 neurons. Remarkably, increased Lhx2 expression was sufficient to disrupt the induction of sLTP in L2/3. This represents the first evidence that higher-order inputs to L4 are required for sensory-evoked plasticity in S1. Previous studies have shown that POm inputs to S1 are necessary for the

induction of sLTP in L2/3 pyramidal neurons (Gambino et al. 2014), and that combined L4 and POm activation is sufficient to induce LTP in brain slices (Williams and Holtmaat 2019). Together, these findings led to the proposal that the convergence of higher-order activity from POm, with first-order activity from VPM via L4, forms the basis of sLTP in L2/3 (Buchan et al. 2021; Chéreau et al. 2021; Roelfsema and Holtmaat 2018). In contrast, the data presented here suggest that sLTP requires the complementary delivery of higher-order information to different neuronal compartments and/or cortical layers.

This raises the question: what purpose might be served by complementary information arriving at L2/3 pyramidal neurons? The morphology of pyramidal neurons allows for the compartmentalisation of inputs (London and Häusser 2005; Spruston 2008). For example, inputs from POm are known to target distal regions of the apical dendrite of L2/3 pyramidal neurons, whereas inputs from L4 are proximal to the soma. Generally, this is thought to increase the complexity of stimulus representations that can be achieved by individual neurons. One notable feature is that the apical dendrites of pyramidal neurons exhibit a number of active processes, including the generation of NMDAR-depedent plateau potentials, that result in the supralinear summation of coincident distal and proximal inputs (Lavzin et al. 2012). Previous work has shown that distal POm inputs are required for the propagation of activity from the aprical dendrite to the soma of L5 pyramidal neurons (Suzuki and Larkum 2020). It is possible that similar inputs are required at the soma to ensure that ascending sensory information propagates in the opposite direction so as to engage with, or contribute to active dendritic processes. Equally, it is increasingly recognised that POm can be divided into sub-regions on the basis of specific patterns of input and output connectivity (Roy et al. 2022). As such, the POm inputs received by L4 and L2/3 may well originate from different subpopulations that convey distinct information, such as arousal and motor signals. Therefore, L2/3 pyramidal neurons might act as coincidence detectors, with plasticity mechanisms only being engaged when an animal is actively exploring the environment with its whiskers in a state of heightened arousal, for example. It has

also been proposed that the extensive connectivity of higher-order thalamic nuclei make them well suited to perform the role of a Bayesian observer, forming the basis of a predictive coding model (Rikhye et al. 2018). In this scenario, direct POm inputs to L2/3 might convey a likelihood signal based upon an internal model of the environment, whereas those arriving via L4 will be integrated with first-order information to provide an updated likelihood signal that incorporates external input. Thus, plasticity mechansisms could be engaged differently depending on whether a given stimulus was expected or not (Gillon et al. 2021).

Given that the overexpression of Lhx2 was not specific to a particular progenitor type, it was important to verify that the observed effects upon sLTP were not the result of increased Lhx2 expression in OP-derived L4 neurons. As such, a second construct was developed to restrict the overexpression of Lhx2 to aIP-derived L4 neurons. As before, RWS failed to induce sLTP, reinforcing the idea that sensory-evoked plasticity in S1 is dependent upon higher-order inputs to aIP-derived neurons. A further possibility was that the effects of increased Lhx2 expression reflected a non-specific reduction in the overall activity levels in L4 or L2/3, perhaps as a result of decreased inputs from POm. However, spiking levels during RWS were similar across conditions. This is consistent with the idea that the major excitatory drive to the cortex is provided via VPM (Armstrong-James et al. 1992; Sherman and Guillery 1996; Sherman and Guillery 1998), whereas POm inputs to aIP-derived neurons carry information that is particularly important for plasticity, as has been previously suggested in L2/3 (Gambino et al. 2014).

These observations raise a further question: what is special about the inputs from POm to aIP-derived L4 neurons? One possibility is that the deflection of several whiskers is itself a cue for plasticity. Given their multi-whisker response properties, aIP-derived L4 neurons may only be activated sufficiently by multi-whisker information, which requires them to be sampling inputs from POm. Alternatively, the observed effects may reflect specific synaptic properties of POm inputs. For example, POm inputs to L4 are known to activate metabotropic glutamate receptors (mGluRs), which can modulate activity over a period of several hundreds of

ms (Sherman 2014; Viaene et al. 2011a). Indeed, **Chapter 5** showed that WT aIP-derived L4 neurons have a substantially larger late response to whisker stimulation compared to Lhx2 aIP-derived L4 neurons. These differences in the relative strength of input over time could have implications for synaptic plasticity rules. These differences in temporal recruitment could also have implications for the recruitment of local interneurons. For example, as aIP-derived neurons receive less input from VPM relative to OP-derived L4 neurons, they may not be subject to the same degree of feedforward inhibition by parvalbumin-expression (PV) interneurons (Yu et al. 2019). Equally, POm inputs to L4 may recruit specific inhibitory circuits, as has been shown in L2/3 (Williams and Holtmaat 2019).

In summary, this chapter supports a model in which higher-order inputs to aIP-derived L4 neurons are required for the induction of sensory-evoked cortical plasticity. This highlights the functional importance of the lineage-dependent expression of Lhx2 with respect to sensory processing. More broadly, these findings support the idea that the cortical circuits underlying the integration of higher-order and first-order activity are the result of developmentally distinct lineages. The implications of these findings, and possible directions for future work will be discussed in **Chapter 7**.

# Chapter 7

# General Discussion

The overarching aim of this thesis was to investigate the role of lineage in the cortical integration of thalamic inputs. This chapter will recapitulate some of the key experimental findings and consider factors that may influence their interpretation. Finally, the broader implications of this thesis will be discussed, highlighting opportunities for future work where appropriate.

## 7.1 Experimental findings

- **Chapter 3** investigated the sensory response properties of S1 L4 excitatory neurons as a function of the progenitor from which they derive. To achieve this, *in vivo* extracellular recordings were performed whilst sensory stimuli were delivered by whisker deflection. In keeping with previous work, the response properties of L4 excitatory neurons were found to be heterogeneous, with some neurons being selective for the deflection of a single whisker, and others exhibiting more multi-whisker responses. By using IUE to express ChR2 in a progenitor-defined manner, neurons could be identified in adult S1 as a function of lineage. This revealed that aIP-derived L4 neurons were more likely to exhibit multi-whisker responses than OP-derived L4 neurons, suggesting that the response properties of neurons in S1 L4 are lineage-dependent. Moreover, it was predicted that the multi-whisker response properties of aIP-derived L4 neurons might reflect the preferential

sampling of inputs from the higher-order thalamic nucleus, POm.

- **Chapter 4** tested this prediction directly. Morphological reconstructions revealed that OP-derived L4 neurons typically targeted the principal barrel with their dendrites, whereas aIP-derived L4 neurons were less likely to do so. Instead, the dendrites of aIP-derived L4 neurons often branched extensively into septa, consistent with the sampling of inputs from POm. This was confirmed by subsequent paired recordings *in vitro*, which found that aIP-derived L4 neurons receive greater POm input, and weaker VPM input, relative to OP-derived L4 neurons. These observations were consistent with the idea that the heterogeneous response properties of L4 excitatory neurons in S1 reflect the lineage-dependent integration of thalamic inputs.

- **Chapter 5** explored the expression of the transcription factor, Lhx2, as a possible mechanism by which the lineage-dependent integration of thalamic inputs is established. Immunohistochemical analysis found that aIP-derived L4 neurons express low levels of Lhx2 relative to neighbouring OP-derived L4 neurons during the period of barrel formation in the first postnatal week. To investigate whether low levels of Lhx2 expression are responsible for establishing the higher-order properties of aIP-derived L4 neurons, a Lhx2 overexpression construct was developed. Increased Lhx2 expression resulted in dendrites that no longer projected outside of the principal barrel, abolished WT differences in how neurons sampled thalamic inputs, and resulted in aIP-derived L4 neurons with reduced multi-whisker response properties. Together, these observations suggest that Lhx2 forms part of a lineage-based mechanism through which the integration of thalamic inputs is established in S1 L4.

- **Chapter 6** explored the functional significance of higher-order inputs to aIP-derived L4 neurons. First, it was demonstrated that a RWS paradigm could be used to induce robust sensory-evoked plasticity in S1 L2/3 *in vivo*. Subsequent experiments found that increased Lhx2 expression in aIP-derived

L4 neurons was sufficient to disrupt the induction of sensory-evoked plasticity in L2/3. This emphasised the functional importance of the lineage-dependent expression of Lhx2 with respect to sensory-processing, and reinforced the idea that the cortical circuits underlying the integration of higher-order and first-order activity are the result of developmentally distinct lineages.

## 7.2 Methodological considerations

In this section I will consider some of the methodological issues that might influence the interpretation of the data and the questions that these raise.

### 7.2.1 *In utero* electroporation and the labelling of specific populations of progenitor cells

The observations of this thesis relied upon the ability to label specific populations of cortical progenitors using IUE. IUE is a well-established tool for the delivery of plasmid DNA to dividing progenitors in the ventricular proliferative zones (Baumgart and Grebe 2015; Bitzenhofer et al. 2017; Martínez-Garay et al. 2016; Szczurkowska et al. 2016), and has become an invaluable technique for the study of key aspects of cortical development. The primary reason for the use of IUE in this thesis was that it is uniquely suited to induce long-lasting expression of multiple constructs in the progeny of labelled progenitors, thereby facilitating the study of neurons in the adult brain as a function of the progenitor from which they derive. Importantly, this is not possible using a number of other techniques, such as FLASH-Tag, due to the decay in expression over time.

In general, one issue with IUE is that it may be biased to label specific progenitor populations based on their location. Given that plasmid DNA is drawn from the ventricle into the proliferative zones, it is possible that the progenitor cells closest to the ventricle are more likely to be transfected. As discussed in **Section 1.3.2**, aIPs are known to reside in the VZ, whereas other progenitor types that contribute to the OP population are found within the SVZ. As a consequence, aIPs may be overrepresented relative to OPs, for example by the dual-colour labelling strategies used here (see **Chapter 4**). Nevertheless, previous studies have successfully used IUE to simultaneously label progenitors that reside in both the VZ and the SVZ (Stancik et al. 2010; Tyler and Haydar 2013; Tyler et al. 2015). And the ability to label two progenitor populations affords important within-animal experimental designs, which can control for the potential effects of neuronal birthdates.

A second question relates to the specificity with which distinct progenitor populations can be targeted. It is increasingly clear that the diversity of progenitor types during embryonic development, and the complexity of transcriptional programs regulating their neurogenic output, have been underappreciated (Llorca et al. 2019; Oberst et al. 2019; Telley et al. 2016; Telley et al. 2019). **Section 1.3.2** gave a basic account of how different progenitors act to contemporaneously generate postmitotic cortical neurons. Central to this model are two concepts: Firstly, that the total neurogenic output of a RGC reflects a major contribution by IPs; and secondly, that IPs can be distinguished based upon their expression of molecular markers (e.g., the T$\alpha$1 promoter for aIPs, and Tbr2 for bIPs). However, as with cell types in the adult brain (Tasic et al. 2016; Tasic et al. 2018), the boundaries between what were previously considered distinct populations are subject to change. For example, it has been demonstrated that RGCs can express T$\alpha$1 in what is thought to represent part of a transcriptional program that promotes aIP fate (Ramos et al. 2020; Tyler and Haydar 2013). However, the temporal profile of T$\alpha$1 expression by RGCs, and their pattern of subsequent division has not yet been explored.

As such, a number of key questions arise that have consequences for the labelling approach used in this thesis: To what extent does T$\alpha$1 expression determine the subsequent proliferative behaviour of RGCs? And is expression transient, or inherited? In one scenario, T$\alpha$1 expression might signal that all future divisions within a given clone, asymmetric or symmetric, would generate aIPs. This would also provide an explanation for the expression of T$\alpha$1 by aIPs, in that they would inherit this from their parent cell. Alternatively, whilst T$\alpha$1 expression may promote aIP fate in a single division, it may not be passed on to the non-aIP progeny (e.g., the self-renewing RGC), which could go on to generate further types of progenitor, such as bIPs. In this second scenario, it is possible that electroporation with T$\alpha$1-Cre could drive recombination in a subpopulation of RGCs that go on to generate non-aIP progenitors, thus labelling false positives within the aIP-derived population. However, previous work specifically targeting bIP-derived L4 neurons

in S1 reported a bias in dendritic targeting toward barrels (Guillamon-Vivancos et al. 2019), consistent with the OP-derived L4 population, and in opposition to the aIP-derived L4 population studied here. This suggests that any contamination is minimal and supports the first scenario outlined above. However, future work could quantify any potential contamination using recently developed molecular tools. For example, Cre- and Flp-based recombinase systems have been combined to generate constructs capable of driving expression that is subject to Boolean logical operations (Fenno et al. 2014). In this case, a T$\alpha$1-Cre/Tbr2-Flp construct could be used to target progenitors that express T$\alpha$1 and do not express Tbr2 to ensure the precise targeting of aIPs.

### 7.2.2 *In vivo* recording of cortical activity in anaesthetised preparations

A major experimental approach in this thesis is the quantification of cortical neuronal activity from *in vivo* electrophysiological recordings in anaesthetised mice. The choice of anaesthetic agent and depth of anaesthesia are known to have fundamental consequences for the nature of single-unit spiking activity that can be observed in the cortex and thalamus (Okun et al. 2012). Under anaesthesia, activity in the cortex is highly correlated, characterised by slow fluctuations between short periods of synchronous activity and silence that are reminiscent of slow-wave sleep, albeit often on a slower timescale (Pachitariu et al. 2015). This is also evident in the response properties of individual neurons. For example, sensory stimuli often evoke larger, longer-lasting responses under anaesthesia (Simons et al. 1992). In part, this is thought to reflect increased synchronicity of inputs from the thalamus to the cortex (Poulet et al. 2012). Notably, if stimuli regularly coincide with periods of synchronous activity, it can be difficult to delineate the contribution of external inputs versus that of internal dynamics to the spiking activity of individual neurons. Similarly, a high frequency of synchronous events is known to affect the success of spike-sorting algorithms (Hildebrandt et al. 2017).

In this thesis, all *in vivo* experiments were performed on urethane-anaesthetised

animals. Urethane was chosen for a number of reasons. Firstly, cortical activity under urethane anaesthesia is known to exhibit fewer and less variable synchronous events than other popular agents, such as ketamine (Hildebrandt et al. 2017). Secondly, unlike isoflurane, urethane does not inhibit the action of NMDARs (Accorsi-Mendonça et al. 2007). This was likely crucial for the investigations into plasticity in **Chapter 6**. Thirdly, there is an established literature in which urethane is used to explore the sensory response properties of neurons in S1 (e.g., Armstrong-James et al. 1992; Simons et al. 1992; Diamond et al. 1992). Finally, because of its long half-life relative to other agents, one dose of urethane can provide stable anaesthesia for an entire recording session, with minimal respiratory complications (Lee and Jones 2018). This was particularly important so as to avoid large anaesthetic depth-dependent shifts in spiking activity in the middle of experiments that might influence interpretation. Generally, the lowest possible dose of urethane was administered such as to ensure that animals were suitably anaesthetised, whilst minimising the negative effects associated with its use.

One important question relates to how thalamic activity is affected by anaesthesia. It is widely stated in the literature that POm is inactive under anaesthesia, due to inhibition by the zona incerta that is strongly dependent on brain state (Lavallée et al. 2005; Sobolewski et al. 2015). Indeed, a reduction in higher-order thalamic input to cortex has been implicated as a possible mechanism of anaesthesia action (Suzuki and Larkum 2020). However, here we show that the multi-whisker responses of L4 excitatory neurons are dependent upon input from POm, and reproduce a sLTP protocol that has been shown to require the action of POm inputs in L2/3 to induce plasticity (Gambino et al. 2014). One possible explanation is that while spontaneous activity in POm (i.e., that driven by non-sensory inputs in the awake brain) is suppressed under anaesthesia, excitation driven by sensory inputs remains strong enough to propagate to the cortex. Alternatively, as discussed in **Chapter 6**, this may reflect the action of different subpopulations within POm (Roy et al. 2022). For example, the neurons that receive inhibitory input from the zona incerta, may not be the same neurons that engage in recurrent connectivity with

S1.

The use of anaesthesia also has implications for the appropriate choice of sensory stimuli. Traditional approaches in sensory physiology have focussed on recording the activity of individual neurons, whilst exploring the sensory periphery to find regions that evoke responses (i.e., receptive field mapping; Hubel and Wiesel 1962). This has contributed enormously to our understanding of the functional organisation of sensory processing and revealed the sheer complexity of stimulus representation that can be achieved by individual neurons. For example, L4 excitatory neurons in S1 are known to be sensitive to a vast array of stimulus features including amplitude, frequency, velocity, vibration, inter-stimulus-interval, and direction (discussed in Estebanez et al. 2018). These features constrain the region of stimulus space in which a neuron will respond, giving rise to the appearance of a sparse network, in which any given stimulus drives only a small subset of neurons (Barth and Poulet 2012; Hong et al. 2007). Importantly, these constraints are relaxed under anaesthesia, such that neurons are more likely to exhibit dense responses, and to a wider variety of stimuli (Ranjbar-Slamloo and Arabzadeh 2019; Ranjbar-Slamloo and Arabzadeh 2019). A consequence of this, is that much of the variance across a population of neurons, in terms of stimulus selectivity, can be accounted for using relatively simple stimuli. For example, experiments using single whisker deflection in **Chapter 3** found that selectivity for the PW varied continuously throughout the recorded population. In this sense, the use of anaesthesia can be considered an advantage, as populations of neurons in awake animals would revert to a sparse regime and be subject to considerable trial-to-trial non-sensory modulation that may impede the study of their response properties as relating to the thalamic inputs that they receive.

### 7.2.3 On the synthesis of rodent literature

It is important to acknowledge that the majority of our understanding of sensory processing in S1 is based on a synthesis of mouse and rat literature. Early experiments were typically performed in rats, owing to their size, however the increasing

genetic tractability of mice has led to them becoming the model of choice (Erzurumlu and Gaspar 2020). Despite this, observations from both species are often cited interchangeably, including within this thesis. One species difference that may be relevant to this thesis is that the septal regions of rats are larger than those in mice (Alloway et al. 2004; Kim and Ebner 1999). This has led to the suggestion that neurons whose soma are located within rat septa play a much more prominent and/or distinct role in sensory processing, compared to mice (Petersen 2007). As such, while there was no evidence of the lineage-dependent localisation of soma here, there may well be in rats. Equally, the extent to which L4 excitatory neurons target specific regions of the barrel field with their dendrites may also have arisen due to a lack of segregation between barrel and septa-related circuitry in L4. A related observation is that the connection density of the mouse cortex is thought to be considerably higher than that of the rat, estimated as 97 % and 80-90 %, respectively (Bota et al. 2015; Gămănuţ et al. 2018). Generally, this is thought to be a function of brain size (e.g., macaque connection density has been reported as 66 %; Markov et al. 2014), and is inversely correlated with the specificity of large-scale functional organisation. This could apply to the organisation of sensory representations in cortex. For example, orientation selectivity in cats is arranged into a coarse topographic representation, often referred to as a pinwheel, whereas that of rodents is heterogeneous and characterised as a salt-and-pepper distribution, as discussed in **Section 1.3** (Ohki et al. 2005). Given the differences in connection density, it may be the case that any large-scale, or coarse, organisation of whisker representation is less pronounced in mice compared to rats. Indeed, an interesting possibility is that the fine-scale organisation that is established by lineage-dependent mechanisms reported in this thesis might represent a compensatory strategy to account for the spatial constraints of the mouse cortex.

### 7.2.4 Optogenetic strategies

Experiments in **Chapter 3** and **Chapter 5** required that the activity of specific populations of excitatory neurons could be identified from *in vivo* extracellular

recordings. This was achieved by optotagging, a well-established method for the targeted identification of neurons based on their expression of ChR2 (Lima et al. 2009). A common problem associated with optotagging excitatory neurons is that the activation of ChR2$^+$ neurons can result in the indirect polysynaptic recruitment of spiking activity in ChR2$^-$ neurons within the local circuit, thereby confounding the identification of the target population. The most common method to account for this, is to use inclusion criteria based on the latency and reliability of the light-evoked responses. The rationale is that ChR2$^+$ neurons will respond faster, and with less trial-to-trial variability than ChR2$^-$ neurons. Here, a mean light-evoked latency of 5 ms was used as the separation criterion, in keeping with some of the more strict criteria used by previous studies in rodent cortex (Okun et al. 2015). As an additional control for the recruitment of polysynaptic activity, the AMPA receptor blocker DNQX was administered topically to the cortical surface in a subset of animals. DNQX reduced the light-evoked responses in the optotagged population (ChR2$^+$ aIP-derived), but the response level remained above spontaneous levels, indicating that direct light-evoked activation was preserved in the absence of synaptic transmission. In contrast, the response of the non-optotagged population (ChR2$^-$ OP-derived) was abolished. Together, this suggested that optotagging was able to correctly identify aIP-derived L4 neurons based upon their expression of ChR2. It is of course possible that a small number of ChR2$^-$ OP-derived L4 neurons were included within the optotagged population, but one would expect these to detract from the effects presented in this thesis, rather than exaggerate them.

In **Chapter 4** and **Chapter 5**, another optogenetic strategy was used to activate thalamic axons in L4. ChR2-GFP was first expressed in either VPM or POm by targeted postnatal intrathalamic injection. Several weeks later, dual patch-clamp recordings were performed from acute brain slices. Given the difference in rostro-caudal position between S1 and VPM or POm, thalamic axons are typically severed from their parent soma by the slicing process. This is not a problem in terms of stimulus efficacy, as ChR2$^+$ axons can be activated independently of their soma. However, it does mean that it is not possible to restrict activation to axons from

the target nucleus. As such, it is possible that axons from other thalamic nuclei that had been mistakenly targeted might contribute to the responses observed in L4. Therefore, it was particularly important to quantify the accuracy of intrathalamic injections. Consequently, control experiments were performed that verified injections were 80 % accurate on average, meaning that only 20 % of expression could be classed as ectopic.

As part of the plasticity experiments in **Chapter 6**, the expression of ChR2-YFP was used to confirm that recordings were targeted to areas of S1 that contained a substantial portion of electroporated neurons. Naturally, the optogenetic confirmation was conducted at the beginning of the experiment to facilitate the accurate placement of the electrode, raising the possibility that repeated ChR2 activation could have affected the recorded neurons. For example, synchronous light-evoked activity is likely to increase excitability, both in terms of the spontaneous activity of individual neurons, and the global synchronous events discussed in **Section 7.2.2**. Additionally, ChR2 activation alone has been shown to be sufficient to induce plasticity under certain conditions (Xie et al. 2013). In an attempt to control for these concerns, all animals were exposed to the same number and intensity of light pulses. Furthermore, experiments did not begin until at least 30 min following electrode placement, both to allow for settling of the tissue surrounding the electrode and to ensure that no persistent effects of ChR2 activation could influence their interpretation.

### 7.2.5 Overexpression of Lhx2

In this thesis, DNA constructs were used to experimentally increase the expression of Lhx2, (see **Section 2.2**). Experiments in **Chapter 5** confirmed that the use of CAG-Lhx2 successfully increased Lhx2 expression. However, expression levels in Lhx2 aIP-derived L4 neurons were several orders of magnitude higher than those in WT aIP-derived L4 neurons, and beyond the physiological range. As such, it was necessary to verify that CAG-Lhx2 did not give rise to neurons with aberrant or pathophysiological properties that could affect the interpretation of

subsequent experiments. This was a particular concern, as complete knockdown of Lhx2 has been associated with cortical malformations, often characterised by aberrant neuronal migration (Bulchand et al. 2003; Chou et al. 2009; Mangale et al. 2008; Monuki et al. 2001). However, the data prevented in this thesis suggest that increased Lhx2 expression did not affect neuronal migration, with Lhx2 and WT aIP-derived L4 neurons occupying a similar position within L4, and with respect to pia. An additional concern was that Lhx2 has been implicated in the coordination of activity-dependent processes (Wang et al. 2017). For this reason, it was relevant to assess the potential effect upon the intrinsic electrical and synaptic properties of the neurons, which revealed that Lhx2 and WT aIP-derived L4 neurons were largely indistinguishable.

## 7.3 Implications of findings

This section will elaborate on the findings presented within this thesis, and speculate how they might be reconciled with previous observations to inform how lineage-dependent circuits contribute to cortical function.

### 7.3.1 Lineage shapes the fine-scale organisation of sensory representation

A longstanding challenge in sensory neuroscience has been to reconcile the apparent dichotomy between the strict topographic organisation of primary sensory areas on a large, or coarse scale, with the heterogeneity of response properties observed between neighbouring neurons. Experiments in **Chapter 3** observed that S1 L4 excitatory neurons exhibit diverse spiking response properties following whisker deflection, in agreement with previous observations. However, by identifying neurons as a function of the progenitor type from which they derive, it was possible to demonstrate that this heterogeneity can be understood as a function of a neuron's lineage. Specifically, aIP-derived L4 neurons were found to be more likely to exhibit multi-whisker response properties compared to OP-derived L4 neurons, which were typically selective for a single whisker. Previous work in the visual system of mice and Xenopus laevis tadpoles has shown that clonally-related neurons that derive from a common progenitor are more likely to exhibit shared orientation selectivity in comparison to unrelated neurons (Li et al. 2012; Muldal et al. 2014; Ohtsuki et al. 2012). The findings of this thesis advance this idea, by revealing that shared sensory response properties are not just a feature of an individual clone, but rather a general feature of neurons derived from different types of cortical progenitor. Moreover, the observation that lineage also plays a role in establishing stimulus selectivity in S1, suggests that lineage-based mechanisms provide a general oganising principle across sensory areas, and across species.

One interesting consideration is how the degree of relatedness between neurons influences their response properties. For example, the similarity in orientation selectivity exhibited by clonally-related neurons has been reported to decrease with

increasing clone size (Li et al. 2012; Ohtsuki et al. 2012). This is thought to reflect the fact that the degree of relatedness between randomly selected pairs of neurons will be less in larger clones than in smaller clones. However, given that large clones inevitably contain the progeny of multiple progenitors, an alternative explanation is that the variance in stimulus selectivity reflects progenitor diversity. Here, the selectivity of L4 excitatory neurons was observed to vary continuously throughout the recorded population, rather than associating into two separate lineage-based clusters. This supports the view that the degree of relatedness is likely to be an important factor in establishing the extent to which a given pair of neurons exhibit similar response properties. In this sense, the degree of relatedness may serve to instruct the weight ascribed to different lineage-based mechanisms that are responsible for shaping various functional properties of neurons. According to such a model, it is tempting to view the heterogenous response properties within a primary sensory area as being solely the result of lineage, with apparent variation emerging as the result of different degrees of relatedness. Perhaps a better prediction would be that the stimuli a neuron is able respond to are largely determined by lineage, but a number of other factors can shape the degree to which lineage exerts its effects.

For example, the observation that aIP-derived L4 neurons show a high degree of coupling to population activity raises a number of predictions about their functional attributes. For example, previous work has shown that the response properties of highly coupled neurons are more variable than those that are weakly coupled, such that they exhibit shifts in stimulus selectivity over time (Sweeney and Clopath 2020). This is consistent with two possible scenarios. Firstly, highly coupled neurons may be subject to a greater degree of modulation by non-sensory variables, such as arousal, or motor-planning. Indeed, evidence from the macaque demonstrates that highly coupled neurons respond strongly to motor intention prior to saccade onset (Okun et al. 2015). A second possibility is that highly coupled neurons are more sensitive to mechanisms of sensory-evoked plasticity, such that their response properties are more readily affected by sensory experience. These

possibilities will be explored further in **Section 7.3.2**, and **Section 7.3.4**.

### 7.3.2 Lineage-dependent subnetworks facilitate the integration of higher-order information

The data presented within this thesis contribute to a growing body of evidence that different progenitor types give rise to neurons with specific patterns of functional connectivity. Indeed, by combining the findings of **Chapter 3** and **Chapter 4** with those of other recent work in S1 (Ellender et al. 2019), a putative cortical circuit model can be constructed from which to consider how lineage-dependent subnetworks might contribute to sensory processing in the cortex (**Figure 7.1**).

Experiments in **Chapter 4** demonstrated that the thalamic inputs received by L4 excitatory neurons in S1 are lineage dependent. Specifically, aIP-derived L4 neurons preferentially sample input from the higher-order thalamic nucleus, POm, whereas OP-derived L4 neurons receive greater input from the first-order nucleus, VPM. Previously, it has been shown that the output of L2/3 pyramidal neurons in S1 is also lineage-dependent, with aIP-derived L2/3 neurons preferentially targeting L5a, and OP-derived L2/3 neurons predominantly projecting to L5b (Ellender et al. 2019). This subdivision is notable as L5a and L5b are associated with distinct cortical and subcortical targets, respectively. Despite the fact that the connections between L2/3 and L5 can be understood in terms of lineage, it is unclear whether these connections, or those between L4 and L2/3, develop preferentially between neurons derived from the same progenitor type. However, given that previous work has found the interlaminar connection probably is considerably higher amongst clonally-related neurons (Cadwell et al. 2020; Yu et al. 2009), one might predict that this would also be observed at a population level between neurons of the same lineage. Importantly, this model shows that both the input and output connectivity of the cortical circuit can be interpreted as a function of lineage.

It is important to consider how lineage-dependent subnetworks, as characterised here, compare to other non-random patterns of connectivity that have previously been described (Perin et al. 2011; Song et al. 2005). The observation that pairs

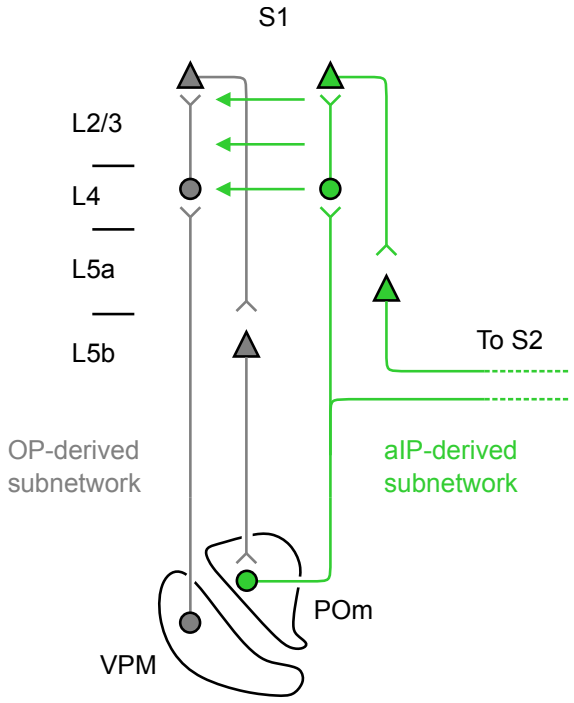


**Figure 7.1: Progenitors give rise to lineage-dependent cortical subnetworks.** In this putative cortical circuit model, OP-derived L4 neurons are primarily driven by the first-order thalamic nucleus, VPM. OP-derived L2/3 neurons predominantly output to L5b, which subsequently projects to subcortical targets, including POm. aIP-derived L4 neurons, preferentially receive inputs from the higher-order nucleus, POm. aIP-derived L2/3 neurons predominantly output to L5a, which then sends projections to long-range cortical targets (e.g., S2). These projections are mirrored by transthalamic pathways that are routed through POm. Within L4 and L2/3, aIP-derived neurons exhibit an out-of-class bias, preferring to connect with OP-derived neurons. Future work is required to determine whether interlaminar connections between L4 and L2/3, and L2/3 and L5, form preferentially as a function of lineage, as has been observed for clonally-related pairs (Cadwell et al. 2020; Yu et al. 2009).

of neurons are more likely to be connected if they receive common input, gave rise to the idea that interconnected subnetworks might act to participate in the segregated, or parallel, processing of different types of information (Brown and Hestrin 2009; Kampa et al. 2006; Yoshimura et al. 2005). This was reinforced by evidence that pairs of interconnected neurons are also likely to exhibit shared stimulus selectivity (Ko et al. 2011). Crucially, these subnetworks were characterised by preferential patterns of intralaminar excitatory connectivity, which was shown to vary as a function of their interlaminar input. Interestingly, previous work has shown that aIP-derived neurons in L4 and L2/3 exhibit an out-of-class connectivity bias such that they avoid connecting to other aIP-derived neurons (Ellender et al. 2019). Instead, they are more likely to connect to nearby OP-derived neurons.

Indeed, this seems to be a feature of lineage relationships, as experiments assessing the interconnectivity of large clones also found no evidence of preferential interlaminar connectivity (Cadwell et al. 2020). Of course, it is possible that a pair of aIP-derived L4 neurons that receive shared input from a thalamic axon are more likely to be connected than a pair that do not, however the probability must still be below average so as to not be observed at a population level. Taken together, this suggests that the lineage-dependent subnetworks observed here do not necessarily arise through the same mechanisms as previously described intralaminar excitatory subnetworks. Further work is therefore required to assess whether lineage relationships are sufficient to give rise to the interlaminar connectivity biases observed within single clones (Cadwell et al. 2020; Yu et al. 2009).

The question remains as to what the lineage-dependent subnetworks outlined in **Figure 7.1** contribute to cortical function. As discussed above, one possibility is that progenitors generate neurons that are specialised for the processing of distinct types of information, acting as independent circuits for parallel processing within the cortex (Nassi and Callaway 2009). This is consistent with the observation that the sampling of thalamic inputs is lineage-dependent, and further supported by observations in **Chapter 3** that suggest these different inputs give rise to distinct stimulus representations. However, one problem with this interpretation is that while the inputs from VPM and POm are segregated in S1, the cortical neurons that receive them are not. Furthermore, the out-of-class connectivity bias exhibited by aIP-derived neurons suggests that, instead of participating in a functionally independent network, they are well-suited to sharing information. Given that aIP-derived L4 neurons preferentially sample inputs from POm, an alternative interpretation is that aIPs give rise to neurons that are specialised for the integration of higher-order information into the local cortical circuit.

As discussed at length, VPM is predominantly driven by sensory input from the periphery (Diamond et al. 1992). Neurons in VPM respond robustly to whisker deflection and give rise to short-latency responses in the cortex that are time locked by feedforward inhibition (Cruikshank et al. 2010). In contrast, POm continually

integrates information from a wide variety of inputs (see **Section 1.2.1**), and is known to evoke long-lasting depolarisations in recipient neurons, typically mediated by mGluRs, that can affect the excitability of cortical circuits over hundreds of ms (Gambino et al. 2014; Mease et al. 2016; Viaene et al. 2011a; Zhang and Bruno 2019). This suggests that POm is well placed to facilitate state change across cortical circuits over a behaviourally relevant timescale, thereby modulating how ascending sensory information is processed. In keeping with this, previous work has demonstrated that responses to coincident whisker deflection and optogenetic stimulation of POm axons sum nonlinearly, both in L2/3 and L5 pyramidal neurons (Mease et al. 2016; Zhang and Bruno 2019). This suggests that higher-order inputs can act like a gain control for sensory responses within the cortex, and raises the question: what are the conditions in which this might be required? One possibility is that POm enhances sensory responses in the cortex during periods of heightened arousal. POm is known to be subject to considerable brain state-dependent inhibition by the zona incerta (Lavallée et al. 2005). Moreover, activity in POm is upregulated during periods of heightened arousal, such as active whisker exploration (Petty et al. 2021). In this scenario, increased POm activity would sensitise the cortex to sensory experience, with the out-of-class connectivity of aIP-derived neurons in L4 and L2/3 acting to propagate this information through the local circuit. This could be tested using two photon imaging in vivo, by asking whether aIP-derived neurons are more heavily modulated by arousal (e.g., during active whisker exploration, or running) than neighbouring OP-derived neurons.

To appreciate what lineage-dependent higher-order subnetworks contribute to cortical function, one could also consider their contribution in terms of the hierarchical organisation of sensory processing. The idea of POm inputs acting as a gain control is consistent with a model whereby ascending first-order information is subject to continuous modulation by higher-order inputs (Sherman 2016). However, the suggestion that POm inputs might sensitise the cortex to upcoming sensory input is indicative of a predictive model (Rikhye et al. 2018). Of course, these suggestions

are not mutually exclusive. One possibility is that POm could operate in different modes depending upon an animal's arousal state. Indeed, one study has shown that under conditions of low arousal, sensory information primarily travels through the cortical circuit in a sequential, hierarchical manner (i.e., from VPM to cortex, and subsequently to POm via descending transthalamic projections). However, in periods of heightened arousal, this circuit is bypassed, with POm providing considerable short latency input to S1 (Sobolewski et al. 2015). This example illustrates that lineage-based circuits could perform multiple distinct roles dependent upon the behavioural context of an animal.

### 7.3.3 Lineage-based transcriptional programs coordinate the action of activity-dependent processes

The anatomical organisation of thalamic inputs to S1 are well understood. Despite this, relatively little is known about the mechanisms that govern how individual neurons are instructed to receive them. One prominent example is that of targeted dendritic orientation, which is known to emerge late in the first postnatal week as the result of an activity-dependent period of remodelling (Espinosa et al. 2009; Matsui et al. 2013). Previous observations found that oriented dendrites often targeted the closest, principal barrel, leading to the suggestion that this represents a strategy by which neurons could preferentially sample incoming input from VPM (Simons and Woolsey 1984; Staiger 2004). Notably, many L4 excitatory neurons do not exhibit targeted dendritic morphology, certainly with respect to barrels, raising the question of how do individual neurons know whether or not to orient their dendrites?

One suggestion is that the extent to which a given neuron exhibits dendritic targeting reflects a relatively passive process, which depends upon the neuron's distance from the nearest barrel, and thus its primary source of excitatory input. However, the observations of **Chapter 3** and other work suggest that this is unlikely, with individual neurons exhibiting considerable heterogeneity in terms of their response properties (Kerr et al. 2007; Sato et al. 2007). In keeping with this, experiments in

**Chapter 4** demonstrated that the dendritic morphology of L4 excitatory neurons varies as a function of the progenitor types studied here. Specifically, while OP-derived L4 neurons typically targeted the principal barrel with their dendrites, the dendrites of aIP-derived neurons branched extensively into the regions outside of barrels, including septa. Importantly, these observations appear to be independent of soma location with respect to barrels, suggesting that the development of targeted dendrites is an active process, through which specific thalamic inputs can be sampled. Previous work has shown that the dendritic morphology of bIP-derived L4 neurons is asymmetric in comparison to neurons derived from other progenitors (Guillamon-Vivancos et al. 2019). Given that the OP-derived population in this thesis likely contains a high proportion of bIP-derived neurons, this complements the observation that OP-derived L4 neurons typically orient their dendrites towards the principal barrel. Broadly, these observations suggest that morphological diversity might represent a general mechanism through which progenitors influence the synaptic connectivity of their progeny. As discussed, targeted dendrites are known to arise through activity dependent mechanisms (Espinosa et al. 2009; Matsui et al. 2013), suggesting that differences between the aIP-derived and OP-derived L4 populations arise from a lineage-dependent transcriptional program that influences their sensitivity to activity.

Experiments in **Chapter 5** revealed that expression of the transcription factor, Lhx2, is lineage-dependent within excitatory L4 neurons. During the first week of postnatal cortical development, aIP-derived L4 neurons exhibited lower Lhx2 protein levels than OP-derived L4 neurons. Lhx2 is known to coordinate the action of several activity-dependent processes, including the expression of Btbd3, a transcription factor that is required for the development of targeted dendritic morphology in L4 excitatory neurons (Matsui et al. 2013; Wang et al. 2017). As such, these findings are consistent with a model in which low Lhx2 expression is associated with neurons that exhibit greater dendritic projections outside of the principal barrel. One important question is whether the action of Lhx2 represents the only mechanism responsible for the development of targeted dendrites. If so,

this would imply that the low expression levels of Lhx2 in aIP-derived L4 neurons allow them to resist activity-dependent remodelling. As such, the proportion of inputs that they receive from VPM and POm become a function of their position with respect to barrels and septa. However, many aIP-derived L4 neurons exhibited a low percentage overlap with barrels, suggesting that an alternative process might be coordinating the active targeting of septal regions. Indeed, given the number of different developmental processes that implicate Lhx2 in their regulation (Chou and Tole 2019), it is likely that numerous candidate mechanisms exist. Particular insight may come from investigating other primary sensory areas, as Btbd3 is exclusively expressed in S1 L4 excitatory neurons.

Consistent with previous work, Lhx2 expression levels had decreased by P21 (Bulchand et al. 2003; Chou and O'Leary 2013; Hsu et al. 2015; Nakagawa et al. 1999), and lineage-dependent differences were no longer observed. This reinforces the idea that Lhx2 forms part of a transient lineage-based mechanism that is only active during the formation of the barrel field. It is possible that lineage-dependent differences in Lhx2 expression persist into the second postnatal week and continue to coordinate activity-dependent processes in L4 excitatory neurons. Notably, this period is associated with widespread intralaminar plasticity within S1 (Erzurumlu and Gaspar 2012; Wen and Barth 2011). One possibility is that connections might be more likely to form if the postsynaptic neuron is expressing high levels of Lhx2. This could provide an explanation for the out-of-class connectivity bias observed between aIP-derived L4 neurons. In order to test this, the fLhx2 construct developed here could be used to increase Lhx2 expression only in aIP-derived L4 neurons, before repeating connectivity assays reported in previous work (Ellender et al. 2019).

As discussed in **Section 1.3.1**, establishing the relative contribution of neuronal-intrinsic factors and activity-dependent processes to the formation of fine-scale connectivity remains a topic of considerable debate (Zador 2019). Observations

that excitatory subnetworks are often defined by shared input supports an activity-dependent Hebbian view (Clopath et al. 2010; Hebb 2002). In contrast, the observation that non-random connectivity is present early in postnatal development suggests a dominant role for genetic programs (Perin et al. 2011; Song et al. 2005). The lineage-dependent expression of Lhx2 represents a reconciliatory mechanism, whereby different progenitor types specify distinct transcriptional programs to their progeny, which then determine how those progeny engage in subsequent activity-dependent processes.

### 7.3.4 Lineage-dependent circuitry is required for plasticity in response to sensory experience

Sensory-evoked plasticity requires an instructive cue to ensure that the strength of synaptic connections is adjusted appropriately in response to sensory experience. A number of studies have implicated higher-order thalamic inputs as critical regulators of sensory-evoked plasticity in the cortex (Audette et al. 2019; Gambino et al. 2014; Williams and Holtmaat 2019). This is thought to reflect the fact that higher-order nuclei integrate sensory information with other sources of inputs, and are therefore well-placed to deliver information regarding the context in which stimuli occur. Previous work in S1 has shown that POm inputs are required for the induction of sLTP in L2/3 pyramidal neurons (Gambino et al. 2014). Furthermore, coincident stimulation of L4 and POm axons is known to be sufficient to induce sLTP in acute brain slices (Williams and Holtmaat 2019). These observations led to the suggestion that the convergence of higher-order activity from POm, with first-order activity from VPM via L4, forms the basis of sLTP in L2/3. However, this does not account for the fact that L4 excitatory neurons receive convergent input from VPM and POm (see **Chapter 4**). As such, ascending connections from L4 to L2/3 also convey a degree of higher-order information, and it is unclear how this contributes to sLTP. Experiments in **Chapter 6** indicate that higher-order inputs to aIP-derived L4 neurons are necessary for sensory-evoked plasticity. This suggests that the induction of sLTP requires that complementary higher-order

information is delivered to different neuronal compartments and/or cortical layers.

As discussed in **Section 6.3**, the significance of this observation is intimately related to questions regarding the nature of information that is encoded by POm. It is increasingly clear that higher-order thalamic nuclei share connections with more-or-less every other part of the brain. As such, it is easier to implicate their involvement in a variety of different processes, rather than attribute a single overarching function (but see Rikhye et al. 2018). This problem is well illustrated by work that has explored the role of POm during self-generated whisker movements, known as whisking. The observation that activity in POm is upregulated by whisking led to the suggestion that the paralemniscal pathway is responsible for conveying motor information about self-generated whisker movements to the cortex (Ahissar et al. 2000; Alloway et al. 2004; Alloway 2008; Petersen 2007). In fact, this has been widely proposed to be the predominant function of POm during sensory processing. Generally, this was attributed to the fact that POm receives inputs from a number of motor areas, primary motor cortex and the facial motor nerves (Alloway et al. 2004; Groh et al. 2014; Lavallée et al. 2005; Lohse et al. 2018; Sobolewski et al. 2015; Theyel et al. 2010; Trageser and Keller 2004; Urbain and Deschênes 2007). However, a recent study found that inhibiting motor inputs to POm, including efferent inputs from S1, did not affect POm activity during whisking (Petty et al. 2021). Furthermore, activity in the higher-order visual thalamic nucleus was similarly upregulated during whisking. The authors conclude that what appears to be movement-related activity in POm, actually reflects the encoding of arousal, which is elevated during movement (Chapin 1986; McCormick et al. 2015; Murata and Colonnese 2018). This is consistent with the model discussed in **Section 7.3.2**, whereby POm is able to increase the excitability of the cortical circuit during periods of heightened arousal. More broadly, this suggests that the encoding of behavioural state is a general feature of higher order nuclei. Therefore, one interpretation of the data presented here is that with reduced higher-order input, aIP-derived L4 neurons can no longer spread arousal-related activity sufficiently throughout the local circuit. As discussed in **Section 7.3.3**,

this could be compounded by changes to intralaminar connectivity due to increased Lhx2 expression in the second postnatal week.

An important caveat relates to the recording conditions of these experiments, and the nature of the protocol used to induce sLTP. When animals are anaesthetised, they are clearly not sensitive to arousal information, aside from fluctuations in anaesthetic depth. Equally, given that RWS involves one min of repetitive stimulation, it does not seem like a physiologically relevant candidate for inducing plasticity in behaving animals. One possible explanation is that the RWS protocol gives rise to sustained activity in POm, similar to that observed during periods of heightened arousal. Interestingly, previous studies using RWS in L2/3 of S1 have not reported changes in spiking activity (Gambino et al. 2014). Rather, they report sLTP in terms of the increased amplitude of postsynaptic potentials following whisker deflection. A key distinction is that, in this thesis, the RWS protocol was adapted to incorporate the simultaneous deflection of multiple whiskers, rather than the single-whisker deflection reported previously. As such, it is likely that a larger proportion of S1 was activated during RWS, perhaps in a manner that is more representative of brain state change in an awake animal.

A second interpretation is that aIP-derived subnetworks are themselves specialised to exhibit plasticity. Conceptually, this could be an advantageous way for the cortical circuit to ensure that the initial weight ascribed to incoming sensory information remains constant, mediated by the hierarchical organisation of lineage-dependent subnetworks outlined in **Section 7.3.2**. In this scenario, first-order inputs might feed sensory information into a recurrent higher-order thalamocortical circuit that exhibits plastic change in response to sensory-experience, subject to contextual modulation. This idea is supported by previous work, discussed in **Section 7.3.1**, that has shown there is an inverse correlation between the coupling of a neuron and the degree to which it exhibits plasticity (Sweeney and Clopath 2020). In practice, this establishes an architecture whereby a highly plastic population of neurons are intermixed with a stable backbone that is relatively invariant to

sensory-experience, reminiscent of plastic and rigid assemblies that have been reported in the hippocampus (Grosmark and Buzsáki 2016). Given that aIP-derived L4 neurons were observed to be highly coupled, this suggests that they might be particularly susceptible to plastic change. This could be tested by optotagging aIP-derived L4 neurons and comparing the extent to which they exhibit sLTP compared to OP-derived L4 neurons. Importantly, understanding the extent to which aIP-derived neurons might act as a plasticity-promoting subnetwork across cortical circuits will require further exploration of whether interlaminar connections are also constrained by lineage, as predicted by earlier clonal work (Cadwell et al. 2020; Yu et al. 2009).

### 7.3.5 On the utility of lineage

A common approach in neuroscience is to think of the identity of neurons as being a collection of different phenotypic characteristics that confer some degree of functional specification. Indeed, the development of new anatomical, physiological, and molecular methods have facilitated the classification of neurons with increasing granularity, toward the creation of a unified taxonomy of cell types (Tasic et al. 2016; Tasic et al. 2018; Yao et al. 2021; Yuste et al. 2020; Zeng and Sanes 2017). One problem with this approach is that it is unclear at what point further granularity of classification becomes a barrier to understanding the function of different neuronal populations. This raises the question: what is the appropriate level at which to study the function of the cortex?

The work presented here shows that the stimulus response properties, morphology, sampling of thalamic inputs, and functional contribution to sensory-evoked plasticity of cortical neurons can all vary as a function of lineage, within a transcriptomically homonogeneous cell-type (Ellender et al. 2019; Tasic et al. 2018). This suggests that an approach based upon lineage may prove to be more effective than a reductionist, cell-by-cell, characterisation in the effort to understand how individual neurons contribute to different aspects of cortical function. Generally, the observation that lineage relationships appear to give rise to functionally specialised

circuits is consistent with the idea that progenitors serve to express evolutionarily conserved patterns of connectivity (Zador 2019). This is an attractive model, as it provides the means to consider how evolutionary pressure might act at a level that is directly relevant to behaviour.

## 7.4 Concluding remarks

The heterogeneity of excitatory cortical progenitor types give rise to the question: what does progenitor diversity contribute to cortical function? Whilst it is accepted that increased numbers of progenitors are responsible for the evolutionary expansion of the cortex, a number of recent studies have shown that different excitatory progenitor types convey specific functional attributes to their progeny, including their morphology, intrinsic electrical properties, and local synaptic connectivity. This thesis has established that lineage is also a critical determinant of how individual neurons sample thalamic inputs, suggesting that common developmental mechanisms govern local and long-range connectivity within the cortex, thereby generating functional excitatory subnetworks. Therefore, the emergence of diverse progenitor types does not only serve to expand cortical volume or increase the representation of postmitotic cell types, but also to generate distinct routes for information flow through the cortex.

# Bibliography

Accorsi-Mendonça, Daniela et al. (2007). "Urethane inhibits the GABAergic neurotransmission in the nucleus of the solitary tract of rat brain stem slices". eng. In: *American Journal of Physiology. Regulatory, Integrative and Comparative Physiology* 292.1, R396–402. DOI: 10.1152/ajpregu.00776.2005.

Agmon, A. et al. (1993). "Organized growth of thalamocortical axons from the deep tier of terminations into layer IV of developing mouse barrel cortex". en. In: *Journal of Neuroscience* 13.12, pp. 5365–5382. DOI: 10.1523/JNEUROSCI.13-12-05365.1993.

Ahissar, Ehud, Ronen Sosnik, and Sebastian Haidarliu (2000). "Transformation from temporal to rate coding in a somatosensory thalamocortical pathway". en. In: *Nature* 406.6793, pp. 302–306. DOI: 10.1038/35018568.

Alloway, Kevin D. (2008). "Information Processing Streams in Rodent Barrel Cortex: The Differential Functions of Barrel and Septal Circuits". In: *Cerebral Cortex* 18.5, pp. 979–989. DOI: 10.1093/cercor/bhm138.

Alloway, Kevin D., Mengliang Zhang, and Shubhodeep Chakrabarti (2004). "Septal columns in rodent barrel cortex: Functional circuits for modulating whisking behavior". en. In: *Journal of Comparative Neurology* 480.3, pp. 299–309. DOI: 10.1002/cne.20339.

Angevine, J. B. and R. L. Sidman (1961). "Autoradiographic Study of Cell Migration during Histogenesis of Cerebral Cortex in the Mouse". en. In: *Nature* 192.4804, pp. 766–768. DOI: 10.1038/192766b0.

Anthony, Todd E et al. (2004). "Radial Glia Serve as Neuronal Progenitors in All Regions of the Central Nervous System". en. In: *Neuron* 41.6, pp. 881–890. DOI: 10.1016/S0896-6273(04)00140-0.

Antic, Srdjan D. et al. (2010). “The decade of the dendritic NMDA spike”. en. In: *Journal of Neuroscience Research* 88.14, pp. 2991–3001. DOI: 10.1002/jnr.22444.

Arabzadeh, Ehsan, Erik Zorzin, and Mathew E. Diamond (2005). “Neuronal Encoding of Texture in the Whisker Sensory Pathway”. en. In: *PLOS Biology* 3.1, e17. DOI: 10.1371/journal.pbio.0030017.

Armstrong-James, M. and C. A. Callahan (1991). “Thalamo-cortical processing of vibrissal information in the rat. II. spatiotemporal convergence in the thalamic ventroposterior medial nucleus (VPm) and its relevance to generation of receptive fields of S1 cortical "barrel" neurones”. eng. In: *The Journal of Comparative Neurology* 303.2, pp. 211–224. DOI: 10.1002/cne.903030204.

Armstrong-James, M., K. Fox, and A. Das-Gupta (1992). “Flow of excitation within rat barrel cortex on striking a single vibrissa”. In: *Journal of Neurophysiology* 68.4, pp. 1345–1358. DOI: 10.1152/jn.1992.68.4.1345.

Armstrong-James, Michael and Kevin Fox (1987). “Spatiotemporal convergence and divergence in the rat S1 “Barrel” cortex”. en. In: *Journal of Comparative Neurology* 263.2. DOI: 10.1002/cne.902630209.

Aroniadou-Anderjaska, V and A Keller (1995). “LTP in the barrel cortex of adult rats”. eng. In: *Neuroreport* 6.17, pp. 2297–2300. DOI: 10.1097/00001756-199511270-00007.

Audette, N. J. et al. (2018). “POm Thalamocortical Input Drives Layer-Specific Microcircuits in Somatosensory Cortex”. en. In: *Cerebral Cortex* 28.4, pp. 1312–1328. DOI: 10.1093/cercor/bhx044.

Audette, N. J. et al. (2019). “Rapid Plasticity of Higher-Order Thalamocortical Inputs during Sensory Learning”. eng. In: *Neuron* 103.2, 277–291.e4. DOI: 10.1016/j.neuron.2019.04.037.

Auladell, Carme et al. (2000). “The early development of thalamocortical and corticothalamic projections in the mouse”. en. In: *Anatomy and Embryology* 201.3, pp. 169–179. DOI: 10.1007/PL00008238.

Barbe, M F and P Levitt (1992). "Attraction of specific thalamic input by cerebral grafts depends on the molecular identity of the implant." In: *Proceedings of the National Academy of Sciences* 89.9, pp. 3706–3710. DOI: 10.1073/pnas.89.9.3706.

Barth, Alison L. and James F. A. Poulet (2012). "Experimental evidence for sparse firing in the neocortex". en. In: *Trends in Neurosciences* 35.6, pp. 345–355. DOI: 10.1016/j.tins.2012.03.008.

Barthó, Peter et al. (2004). "Characterization of Neocortical Principal Cells and Interneurons by Network Interactions and Extracellular Features". In: *Journal of Neurophysiology* 92.1, pp. 600–608. DOI: 10.1152/jn.01170.2003.

Baumgart, Jan and Nadine Grebe (2015). "C57BL/6-specific conditions for efficient in utero electroporation of the central nervous system". eng. In: *Journal of Neuroscience Methods* 240, pp. 116–124. DOI: 10.1016/j.jneumeth.2014.11.004.

Bender, D. B. (1983). "Visual activation of neurons in the primate pulvinar depends on cortex but not colliculus". en. In: *Brain Research* 279.1, pp. 258–261. DOI: 10.1016/0006-8993(83)90188-9.

Bicks, Lucy K. et al. (2015). "Prefrontal Cortex and Social Cognition in Mouse and Man". In: *Frontiers in Psychology* 6.

Binzegger, Tom, Rodney J. Douglas, and Kevan A. C. Martin (2004). "A Quantitative Map of the Circuit of Cat Primary Visual Cortex". en. In: *Journal of Neuroscience* 24.39, pp. 8441–8453. DOI: 10.1523/JNEUROSCI.1400-04.2004.

Bishop, Kathie M., Guy Goudreau, and Dennis D. M. O'Leary (2000). "Regulation of Area Identity in the Mammalian Neocortex by Emx2 and Pax6". In: *Science* 288.5464, pp. 344–349. DOI: 10.1126/science.288.5464.344.

Bitzenhofer, Sebastian H., Joachim Ahlbeck, and Ileana L. Hanganu-Opatz (2017). "Methodological Approach for Optogenetic Manipulation of Neonatal Neuronal Networks". In: *Frontiers in Cellular Neuroscience* 11, p. 239. DOI: 10.3389/fncel.2017.00239.

Borgdorff, Aren J., James F. A. Poulet, and Carl C. H. Petersen (2007). "Facilitating Sensory Responses in Developing Mouse Somatosensory Barrel Cortex". In: *Journal of Neurophysiology* 97.4, pp. 2992–3003. DOI: 10.1152/jn.00013.2007.

Bota, Mihail, Olaf Sporns, and Larry W. Swanson (2015). "Architecture of the cerebral cortical association connectome underlying cognition". In: *Proceedings of the National Academy of Sciences* 112.16, E2093–E2101. DOI: 10.1073/pnas.1504394112.

Bota, Mihail and Larry W. Swanson (2007). "The neuron classification problem". en. In: *Brain Research Reviews* 56.1, pp. 79–88. DOI: 10.1016/j.brainresrev.2007.05.005.

Braitenberg, Valentino and Almut Schüz (1998). *Cortex: Statistics and Geometry of Neuronal Connectivity*. en. Berlin, Heidelberg: Springer. DOI: 10.1007/978-3-662-03733-1.

Brodmann, Korbinian (1909). "Vergleichende Lokalisationslehre der Grosshirnrinde in ihren Prinzipien dargestellt auf Grund des Zellenbaues / [K. Brodmann]". In.

Brown, Solange P. and Shaul Hestrin (2009). "Intracortical circuits of pyramidal neurons reflect their long-range axonal targets". en. In: *Nature* 457.7233, pp. 1133–1136. DOI: 10.1038/nature07658.

Bruno, Randy M. and Daniel J. Simons (2002). "Feedforward Mechanisms of Excitatory and Inhibitory Cortical Receptive Fields". en. In: *The Journal of Neuroscience* 22.24, pp. 10966–10975. DOI: 10.1523/JNEUROSCI.22-24-10966.2002.

Buchan, Matthew J. (2020). "A subpopulation of L6b neurons provides driver-like input to the posteromedial thalamus". en. In: *The Journal of Physiology* 598.23. DOI: 10.1113/JP280472.

Buchan, Matthew J. and James M. Rowland (2018). "Stimulation of Individual Neurons Is Sufficient to Influence Sensory-Guided Decision-Making". In: *The Journal of Neuroscience* 38.30, pp. 6609–6611. DOI: 10.1523/JNEUROSCI.1026-18.2018.

Buchan, Matthew J. et al. (2021). "Diverse roles for the posteromedial thalamus in sensory-evoked cortical plasticity". In: *Journal of Neurophysiology* 125.2, pp. 537–539. DOI: 10.1152/jn.00291.2020.

Buckner, Randy L. and Fenna M. Krienen (2013). "The evolution of distributed association networks in the human brain". en. In: *Trends in Cognitive Sciences*. Special Issue: The Connectome 17.12, pp. 648–665. DOI: 10.1016/j.tics.2013.09.017.

Bulchand, S., L. Subramanian, and S. Tole (2003). "Dynamic spatiotemporal expression of LIM genes and cofactors in the embryonic and postnatal cerebral cortex". English. In: *Developmental Dynamics* 226.3, pp. 460–469. DOI: 10.1002/dvdy.10235.

Bureau, Ingrid, Francisca von Saint Paul, and Karel Svoboda (2006). "Interdigitated Paralemniscal and Lemniscal Pathways in the Mouse Barrel Cortex". en. In: *PLoS Biology* 4.12. Ed. by Ford Ebner, e382. DOI: 10.1371/journal.pbio.0040382.

Buzsáki, György and Kenji Mizuseki (2014). "The log-dynamic brain: how skewed distributions affect network operations". en. In: *Nature Reviews Neuroscience* 15.4, pp. 264–278. DOI: 10.1038/nrn3687.

Cadwell, Cathryn R et al. (2020). "Cell type composition and circuit organization of clonally related excitatory neurons in the juvenile mouse neocortex". en. In: *eLife* 9, e52951. DOI: 10.7554/eLife.52951.

Cajal, S. Ramon y and L. Azoulay (1955). "Histologie du systeme nerveux de l'homme et des vertebres". es. In: *Histologie du systeme nerveux de l'homme et des vertebres*, pp. 2v–2v.

Casanova, C. et al. (2001). "Chapter 5 Higher-order motion processing in the pulvinar". en. In: *Progress in Brain Research*. Vol. 134. Vision: From Neurons to Cognition. Elsevier, pp. 71–82. DOI: 10.1016/S0079-6123(01)34006-2.

Castejon, Carlos, Natali Barros-Zulaica, and Angel Nuñez (2016). "Control of Somatosensory Cortical Processing by Thalamic Posterior Medial Nucleus: A New

Role of Thalamus in Cortical Function". eng. In: *PloS One* 11.1, e0148169. DOI: 10.1371/journal.pone.0148169.

Castro-Alamancos, M. A., J. P. Donoghue, and B. W. Connors (1995). "Different forms of synaptic plasticity in somatosensory and motor areas of the neocortex". en. In: *Journal of Neuroscience* 15.7, pp. 5324–5333. DOI: 10.1523/JNEUROSCI.15-07-05324.1995.

Castro-alamancos, MANUEL A. and BARRY W. Connors (1997). "THALAMOCORTICAL SYNAPSES". en. In: *Progress in Neurobiology* 51.6, pp. 581–606. DOI: 10.1016/S0301-0082(97)00002-6.

Cauller, L. (1995). "Layer I of primary sensory neocortex: where top-down converges upon bottom-up". eng. In: *Behavioural Brain Research* 71.1-2, pp. 163–170. DOI: 10.1016/0166-4328(95)00032-1.

Chalupa, Leo M., Harvey Anchel, and Donald B. Lindsley (1972). "Visual input to the pulvinar via lateral geniculate, superior colliculus and visual cortex in the cat". en. In: *Experimental Neurology* 36.3, pp. 449–462. DOI: 10.1016/0014-4886(72)90005-2.

Chapin, J. K. (1986). "Laminar differences in sizes, shapes, and response profiles of cutaneous receptive fields in the rat SI cortex". en. In: *Experimental Brain Research* 62.3, pp. 549–559. DOI: 10.1007/BF00236033.

Chiaia, Nicolas L. et al. (1991). "Thalamic processing of vibrissal information in the rat: II. Morphological and functional properties of medial ventral posterior nucleus and posterior nucleus neurons". en. In: *The Journal of Comparative Neurology* 314.2, pp. 217–236. DOI: 10.1002/cne.903140203.

Chou, Shen-Ju and Dennis D. M. O'Leary (2013). "Role for Lhx2 in corticogenesis through regulation of progenitor differentiation". en. In: *Molecular and Cellular Neuroscience*. RNA and splicing regulation in neurodegeneration 56, pp. 1–9. DOI: 10.1016/j.mcn.2013.02.006.

Chou, Shen-Ju and Shubha Tole (2019). "Lhx2, an evolutionarily conserved, multifunctional regulator of forebrain development". en. In: *Brain Research*. Emerging roles of transcription factors in the brain: from developmental programming to

neuronal reprogramming 1705, pp. 1–14. DOI: 10.1016/j.brainres.2018.02.046.

Chou, Shen-Ju et al. (2009). "Lhx2 specifies regional fate in Emx1 lineage of telencephalic progenitors generating cerebral cortex". en. In: *Nature Neuroscience* 12.11, pp. 1381–1389. DOI: 10.1038/nn.2427.

Chéreau, Ronan et al. (2021). "Circuit mechanisms for cortical plasticity and learning". en. In: *Seminars in Cell & Developmental Biology*. DOI: 10.1016/j.semcdb.2021.07.012.

Clascá, Francisco, Pablo Rubio-Garrido, and Denis Jabaudon (2012). "Unveiling the diversity of thalamocortical neuron subtypes". en. In: *European Journal of Neuroscience* 35.10. DOI: 10.1111/j.1460-9568.2012.08033.x.

Clopath, Claudia et al. (2010). "Connectivity reflects coding: a model of voltage-based STDP with homeostasis". en. In: *Nature Neuroscience* 13.3, pp. 344–352. DOI: 10.1038/nn.2479.

Collins, David P. and Paul G. Anastasiades (2019). "Cellular Specificity of Cortico-Thalamic Loops for Motor Planning". en. In: *Journal of Neuroscience* 39.14, pp. 2577–2580. DOI: 10.1523/JNEUROSCI.2964-18.2019.

Costa, Marcos R. and Ulrich Müller (2015). "Specification of excitatory neurons in the developing cerebral cortex: progenitor diversity and environmental influences". In: *Frontiers in Cellular Neuroscience* 8.

Crabtree, John W. (2018). "Functional Diversity of Thalamic Reticular Subnetworks". In: *Frontiers in Systems Neuroscience* 12.

Cruikshank, Scott J. et al. (2010). "Pathway-Specific Feedforward Circuits between Thalamus and Neocortex Revealed by Selective Optical Stimulation of Axons". en. In: *Neuron* 65.2, pp. 230–245. DOI: 10.1016/j.neuron.2009.12.025.

Datwani, Akash et al. (2002). "Lesion-Induced Thalamocortical Axonal Plasticity in the S1 Cortex Is Independent of NMDA Receptor Function in Excitatory Cortical Neurons". en. In: *Journal of Neuroscience* 22.21, pp. 9171–9175. DOI: 10.1523/JNEUROSCI.22-21-09171.2002.

Diamond, Mathew E. et al. (1992). "Somatic sensory responses in the rostral sector of the posterior group (POm) and in the ventral posterior medial nucleus (VPM) of the rat thalamus: Dependence on the barrel field cortex". en. In: *The Journal of Comparative Neurology* 319.1, pp. 66–84. DOI: 10.1002/cne.903190108.

Donoghue, Maria J. and Pasko Rakic (1999). "Molecular Evidence for the Early Specification of Presumptive Functional Domains in the Embryonic Primate Cerebral Cortex". en. In: *Journal of Neuroscience* 19.14, pp. 5967–5979. DOI: 10.1523/JNEUROSCI.19-14-05967.1999.

Douglas, Rodney J. and Kevan A.C. Martin (2004). "Neuronal Circuits of the Neocortex". In: *Annual Review of Neuroscience* 27.1. DOI: 10.1146/annurev.neuro.27.070203.144152.

Douglas, Rodney J., Kevan A.C. Martin, and David Whitteridge (1989). "A Canonical Microcircuit for Neocortex". In: *Neural Computation* 1.4, pp. 480–488. DOI: 10.1162/neco.1989.1.4.480.

Durham, Dianne and Thomas A. Woolsey (1984). "Effects of neonatal whisker lesions on mouse central trigeminal pathways". fr. In: *Journal of Comparative Neurology* 223.3. DOI: 10.1002/cne.902230308.

Egger, Veronica, Thomas Nevian, and Randy M. Bruno (2008). "Subcolumnar Dendritic and Axonal Organization of Spiny Stellate and Star Pyramid Neurons within a Barrel in Rat Somatosensory Cortex". In: *Cerebral Cortex* 18.4, pp. 876–889. DOI: 10.1093/cercor/bhm126.

El-Boustani, Sami et al. (2020). "Anatomically and functionally distinct thalamocortical inputs to primary and secondary mouse whisker somatosensory cortices". en. In: *Nature Communications* 11.1, p. 3342. DOI: 10.1038/s41467-020-17087-7.

Ellender, Tommas J. et al. (2019). "Embryonic progenitor pools generate diversity in fine-scale excitatory cortical subnetworks". en. In: *Nature Communications* 10.1, p. 5224. DOI: 10.1038/s41467-019-13206-1.

Emmers, Raimond (1965). "Organization of the first and the second somesthetic regions (SI and SII) in the rat thalamus". en. In: *Journal of Comparative Neurology* 124.2. DOI: 10.1002/cne.901240207.

Englund, Chris et al. (2005). "Pax6, Tbr2, and Tbr1 Are Expressed Sequentially by Radial Glia, Intermediate Progenitor Cells, and Postmitotic Neurons in Developing Neocortex". en. In: *Journal of Neuroscience* 25.1, pp. 247–251. DOI: 10.1523/JNEUROSCI.2899-04.2005.

Erzurumlu, Reha S., Carolyn A. Bates, and Herbert P. Killackey (1980). "Differential organization of thalamic projection cells in the brain stem trigeminal complex of the rat". en. In: *Brain Research* 198.2, pp. 427–433. DOI: 10.1016/0006-8993(80)90756-8.

Erzurumlu, Reha S. and Patricia Gaspar (2012). "Development and critical period plasticity of the barrel cortex". en. In: *European Journal of Neuroscience* 35.10, pp. 1540–1553. DOI: 10.1111/j.1460-9568.2012.08075.x.

– (2020). "How the Barrel Cortex Became a Working Model for Developmental Plasticity: A Historical Perspective". en. In: *Journal of Neuroscience* 40.34, pp. 6460–6473. DOI: 10.1523/JNEUROSCI.0582-20.2020.

Erzurumlu, Reha S and Peter C Kind (2001). "Neural activity: sculptor of 'barrels' in the neocortex". en. In: *Trends in Neurosciences* 24.10, pp. 589–595. DOI: 10.1016/S0166-2236(00)01958-5.

Espinosa, J. Sebastian et al. (2009). "Uncoupling Dendrite Growth and Patterning: Single-Cell Knockout Analysis of NMDA Receptor 2B". en. In: *Neuron* 62.2, pp. 205–217. DOI: 10.1016/j.neuron.2009.03.006.

Estebanez, Luc et al. (2018). "Representation of Tactile Scenes in the Rodent Barrel Cortex". en. In: *Neuroscience*. Barrel Cortex Function 368, pp. 81–94. DOI: 10.1016/j.neuroscience.2017.08.039.

Feldman, Daniel E (2000). "Timing-Based LTP and LTD at Vertical Inputs to Layer II/III Pyramidal Cells in Rat Barrel Cortex". en. In: *Neuron* 27.1, pp. 45–56. DOI: 10.1016/S0896-6273(00)00008-8.

Feldman, Daniel E. and Michael Brecht (2005). "Map Plasticity in Somatosensory Cortex". In: *Science* 310.5749, pp. 810–815. DOI: 10.1126/science.1115807.

Feldmeyer, Dirk (2012). "Excitatory neuronal connectivity in the barrel cortex". eng. In: *Frontiers in Neuroanatomy* 6, p. 24. DOI: 10.3389/fnana.2012.00024.

Felleman, D J and D C Van Essen (1991). "Distributed hierarchical processing in the primate cerebral cortex". eng. In: *Cerebral cortex (New York, N.Y.* 1.1, pp. 1–47. DOI: 10.1093/cercor/1.1.1-a.

Fenno, Lief E. et al. (2014). "INTRSECT: single-component targeting of cells using multiple-feature Boolean logic". In: *Nature methods* 11.7, pp. 763–772. DOI: 10.1038/nmeth.2996.

Ferster, David, Sooyoung Chung, and Heidi Wheat (1996). "Orientation selectivity of thalamic input to simple cells of cat visual cortex". en. In: *Nature* 380.6571, pp. 249–252. DOI: 10.1038/380249a0.

Fishell, Gord and Nathaniel Heintz (2013). "The Neuron Identity Problem: Form Meets Function". en. In: *Neuron* 80.3, pp. 602–612. DOI: 10.1016/j.neuron.2013.10.035.

Florio, Marta and Wieland B. Huttner (2014). "Neural progenitors, neurogenesis and the evolution of the neocortex". In: *Development* 141.11, pp. 2182–2194. DOI: 10.1242/dev.090571.

Fox, Kevin et al. (2003). "The Origin of Cortical Surround Receptive Fields Studied in the Barrel Cortex". en. In: *The Journal of Neuroscience* 23.23, pp. 8380–8391. DOI: 10.1523/JNEUROSCI.23-23-08380.2003.

Franco, S. J. et al. (2012). "Fate-Restricted Neural Progenitors in the Mammalian Cerebral Cortex". en. In: *Science* 337.6095, pp. 746–749. DOI: 10.1126/science.1223616.

Franco, Santos J. and Ulrich Müller (2013). "Shaping Our Minds: Stem and Progenitor Cell Diversity in the Mammalian Neocortex". en. In: *Neuron* 77.1, pp. 19–34. DOI: 10.1016/j.neuron.2012.12.022.

Frangeul, Laura et al. (2014). "Specific activation of the paralemniscal pathway during nociception". en. In: *European Journal of Neuroscience* 39.9. DOI: 10.1111/ejn.12524.

Frey, Uwe and Richard G. M. Morris (1997). "Synaptic tagging and long-term potentiation". en. In: *Nature* 385.6616, pp. 533–536. DOI: 10.1038/385533a0.

Fukuchi-Shimogori, Tomomi and Elizabeth A. Grove (2001). "Neocortex Patterning by the Secreted Signaling Molecule FGF8". In: *Science* 294.5544, pp. 1071–1074. DOI: 10.1126/science.1064252.

Gal, J. S. (2006). "Molecular and Morphological Heterogeneity of Neural Precursors in the Mouse Neocortical Proliferative Zones". en. In: *Journal of Neuroscience* 26.3, pp. 1045–1056. DOI: 10.1523/JNEUROSCI.4499-05.2006.

Gambino, Frédéric et al. (2014). "Sensory-evoked LTP driven by dendritic plateau potentials in vivo". en. In: *Nature* 515.7525, pp. 116–119. DOI: 10.1038/nature13664.

Gao, Pan-Pan et al. (1998). "Regulation of thalamic neurite outgrowth by the Eph ligand ephrin-A5: Implications in the development of thalamocortical projections". In: *Proceedings of the National Academy of Sciences* 95.9, pp. 5329–5334. DOI: 10.1073/pnas.95.9.5329.

Gao, Peng et al. (2014). "Deterministic progenitor behavior and unitary production of neurons in the neocortex". eng. In: *Cell* 159.4, pp. 775–788. DOI: 10.1016/j.cell.2014.10.027.

Garcia-Junco-Clemente, Pablo et al. (2017). "An inhibitory pull–push circuit in frontal cortex". en. In: *Nature Neuroscience* 20.3, pp. 389–392. DOI: 10.1038/nn.4483.

Gilbert, Charles D. and Wu Li (2013). "Top-down influences on visual processing". eng. In: *Nature Reviews. Neuroscience* 14.5, pp. 350–363. DOI: 10.1038/nrn3476.

Gillon, Colleen J. et al. (2021). *Learning from unexpected events in the neocortical microcircuit*. en. Tech. rep. bioRxiv, p. 2021.01.15.426915. DOI: 10.1101/2021.01.15.426915.

Glazewski, Stanislaw et al. (1998). "Long-term potentiation in vivo in layers II/III of rat barrel cortex". en. In: *Neuropharmacology* 37.4, pp. 581–592. DOI: 10.1016/S0028-3908(98)00039-2.

Goetz, Lea, Arnd Roth, and Michael Häusser (2021). "Active dendrites enable strong but sparse inputs to determine orientation selectivity". eng. In: *Proceedings of the National Academy of Sciences of the United States of America* 118.30, e2017339118. DOI: 10.1073/pnas.2017339118.

Greig, Luciano Custo et al. (2013). "Molecular logic of neocortical projection neuron specification, development and diversity". en. In: *Nature Reviews Neuroscience* 14.11, pp. 755–769. DOI: 10.1038/nrn3586.

Groh, Alexander et al. (2014). "Convergence of Cortical and Sensory Driver Inputs on Single Thalamocortical Cells". In: *Cerebral Cortex* 24.12, pp. 3167–3179. DOI: 10.1093/cercor/bht173.

Grosmark, Andres D. and György Buzsáki (2016). "Diversity in neural firing dynamics supports both rigid and learned hippocampal sequences". In: *Science* 351.6280, pp. 1440–1443. DOI: 10.1126/science.aad1935.

Guillamon-Vivancos, Teresa et al. (2019). "Distinct Neocortical Progenitor Lineages Fine-tune Neuronal Diversity in a Layer-specific Manner". en. In: *Cerebral Cortex* 29.3, pp. 1121–1138. DOI: 10.1093/cercor/bhy019.

Guo, KuangHua et al. (2018). "Anterolateral motor cortex connects with a medial subdivision of ventromedial thalamus through cell-type-specific circuits, forming an excitatory thalamo-cortico-thalamic loop via layer 1 apical tuft dendrites of layer 5B pyramidal tract type neurons". en. In: *Journal of Neuroscience*. DOI: 10.1523/JNEUROSCI.1333-18.2018.

Guo, KuangHua et al. (2020). "Cortico-Thalamo-Cortical Circuits of Mouse Forelimb S1 Are Organized Primarily as Recurrent Loops". In: *The Journal of Neuroscience* 40.14, pp. 2849–2858. DOI: 10.1523/JNEUROSCI.2277-19.2020.

Gămănuţ, Răzvan et al. (2018). "The Mouse Cortical Connectome, Characterized by an Ultra-Dense Cortical Graph, Maintains Specificity by Distinct Connectivity Profiles". en. In: *Neuron* 97.3, 698–715.e10. DOI: 10.1016/j.neuron.2017.12.037.

Hage, Steffen R. and Andreas Nieder (2016). "Dual Neural Network Model for the Evolution of Speech and Language". en. In: *Trends in Neurosciences* 39.12, pp. 813–829. DOI: 10.1016/j.tins.2016.10.006.

Halassa, Michael M. and Sabine Kastner (2017). "Thalamic functions in distributed cognitive control". en. In: *Nature Neuroscience* 20.12, pp. 1669–1679. DOI: 10.1038/s41593-017-0020-1.

Halassa, Michael M. and S. Murray Sherman (2019). "Thalamocortical Circuit Motifs: A General Framework". en. In: *Neuron* 103.5, pp. 762–770. DOI: 10.1016/j.neuron.2019.06.005.

Hansen, David V. et al. (2010). "Neurogenic radial glia in the outer subventricular zone of human neocortex". en. In: *Nature* 464.7288, pp. 554–561. DOI: 10.1038/nature08845.

Harris, Julie A. et al. (2019). "Hierarchical organization of cortical and thalamic connectivity". In: *Nature* 575.7781, pp. 195–202. DOI: 10.1038/s41586-019-1716-z.

Harris, Kenneth D. and Thomas D. Mrsic-Flogel (2013). "Cortical connectivity and sensory coding". en. In: *Nature* 503.7474, pp. 51–58. DOI: 10.1038/nature12654.

Harris, Kenneth D. and Gordon M. G. Shepherd (2015). "The neocortical circuit: themes and variations". en. In: *Nature Neuroscience* 18.2, pp. 170–181. DOI: 10.1038/nn.3917.

Hattox, Alexis M. and Sacha B. Nelson (2007). "Layer V neurons in mouse cortex projecting to different targets have distinct physiological properties". eng. In: *Journal of Neurophysiology* 98.6, pp. 3330–3340. DOI: 10.1152/jn.00397.2007.

Haubensak, Wulf et al. (2004). "Neurons arise in the basal neuroepithelium of the early mammalian telencephalon: A major site of neurogenesis". In: *Proceedings*

*of the National Academy of Sciences* 101.9, pp. 3196–3201. DOI: 10.1073/pnas.0308600100.

Hebb, D. O. (2002). *The Organization of Behavior: A Neuropsychological Theory*. New York: Psychology Press. DOI: 10.4324/9781410612403.

Hellwig, Bernhard (2000). "A quantitative analysis of the local connectivity between pyramidal neurons in layers 2/3 of the rat visual cortex". en. In: *Biological Cybernetics* 82.2, pp. 111–121. DOI: 10.1007/PL00007964.

Hellwig, Bernhard, Almut Schüz, and Ad Aertsen (1994). "Synapses on axon collaterals of pyramidal cells are spaced at random intervals: a Golgi study in the mouse cerebral cortex". en. In: *Biological Cybernetics* 71.1, pp. 1–12. DOI: 10.1007/BF00198906.

Herkenham, Miles (1986). "New Perspectives on the Organization and Evolution of Nonspecific Thalamocortical Projections". en. In: *Sensory-Motor Areas and Aspects of Cortical Connectivity*. Ed. by Edward G. Jones and Alan Peters. Cerebral Cortex. Boston, MA: Springer US, pp. 403–445. DOI: 10.1007/978-1-4613-2149-1_11.

Hildebrandt, K. Jannis, Maneesh Sahani, and Jennifer F. Linden (2017). "The Impact of Anesthetic State on Spike-Sorting Success in the Cortex: A Comparison of Ketamine and Urethane Anesthesia". In: *Frontiers in Neural Circuits* 11.

Hong, Sungho, Blaise Agüera y Arcas, and Adrienne L. Fairhall (2007). "Single Neuron Computation: From Dynamical System to Feature Detector". In: *Neural Computation* 19.12, pp. 3133–3172. DOI: 10.1162/neco.2007.19.12.3133.

Hooks, B. M. et al. (2011). "Laminar Analysis of Excitatory Local Circuits in Vibrissal Motor and Sensory Cortical Areas". en. In: *PLOS Biology* 9.1, e1000572. DOI: 10.1371/journal.pbio.1000572.

Hooser, Stephen D. Van et al. (2006). "Lack of Patchy Horizontal Connectivity in Primary Visual Cortex of a Mammal without Orientation Maps". en. In: *Journal of Neuroscience* 26.29, pp. 7680–7692. DOI: 10.1523/JNEUROSCI.0108-06.2006.

Hsu, Lea Chia-Ling et al. (2015). "Lhx2 regulates the timing of -catenin-dependent cortical neurogenesis". In: *Proceedings of the National Academy of Sciences* 112.39, pp. 12199–12204. DOI: 10.1073/pnas.1507145112.

Huang, Z. Josh (2014). "Toward a Genetic Dissection of Cortical Circuits in the Mouse". en. In: *Neuron* 83.6, pp. 1284–1302. DOI: 10.1016/j.neuron.2014.08.041.

Hubel, D. H. and T. N. Wiesel (1962). "Receptive fields, binocular interaction and functional architecture in the cat's visual cortex". en. In: *The Journal of Physiology* 160.1, pp. 106–154. DOI: 10.1113/jphysiol.1962.sp006837.

Huilgol, Dhananjay et al. (2022). *Direct and indirect neurogenesis generate a mosaic of distinct glutamatergic projection neuron types and cortical subnetworks*. en. Tech. rep. bioRxiv, p. 2022.03.13.484161. DOI: 10.1101/2022.03.13.484161.

Ibrahim, Leena A. et al. (2016). "Cross-Modality Sharpening of Visual Cortical Processing through Layer-1-Mediated Inhibition and Disinhibition". en. In: *Neuron* 89.5, pp. 1031–1045. DOI: 10.1016/j.neuron.2016.01.027.

Inan, Melis and Michael C. Crair (2007). "Development of Cortical Maps: Perspectives From the Barrel Cortex". en. In: *The Neuroscientist* 13.1. DOI: 10.1177/1073858406296257.

Ince-Dunn, Gulayse et al. (2006). "Regulation of Thalamocortical Patterning and Synaptic Maturation by NeuroD2". en. In: *Neuron* 49.5, pp. 683–695. DOI: 10.1016/j.neuron.2006.01.031.

Ito, M. (1988). "Response properties and topography of vibrissa-sensitive VPM neurons in the rat". In: *Journal of Neurophysiology* 60.4, pp. 1181–1197. DOI: 10.1152/jn.1988.60.4.1181.

Iwasato, Takuji et al. (2000). "Cortex-restricted disruption of NMDAR1 impairs neuronal patterns in the barrel cortex". en. In: *Nature* 406.6797, pp. 726–731. DOI: 10.1038/35021059.

Jacquin, M. F., M. Barcia, and R. W. Rhoades (1989). "Structure-function relationships in rat brainstem subnucleus interpolaris: IV. Projection neurons". eng.

In: *The Journal of Comparative Neurology* 282.1, pp. 45–62. DOI: 10.1002/cne.902820105.

Jaramillo, Jorge, Jorge F. Mejias, and Xiao-Jing Wang (2019). "Engagement of Pulvino-cortical Feedforward and Feedback Pathways in Cognitive Computations". en. In: *Neuron* 101.2, 321–336.e9. DOI: 10.1016/j.neuron.2018.11.023.

Jiang, Xiaolong et al. (2015). "Principles of connectivity among morphologically defined cell types in adult neocortex". In: *Science (New York, N.Y.)* 350.6264, aac9462. DOI: 10.1126/science.aac9462.

Jones, Edward G. (1985). "Principles of Thalamic Organization". en. In: *The Thalamus*. Ed. by Edward G. Jones. Boston, MA: Springer US, pp. 85–149. DOI: 10.1007/978-1-4615-1749-8_3.

Jones, Lauren M. et al. (2004). "Robust Temporal Coding in the Trigeminal System". In: *Science* 304.5679, pp. 1986–1989. DOI: 10.1126/science.1097779.

Jouhanneau, Jean-Sébastien et al. (2014). "Cortical fosGFP Expression Reveals Broad Receptive Field Excitatory Neurons Targeted by POm". en. In: *Neuron* 84.5, pp. 1065–1078. DOI: 10.1016/j.neuron.2014.10.014.

Kampa, Björn M., Johannes J. Letzkus, and Greg J. Stuart (2006). "Cortical feedforward networks for binding different streams of sensory information". en. In: *Nature Neuroscience* 9.12, pp. 1472–1473. DOI: 10.1038/nn1798.

Kanold, Patrick O. and Heiko J. Luhmann (2010). "The Subplate and Early Cortical Circuits". In: *Annual Review of Neuroscience* 33.1, pp. 23–48. DOI: 10.1146/annurev-neuro-060909-153244.

Kashani, Amir H. et al. (2006). "Calcium Activation of the LMO4 Transcription Complex and Its Role in the Patterning of Thalamocortical Connections". en. In: *Journal of Neuroscience* 26.32, pp. 8398–8408. DOI: 10.1523/JNEUROSCI.0618-06.2006.

Kasper, Ekkehard M. et al. (1994). "Pyramidal neurons in layer 5 of the rat visual cortex. I. Correlation among cell morphology, intrinsic electrophysiological properties, and axon targets". fr. In: *Journal of Comparative Neurology* 339.4. DOI: 10.1002/cne.903390402.

Keller, Andreas J., Morgane M. Roth, and Massimo Scanziani (2020). "Feedback generates a second receptive field in neurons of the visual cortex". en. In: *Nature* 582.7813, pp. 545–549. DOI: 10.1038/s41586-020-2319-4.

Kelly, Larry R. et al. (2003). "Ultrastructure and synaptic targets of tectothalamic terminals in the cat lateral posterior nucleus". en. In: *Journal of Comparative Neurology* 464.4. DOI: 10.1002/cne.10800.

Kerr, Jason N. D. et al. (2007). "Spatial Organization of Neuronal Population Responses in Layer 2/3 of Rat Barrel Cortex". en. In: *Journal of Neuroscience* 27.48, pp. 13316–13328. DOI: 10.1523/JNEUROSCI.2210-07.2007.

Kichula, Elizabeth A. and George W. Huntley (2008). "Developmental and comparative aspects of posterior medial thalamocortical innervation of the barrel cortex in mice and rats". eng. In: *The Journal of Comparative Neurology* 509.3, pp. 239–258. DOI: 10.1002/cne.21690.

Kim, Euiseok J. et al. (2015). "Three Types of Cortical Layer 5 Neurons That Differ in Brain-wide Connectivity and Function". en. In: *Neuron* 88.6, pp. 1253–1267. DOI: 10.1016/j.neuron.2015.11.002.

Kim, Mean-Hwan et al. (2018). "Segregated Subnetworks of Intracortical Projection Neurons in Primary Visual Cortex". en. In: *Neuron* 100.6, 1313–1321.e6. DOI: 10.1016/j.neuron.2018.10.023.

Kim, Uhnoh and Ford F. Ebner (1999). "Barrels and septa: Separate circuits in rat barrel field cortex". en. In: *Journal of Comparative Neurology* 408.4, pp. 489–505. DOI: 10.1002/(SICI)1096-9861(19990614)408:4<489::AID-CNE4>3.0.CO;2-E.

Kirchgessner, Megan A., Alexis D. Franklin, and Edward M. Callaway (2020). "Context-dependent and dynamic functional influence of corticothalamic pathways to first- and higher-order visual thalamus". en. In: *Proceedings of the National Academy of Sciences* 117.23, pp. 13066–13077. DOI: 10.1073/pnas.2002080117.

Ko, Ho et al. (2011). "Functional specificity of local synaptic connections in neocortical networks". en. In: *Nature* 473.7345, pp. 87–91. DOI: 10.1038/nature09880.

Koralek, Katherine-Ann, Karl F. Jensen, and Herbert P. Killackey (1988). "Evidence for two complementary patterns of thalamic input to the rat somatosensory cortex". en. In: *Brain Research* 463.2, pp. 346–351. DOI: 10.1016/0006-8993(88)90408-8.

Kowalczyk, Tom et al. (2009). "Intermediate Neuronal Progenitors (Basal Progenitors) Produce Pyramidal–Projection Neurons for All Layers of Cerebral Cortex". en. In: *Cerebral Cortex* 19.10, pp. 2439–2450. DOI: 10.1093/cercor/bhn260.

Kriegstein, Arnold, Stephen Noctor, and Verónica Martínez-Cerdeño (2006). "Patterns of neural stem and progenitor cell division may underlie evolutionary cortical expansion". en. In: *Nature Reviews Neuroscience* 7.11, pp. 883–890. DOI: 10.1038/nrn2008.

Krubitzer, Leah A. and Tony J. Prescott (2018). "The Combinatorial Creature: Cortical Phenotypes within and across Lifetimes". en. In: *Trends in Neurosciences*. Special Issue: Time in the Brain 41.10, pp. 744–762. DOI: 10.1016/j.tins.2018.08.002.

Kwegyir-Afful, E. E. (2005). "The Role of Thalamic Inputs in Surround Receptive Fields of Barrel Neurons". en. In: *Journal of Neuroscience* 25.25, pp. 5926–5934. DOI: 10.1523/JNEUROSCI.1360-05.2005.

Kwon, Sung Eun et al. (2016). "Sensory and decision-related activity propagate in a cortical feedback loop during touch perception". eng. In: *Nature Neuroscience* 19.9, pp. 1243–1249. DOI: 10.1038/nn.4356.

Landers, Margo and H. Philip Zeigler (2006). "Development of rodent whisking: Trigeminal input and central pattern generation". In: *Somatosensory & Motor Research* 23.1-2, pp. 1–10. DOI: 10.1080/08990220600700768.

Langevin, Lisa Marie et al. (2007). "Validating in utero electroporation for the rapid analysis of gene regulatory elements in the murine telencephalon". eng. In: *Developmental Dynamics: An Official Publication of the American Association of Anatomists* 236.5, pp. 1273–1286. DOI: 10.1002/dvdy.21126.

Lavallée, Philippe et al. (2005). "Feedforward Inhibitory Control of Sensory Information in Higher-Order Thalamic Nuclei". en. In: *Journal of Neuroscience* 25.33, pp. 7489–7498. DOI: 10.1523/JNEUROSCI.2301-05.2005.

Lavzin, Maria et al. (2012). "Nonlinear dendritic processing determines angular tuning of barrel cortex neurons in vivo". en. In: *Nature* 490.7420, pp. 397–401. DOI: 10.1038/nature11451.

Lee, Brian R et al. (2021). "Scaled, high fidelity electrophysiological, morphological, and transcriptomic cell characterization". In: *eLife* 10. Ed. by Sacha B Nelson et al., e65482. DOI: 10.7554/eLife.65482.

Lee, Choongheon and Timothy A Jones (2018). "Effects of Ketamine Compared with Urethane Anesthesia on Vestibular Sensory Evoked Potentials and Systemic Physiology in Mice". In: *Journal of the American Association for Laboratory Animal Science : JAALAS* 57.3, pp. 268–277. DOI: 10.30802/AALAS-JAALAS-17-000131.

Lee, Li-Jen and Reha S. Erzurumlu (2005). "Altered parcellation of neocortical somatosensory maps in N-methyl-D-aspartate receptor-deficient mice". en. In: *Journal of Comparative Neurology* 485.1. DOI: 10.1002/cne.20514.

Lee, Seung-Chan et al. (2014). "Two Functionally Distinct Networks of Gap Junction-Coupled Inhibitory Neurons in the Thalamic Reticular Nucleus". en. In: *Journal of Neuroscience* 34.39, pp. 13170–13182. DOI: 10.1523/JNEUROSCI.0562-14.2014.

Lee, Soohyun et al. (2013). "A disinhibitory circuit mediates motor integration in the somatosensory cortex". en. In: *Nature Neuroscience* 16.11, pp. 1662–1670. DOI: 10.1038/nn.3544.

Lendvai, Balazs et al. (2000). "Experience-dependent plasticity of dendritic spines in the developing rat barrel cortex in vivo". en. In: *Nature* 404.6780, pp. 876–881. DOI: 10.1038/35009107.

Letzkus, Johannes J., Steffen B. E. Wolff, and Andreas Lüthi (2015). "Disinhibition, a Circuit Mechanism for Associative Learning and Memory". en. In: *Neuron* 88.2, pp. 264–276. DOI: 10.1016/j.neuron.2015.09.024.

Li, Hong and Michael C. Crair (2011). "How do barrels form in somatosensory cortex?" en. In: *Annals of the New York Academy of Sciences* 1225.1. DOI: 10.1111/j.1749-6632.2011.06024.x.

Li, Ye et al. (2012). "Clonally related visual cortical neurons show similar stimulus feature selectivity". en. In: *Nature* 486.7401, pp. 118–121. DOI: 10.1038/nature11110.

Lima, Susana Q. et al. (2009). "PINP: A New Method of Tagging Neuronal Populations for Identification during In Vivo Electrophysiological Recording". en. In: *PLoS ONE* 4.7. Ed. by Michael N. Nitabach, e6099. DOI: 10.1371/journal.pone.0006099.

Llorca, Alfredo et al. (2019). "A stochastic framework of neurogenesis underlies the assembly of neocortical cytoarchitecture". In: *eLife* 8. Ed. by Sonia Garel, Eve Marder, and Denis Jabaudon, e51381. DOI: 10.7554/eLife.51381.

Lohse, Michael et al. (2018). *Motor cortex can modulate somatosensory processing via cortico-thalamo-cortical pathway*. en. Tech. rep. bioRxiv, p. 366567. DOI: 10.1101/366567.

London, Michael and Michael Häusser (2005). "Dendritic Computation". In: *Annual Review of Neuroscience* 28.1, pp. 503–532. DOI: 10.1146/annurev.neuro.28.061604.135703.

Lu, Shao-Ming and Rick C.-S. Lin (1993). "Thalamic Afferents of the Rat Barrel Cortex: A Light-and Electron-Microscopic Study Using Phaseolus vulgaris Leucoagglutinin as an Anterograde Tracer". en. In: *Somatosensory & Motor Research* 10.1, pp. 1–16. DOI: 10.3109/08990229309028819.

Luczak, Artur, Peter Bartho, and Kenneth D. Harris (2013). "Gating of Sensory Input by Spontaneous Cortical Activity". en. In: *Journal of Neuroscience* 33.4, pp. 1684–1695. DOI: 10.1523/JNEUROSCI.2928-12.2013.

Luhmann, Heiko J. and Rustem Khazipov (2018). "Neuronal Activity Patterns in the Developing Barrel Cortex". en. In: *Neuroscience*. Barrel Cortex Function 368, pp. 256–267. DOI: 10.1016/j.neuroscience.2017.05.025.

Lund, R. D. and M. J. Mustari (1977). "Development of the geniculocortical pathway in rat". fr. In: *Journal of Comparative Neurology* 173.2. DOI: 10.1002/cne.901730206.

Lund, R. D. and K. E. Webster (1967). "Thalamic afferents from the spinal cord and trigeminal nuclei. An experimental anatomical study in the rat." en. In: *Journal of Comparative Neurology* 130.4. DOI: 10.1002/cne.901300404.

López-Bendito, Guillermina and Zoltán Molnár (2003). "Thalamocortical development: how are we going to get there?" en. In: *Nature Reviews Neuroscience* 4.4, pp. 276–289. DOI: 10.1038/nrn1075.

Major, Guy, Matthew E. Larkum, and Jackie Schiller (2013). "Active Properties of Neocortical Pyramidal Neuron Dendrites". In: *Annual Review of Neuroscience* 36.1, pp. 1–24. DOI: 10.1146/annurev-neuro-062111-150343.

Malatesta, P., E. Hartfuss, and M. Gotz (2000). "Isolation of radial glial cells by fluorescent-activated cell sorting reveals a neuronal lineage". In: *Development* 127.24, pp. 5253–5263. DOI: 10.1242/dev.127.24.5253.

Mangale, Vishakha S. et al. (2008). "Lhx2 Selector Activity Specifies Cortical Identity and Suppresses Hippocampal Organizer Fate". In: *Science* 319.5861, pp. 304–309. DOI: 10.1126/science.1151695.

Mansouri, Farshad Alizadeh et al. (2017). "Managing competing goals — a key role for the frontopolar cortex". en. In: *Nature Reviews Neuroscience* 18.11, pp. 645–657. DOI: 10.1038/nrn.2017.111.

Maravall, Miguel, Edward A. Stern, and Karel Svoboda (2004). "Development of Intrinsic Properties and Excitability of Layer 2/3 Pyramidal Neurons During a Critical Period for Sensory Maps in Rat Barrel Cortex". In: *Journal of Neurophysiology* 92.1, pp. 144–156. DOI: 10.1152/jn.00598.2003.

Markov, Nikola T. et al. (2014). "Anatomy of hierarchy: Feedforward and feedback pathways in macaque visual cortex". en. In: *Journal of Comparative Neurology* 522.1. DOI: 10.1002/cne.23458.

Markram, H (1997). "A network of tufted layer 5 pyramidal neurons." In: *Cerebral Cortex* 7.6, pp. 523–533. DOI: 10.1093/cercor/7.6.523.

Martínez-Cerdeño, Verónica, Stephen C. Noctor, and Arnold R. Kriegstein (2006). "The Role of Intermediate Progenitor Cells in the Evolutionary Expansion of the Cerebral Cortex". In: *Cerebral Cortex* 16.suppl_1, pp. i152–i161. DOI: 10.1093/cercor/bhk017.

Martínez-Garay, Isabel et al. (2016). "In Utero Electroporation Methods in the Study of Cerebral Cortical Development". en. In: *Prenatal and Postnatal Determinants of Development*. Ed. by David W. Walker. Neuromethods. New York, NY: Springer, pp. 21–39. DOI: 10.1007/978-1-4939-3014-2_2.

Masri, Radi et al. (2006). "Cholinergic Regulation of the Posterior Medial Thalamic Nucleus". In: *Journal of Neurophysiology* 96.5, pp. 2265–2273. DOI: 10.1152/jn.00476.2006.

Matho, Katherine S. et al. (2021). "Genetic dissection of the glutamatergic neuron system in cerebral cortex". en. In: *Nature* 598.7879, pp. 182–187. DOI: 10.1038/s41586-021-03955-9.

Matsui, Asuka et al. (2013). "BTBD3 Controls Dendrite Orientation Toward Active Axons in Mammalian Neocortex". In: *Science* 342.6162, pp. 1114–1118. DOI: 10.1126/science.1244505.

McCormick, David A., Matthew McGinley, and David Salkoff (2015). "Brain State Dependent Activity in the Cortex and Thalamus". In: *Current opinion in neurobiology* 31, pp. 133–140. DOI: 10.1016/j.conb.2014.10.003.

Mease, Rebecca A., Markus Metz, and Alexander Groh (2016). "Cortical Sensory Responses Are Enhanced by the Higher-Order Thalamus". en. In: *Cell Reports* 14.2, pp. 208–215. DOI: 10.1016/j.celrep.2015.12.026.

Meyer, Hanno S. et al. (2010). "Cell Type–Specific Thalamic Innervation in a Column of Rat Vibrissal Cortex". In: *Cerebral Cortex* 20.10, pp. 2287–2303. DOI: 10.1093/cercor/bhq069.

Migliore, Michele and Gordon M. Shepherd (2005). "An integrated approach to classifying neuronal phenotypes". en. In: *Nature Reviews Neuroscience* 6.10, pp. 810–818. DOI: 10.1038/nrn1769.

Miyashita-Lin, Emily M. et al. (1999). "Early Neocortical Regionalization in the Absence of Thalamic Innervation". In: *Science* 285.5429, pp. 906–909. DOI: 10.1126/science.285.5429.906.

Miyata, Takaki et al. (2001). "Asymmetric Inheritance of Radial Glial Fibers by Cortical Neurons". en. In: *Neuron* 31.5, pp. 727–741. DOI: 10.1016/S0896-6273(01)00420-2.

Miyata, Takaki et al. (2004). "Asymmetric production of surface-dividing and non-surface-dividing cortical progenitor cells". In: *Development* 131.13, pp. 3133–3145. DOI: 10.1242/dev.01173.

Mizuno, Hidenobu et al. (2018). "Patchwork-Type Spontaneous Activity in Neonatal Barrel Cortex Layer 4 Transmitted via Thalamocortical Projections". en. In: *Cell Reports* 22.1, pp. 123–135. DOI: 10.1016/j.celrep.2017.12.012.

Mo, Christina and S. Murray Sherman (2019). "A Sensorimotor Pathway via Higher-Order Thalamus". en. In: *Journal of Neuroscience* 39.4, pp. 692–704. DOI: 10.1523/JNEUROSCI.1467-18.2018.

Molnár, Zoltán, Richard Adams, and Colin Blakemore (1998). "Mechanisms Underlying the Early Establishment of Thalamocortical Connections in the Rat". en. In: *Journal of Neuroscience* 18.15, pp. 5723–5745. DOI: 10.1523/JNEUROSCI.18-15-05723.1998.

Molnár, Zoltán and Ann B. Butler (2002). "The corticostriatal junction: A crucial region for forebrain development and evolution". en. In: *BioEssays* 24.6, pp. 530–541. DOI: 10.1002/bies.10100.

Molnár, Zoltán, Shuji Higashi, and Guillermina López-Bendito (2003). "Choreography of Early Thalamocortical Development". In: *Cerebral Cortex* 13.6, pp. 661–669. DOI: 10.1093/cercor/13.6.661.

Monuki, Edwin S, Forbes D Porter, and Christopher A Walsh (2001). "Patterning of the Dorsal Telencephalon and Cerebral Cortex by a Roof Plate-Lhx2 Pathway". en. In: *Neuron* 32.4, pp. 591–604. DOI: 10.1016/S0896-6273(01)00504-9.

Muldal, Alistair M. et al. (2014). "Clonal relationships impact neuronal tuning within a phylogenetically ancient vertebrate brain structure". eng. In: *Current biology: CB* 24.16, pp. 1929–1933. DOI: 10.1016/j.cub.2014.07.015.

Murata, Yasunobu and Matthew T. Colonnese (2018). "Thalamus Controls Development and Expression of Arousal States in Visual Cortex". en. In: *Journal of Neuroscience* 38.41, pp. 8772–8786. DOI: 10.1523/JNEUROSCI.1519-18.2018.

Mégevand, Pierre et al. (2009). "Long-Term Plasticity in Mouse Sensorimotor Circuits after Rhythmic Whisker Stimulation". en. In: *Journal of Neuroscience* 29.16, pp. 5326–5335. DOI: 10.1523/JNEUROSCI.5965-08.2009.

Nakagawa, Yasushi, Jane E. Johnson, and Dennis D. M. O'Leary (1999). "Graded and Areal Expression Patterns of Regulatory Genes and Cadherins in Embryonic Neocortex Independent of Thalamocortical Input". en. In: *Journal of Neuroscience* 19.24, pp. 10877–10885. DOI: 10.1523/JNEUROSCI.19-24-10877.1999.

Nakajima, Miho and Michael M Halassa (2017). "Thalamic control of functional cortical connectivity". en. In: *Current Opinion in Neurobiology*. Neurobiology of Sleep 44, pp. 127–131. DOI: 10.1016/j.conb.2017.04.001.

Narboux-Nême, Nicolas et al. (2012). "Neurotransmitter Release at the Thalamocortical Synapse Instructs Barrel Formation But Not Axon Patterning in the Somatosensory Cortex". en. In: *Journal of Neuroscience* 32.18, pp. 6183–6196. DOI: 10.1523/JNEUROSCI.0343-12.2012.

Nassi, Jonathan J. and Edward M. Callaway (2009). "Parallel processing strategies of the primate visual system". en. In: *Nature Reviews Neuroscience* 10.5, pp. 360–372. DOI: 10.1038/nrn2619.

Nelson, Sacha (2002). "Cortical microcircuits: diverse or canonical?" eng. In: *Neuron* 36.1, pp. 19–27. DOI: 10.1016/s0896-6273(02)00944-3.

Nelson, Sacha B., Ken Sugino, and Chris M. Hempel (2006). "The problem of neuronal cell types: a physiological genomics approach". en. In: *Trends in Neurosciences*. Neural substrates of cognition 29.6, pp. 339–345. DOI: 10.1016/j.tins.2006.05.004.

Nieh, Edward H. et al. (2015). "Decoding Neural Circuits that Control Compulsive Sucrose Seeking". en. In: *Cell* 160.3, pp. 528–541. DOI: 10.1016/j.cell.2015.01.003.

Niell, Cristopher M. and Michael P. Stryker (2008). "Highly Selective Receptive Fields in Mouse Visual Cortex". en. In: *Journal of Neuroscience* 28.30, pp. 7520–7536. DOI: 10.1523/JNEUROSCI.0623-08.2008.

Nixon, Sophie L. (2017). "Examining the influence of lineage relationships upon mammalian excitatory neocortical development". PhD thesis. University of Oxford.

Noctor, Stephen C. et al. (2001). "Neurons derived from radial glial cells establish radial units in neocortex". en. In: *Nature* 409.6821, pp. 714–720. DOI: 10.1038/35055553.

Noctor, Stephen C. et al. (2002). "Dividing Precursor Cells of the Embryonic Cortical Ventricular Zone Have Morphological and Molecular Characteristics of Radial Glia". en. In: *Journal of Neuroscience* 22.8, pp. 3161–3173. DOI: 10.1523/JNEUROSCI.22-08-03161.2002.

Noctor, Stephen C et al. (2004). "Cortical neurons arise in symmetric and asymmetric division zones and migrate through specific phases". en. In: *Nature Neuroscience* 7.2, pp. 136–144. DOI: 10.1038/nn1172.

Nurminen, Lauri et al. (2018). "Top-down feedback controls spatial summation and response amplitude in primate visual cortex". en. In: *Nature Communications* 9.1, p. 2281. DOI: 10.1038/s41467-018-04500-5.

Oberlaender, Marcel et al. (2012). "Cell Type–Specific Three-Dimensional Structure of Thalamocortical Circuits in a Column of Rat Vibrissal Cortex". In: *Cerebral Cortex* 22.10, pp. 2375–2391. DOI: 10.1093/cercor/bhr317.

Oberst, Polina et al. (2019). "Temporal plasticity of apical progenitors in the developing mouse neocortex". en. In: *Nature* 573.7774, pp. 370–374. DOI: 10.1038/s41586-019-1515-6.

Oh, Seung Wook et al. (2014). "A mesoscale connectome of the mouse brain". en. In: *Nature* 508.7495, pp. 207–214. DOI: 10.1038/nature13186.

Ohki, Kenichi et al. (2005). "Functional imaging with cellular resolution reveals precise micro-architecture in visual cortex". en. In: *Nature* 433.7026, pp. 597–603. DOI: 10.1038/nature03274.

Ohtsuki, Gen et al. (2012). "Similarity of Visual Selectivity among Clonally Related Neurons in Visual Cortex". English. In: *Neuron* 75.1, pp. 65–72. DOI: 10.1016/j.neuron.2012.05.023.

Okun, Michael, Amir Naim, and Ilan Lampl (2010). "The Subthreshold Relation between Cortical Local Field Potential and Neuronal Firing Unveiled by Intracellular Recordings in Awake Rats". en. In: *Journal of Neuroscience* 30.12, pp. 4440–4448. DOI: 10.1523/JNEUROSCI.5062-09.2010.

Okun, Michael et al. (2012). "Population Rate Dynamics and Multineuron Firing Patterns in Sensory Cortex". In: *The Journal of Neuroscience* 32.48, pp. 17108–17119. DOI: 10.1523/JNEUROSCI.1831-12.2012.

Okun, Michael et al. (2015). "Diverse coupling of neurons to populations in sensory cortex". en. In: *Nature* 521.7553, pp. 511–515. DOI: 10.1038/nature14273.

Olsen, Grethe M. and Menno P. Witter (2016). "Posterior parietal cortex of the rat: Architectural delineation and thalamic differentiation". en. In: *Journal of Comparative Neurology* 524.18. DOI: 10.1002/cne.24032.

Pachitariu, Marius et al. (2015). "State-Dependent Population Coding in Primary Auditory Cortex". en. In: *Journal of Neuroscience* 35.5, pp. 2058–2073. DOI: 10.1523/JNEUROSCI.3318-14.2015.

Pachitariu, Marius et al. (2016). *Kilosort: realtime spike-sorting for extracellular electrophysiology with hundreds of channels*. en. Tech. rep., p. 061481. DOI: 10.1101/061481.

Pal, Suranjana et al. (2021). "An Early Cortical Progenitor-Specific Mechanism Regulates Thalamocortical Innervation". en. In: *Journal of Neuroscience* 41.32, pp. 6822–6835. DOI: 10.1523/JNEUROSCI.0226-21.2021.

Palmer, Lucy M. et al. (2014). "NMDA spikes enhance action potential generation during sensory input". en. In: *Nature Neuroscience* 17.3, pp. 383–390. DOI: 10.1038/nn.3646.

Peng, Hanchuan et al. (2021). "Morphological diversity of single neurons in molecularly defined cell types". In: *Nature* 598.7879, pp. 174–181.

Perin, Rodrigo, Thomas K. Berger, and Henry Markram (2011). "A synaptic organizing principle for cortical neuronal groups". In: *Proceedings of the National Academy of Sciences* 108.13, pp. 5419–5424. DOI: 10.1073/pnas.1016051108.

Petersen, Carl C. H. et al. (2003). "Interaction of sensory responses with spontaneous depolarization in layer 2/3 barrel cortex". In: *Proceedings of the National Academy of Sciences* 100.23, pp. 13638–13643. DOI: 10.1073/pnas.2235811100.

Petersen, Carl C.H. (2007). "The Functional Organization of the Barrel Cortex". en. In: *Neuron* 56.2, pp. 339–355. DOI: 10.1016/j.neuron.2007.09.017.

Petreanu, Leopoldo et al. (2009). "The subcellular organization of neocortical excitatory connections". eng. In: *Nature* 457.7233, pp. 1142–1145. DOI: 10.1038/nature07709.

Petty, Gordon H. et al. (2021). *Effects of arousal and movement on secondary somatosensory and visual thalamus*. en. DOI: 10.7554/eLife.67611.

Pi, Hyun-Jae et al. (2013). "Cortical interneurons that specialize in disinhibitory control". en. In: *Nature* 503.7477, pp. 521–524. DOI: 10.1038/nature12676.

Pinault, Didier (2004). "The thalamic reticular nucleus: structure, function and concept". en. In: *Brain Research Reviews* 46.1, pp. 1–31. DOI: 10.1016/j.brainresrev.2004.04.008.

Pinault, Didier and Martin Deschênes (1998). "Anatomical evidence for a mechanism of lateral inhibition in the rat thalamus". en. In: *European Journal of Neuroscience* 10.11. DOI: 10.1046/j.1460-9568.1998.00362.x.

Piñon, Maria Carmen et al. (2009). "Dynamic integration of subplate neurons into the cortical barrel field circuitry during postnatal development in the Golli-tau-eGFP (GTE) mouse". en. In: *The Journal of Physiology* 587.9, pp. 1903–1915. DOI: 10.1113/jphysiol.2008.167767.

Pouchelon, Gabrielle et al. (2014). "Modality-specific thalamocortical inputs instruct the identity of postsynaptic L4 neurons". en. In: *Nature* 511.7510, pp. 471–474. DOI: 10.1038/nature13390.

Poulet, James F. A. et al. (2012). "Thalamic control of cortical states". en. In: *Nature Neuroscience* 15.3, pp. 370–372. DOI: 10.1038/nn.3035.

Puelles, Luis et al. (2000). "Pallial and subpallial derivatives in the embryonic chick and mouse telencephalon, traced by the expression of the genes Dlx-2, Emx-1, Nkx-2.1, Pax-6, and Tbr-1". en. In: *Journal of Comparative Neurology* 424.3. DOI: 10.1002/1096-9861(20000828)424:3<409::AID-CNE3>3.0.CO;2-7.

Qian, Xueming et al. (2000). "Timing of CNS Cell Generation: A Programmed Sequence of Neuron and Glial Cell Production from Isolated Murine Cortical Stem Cells". en. In: *Neuron* 28.1, pp. 69–80. DOI: 10.1016/S0896-6273(00)00086-6.

Rakic, P. (1988). "Specification of cerebral cortical areas". eng. In: *Science (New York, N.Y.)* 241.4862, pp. 170–176. DOI: 10.1126/science.3291116.

Ramos, Susana I. et al. (2020). "Tuba8 Drives Differentiation of Cortical Radial Glia into Apical Intermediate Progenitors by Tuning Modifications of Tubulin C Termini". en. In: *Developmental Cell* 52.4, 477–491.e8. DOI: 10.1016/j.devcel.2020.01.036.

Ranjbar-Slamloo, Yadollah and Ehsan Arabzadeh (2019). "Diverse tuning underlies sparse activity in layer 2/3 vibrissal cortex of awake mice". en. In: *The Journal of Physiology* 597.10, pp. 2803–2817. DOI: 10.1113/JP277506.

Rebsam, Alexandra, Isabelle Seif, and Patricia Gaspar (2002). "Refinement of Thalamocortical Arbors and Emergence of Barrel Domains in the Primary Somatosensory Cortex: A Study of Normal and Monoamine Oxidase A Knock-Out Mice". en. In: *Journal of Neuroscience* 22.19, pp. 8541–8552. DOI: 10.1523/JNEUROSCI.22-19-08541.2002.

– (2005). "Dissociating Barrel Development and Lesion-Induced Plasticity in the Mouse Somatosensory Cortex". en. In: *Journal of Neuroscience* 25.3, pp. 706–710. DOI: 10.1523/JNEUROSCI.4191-04.2005.

Redondo, Roger L. and Richard G. M. Morris (2011). "Making memories last: the synaptic tagging and capture hypothesis". en. In: *Nature Reviews Neuroscience* 12.1, pp. 17–30. DOI: 10.1038/nrn2963.

Reid, R. C. and J. M. Alonso (1995). "Specificity of monosynaptic connections from thalamus to visual cortex". eng. In: *Nature* 378.6554, pp. 281–284. DOI: 10.1038/378281a0.

Rey, Hernan Gonzalo, Carlos Pedreira, and Rodrigo Quian Quiroga (2015). "Past, present and future of spike sorting techniques". en. In: *Brain Research Bulletin*. Advances in electrophysiological data analysis 119, pp. 106–117. DOI: 10.1016/j.brainresbull.2015.04.007.

Rice, Frank Lambert et al. (1985). "AComparative analysis of the development of the primary somatosensory cortex: Interspecies similarities during barrel and laminar development". en. In: *Journal of Comparative Neurology* 236.4. DOI: 10.1002/cne.902360405.

Rikhye, Rajeev V., Ralf D. Wimmer, and Michael M. Halassa (2018). "Toward an Integrative Theory of Thalamic Function". In: *Annual Review of Neuroscience* 41.1, pp. 163–183. DOI: 10.1146/annurev-neuro-080317-062144.

Roelfsema, Pieter R. and Anthony Holtmaat (2018). "Control of synaptic plasticity in deep cortical networks". en. In: *Nature Reviews Neuroscience* 19.3, pp. 166–180. DOI: 10.1038/nrn.2018.6.

Rossant, Cyrille et al. (2016). "Spike sorting for large, dense electrode arrays". In: *Nature neuroscience* 19.4, pp. 634–641. DOI: 10.1038/nn.4268.

Roth, Morgane M et al. (2016). "Thalamic nuclei convey diverse contextual information to layer 1 of visual cortex". en. In: *Nature Neuroscience* 19.2, pp. 299–307. DOI: 10.1038/nn.4197.

Rovó, Zita, István Ulbert, and László Acsády (2012). "Drivers of the Primate Thalamus". en. In: *Journal of Neuroscience* 32.49, pp. 17894–17908. DOI: 10.1523/JNEUROSCI.2815-12.2012.

Roy, Dheeraj S. et al. (2022). "Thalamic subnetworks as units of function". en. In: *Nature Neuroscience* 25.2, pp. 140–153. DOI: 10.1038/s41593-021-00996-1.

Sachdev, Robert N. S., Ford F. Ebner, and Charles J. Wilson (2004). "Effect of Subthreshold Up and Down States on the Whisker-Evoked Response in Somatosensory Cortex". In: *Journal of Neurophysiology* 92.6, pp. 3511–3521. DOI: 10.1152/jn.00347.2004.

Sato, Takashi R. et al. (2007). "The Functional Microarchitecture of the Mouse Barrel Cortex". en. In: *PLOS Biology* 5.7, e189. DOI: 10.1371/journal.pbio.0050189.

Senft, Stephen L. and Thomas A. Woolsey (1991). "Growth of Thalamic Afferents into Mouse Barrel Cortex". In: *Cerebral Cortex* 1.4, pp. 308–335. DOI: 10.1093/cercor/1.4.308.

Sermet, B Semihcan et al. (2019). "Pathway-, layer- and cell-type-specific thalamic input to mouse barrel cortex". In: *eLife* 8. Ed. by Sacha B Nelson et al., e52665. DOI: 10.7554/eLife.52665.

Sherman, S. M. and R. W. Guillery (1996). "Functional organization of thalamocortical relays". en. In: *Journal of Neurophysiology* 76.3, pp. 1367–1395. DOI: 10.1152/jn.1996.76.3.1367.

– (1998). "On the actions that one nerve cell can have on another: Distinguishing "drivers" from "modulators"". en. In: *Proceedings of the National Academy of Sciences* 95.12, pp. 7121–7126. DOI: 10.1073/pnas.95.12.7121.

Sherman, S Murray (2012). "Thalamocortical interactions". en. In: *Current Opinion in Neurobiology* 22.4, pp. 575–579. DOI: 10.1016/j.conb.2012.03.005.

Sherman, S. Murray (2014). "The Function of Metabotropic Glutamate Receptors in Thalamus and Cortex". en. In: *The Neuroscientist* 20.2, pp. 136–149. DOI: 10.1177/1073858413478490.

Sherman, S Murray (2016). "Thalamus plays a central role in ongoing cortical functioning". en. In: *Nature Neuroscience* 19.4, pp. 533–541. DOI: 10.1038/nn.4269.

Sherman, S. Murray and R. W. Guillery (2005). *Exploring the Thalamus and Its Role in Cortical Function*. en. 2nd ed. Cambridge, MA, USA: MIT Press.

Sherman, S. Murray and R. W. Guillery (2013). *Functional Connections of Cortical Areas: A New View from the Thalamus*. en. Cambridge, MA, USA: MIT Press.

Shetty, Ashwin S. et al. (2013). "Lhx2 regulates a cortex-specific mechanism for barrel formation". en. In: *Proceedings of the National Academy of Sciences* 110.50, E4913–E4921. DOI: 10.1073/pnas.1311158110.

Shoykhet, Michael, Peter W. Land, and Daniel J. Simons (2005). "Whisker Trimming Begun at Birth or on Postnatal Day 12 Affects Excitatory and Inhibitory Receptive Fields of Layer IV Barrel Neurons". In: *Journal of Neurophysiology* 94.6, pp. 3987–3995. DOI: 10.1152/jn.00569.2005.

Siegle, Joshua H. et al. (2021). "Survey of spiking in the mouse visual system reveals functional hierarchy". en. In: *Nature*. DOI: 10.1038/s41586-020-03171-x.

Siggs, Owen and Bruce Beutler (2012). "The BTB-ZF transcription factors". In: *Cell Cycle* 11.18, pp. 3358–3369. DOI: 10.4161/cc.21277.

Silberberg, Gilad and Henry Markram (2007). "Disynaptic Inhibition between Neocortical Pyramidal Cells Mediated by Martinotti Cells". en. In: *Neuron* 53.5, pp. 735–746. DOI: 10.1016/j.neuron.2007.02.012.

Simons, D. J. (1978). "Response properties of vibrissa units in rat SI somatosensory neocortex". In: *Journal of Neurophysiology* 41.3, pp. 798–820. DOI: 10.1152/jn.1978.41.3.798.

Simons, D. J. and G. E. Carvell (1989). "Thalamocortical response transformation in the rat vibrissa/barrel system". en. In: *Journal of Neurophysiology* 61.2, pp. 311–330. DOI: 10.1152/jn.1989.61.2.311.

Simons, Daniel J. and Thomas A. Woolsey (1984). "Morphology of Golgi-Cox-impregnated barrel neurons in rat SmI cortex". en. In: *The Journal of Comparative Neurology* 230.1, pp. 119–132. DOI: 10.1002/cne.902300111.

Simons, DanielJ. et al. (1992). "Responses of barrel cortex neurons in awake rats and effects of urethane anesthesia". en. In: *Experimental Brain Research* 91.2. DOI: 10.1007/BF00231659.

Sobolewski, Aleksander et al. (2015). "Alertness opens the effective flow of sensory information through rat thalamic posterior nucleus". en. In: *European Journal of Neuroscience* 41.10. DOI: 10.1111/ejn.12901.

Somogyi, Peter and Thomas Klausberger (2005). "Defined types of cortical interneurone structure space and spike timing in the hippocampus". en. In: *The Journal of Physiology* 562.1. DOI: 10.1113/jphysiol.2004.078915.

Song, Sen et al. (2005). "Highly Nonrandom Features of Synaptic Connectivity in Local Cortical Circuits". en. In: *PLOS Biology* 3.3, e68. DOI: 10.1371/journal.pbio.0030068.

Spruston, Nelson (2008). "Pyramidal neurons: dendritic structure and synaptic integration". en. In: *Nature Reviews Neuroscience* 9.3, pp. 206–221. DOI: 10.1038/nrn2286.

Staiger, J. F. (2004). "Functional Diversity of Layer IV Spiny Neurons in Rat Somatosensory Cortex: Quantitative Morphology of Electrophysiologically Characterized and Biocytin Labeled Cells". en. In: *Cerebral Cortex* 14.6, pp. 690–701. DOI: 10.1093/cercor/bhh029.

Stancik, E. K. et al. (2010). "Heterogeneity in Ventricular Zone Neural Precursors Contributes to Neuronal Fate Diversity in the Postnatal Neocortex". en. In: *Journal of Neuroscience* 30.20, pp. 7028–7036. DOI: 10.1523/JNEUROSCI.6131-09.2010.

Stepanyants, Armen et al. (2009). "The fractions of short- and long-range connections in the visual cortex". In: *Proceedings of the National Academy of Sciences* 106.9, pp. 3555–3560. DOI: 10.1073/pnas.0810390106.

Stern, Edward A, Miguel Maravall, and Karel Svoboda (2001). "Rapid Development and Plasticity of Layer 2/3 Maps in Rat Barrel Cortex In Vivo". en. In: *Neuron* 31.2, pp. 305–315. DOI: 10.1016/S0896-6273(01)00360-9.

Stevens, Charles F (1998). "Neuronal diversity: Too many cell types for comfort?" en. In: *Current Biology* 8.20, R708–R710. DOI: 10.1016/S0960-9822(98)70454-3.

Stoykova, A. and P. Gruss (1994). "Roles of Pax-genes in developing and adult brain as suggested by expression patterns". en. In: *Journal of Neuroscience* 14.3, pp. 1395–1412. DOI: 10.1523/JNEUROSCI.14-03-01395.1994.

Suzuki, Mototaka and Matthew E. Larkum (2020). "General Anesthesia Decouples Cortical Pyramidal Neurons". en. In: *Cell* 180.4, 666–676.e13. DOI: 10.1016/j.cell.2020.01.024.

Suzuki, Sachihiro C. et al. (1997). "Neuronal Circuits Are Subdivided by Differential Expression of Type-II Classic Cadherins in Postnatal Mouse Brains". en. In: *Molecular and Cellular Neuroscience* 9.5, pp. 433–447. DOI: 10.1006/mcne.1997.0626.

Svoboda, Karel and Nuo Li (2018). "Neural mechanisms of movement planning: motor cortex and beyond". eng. In: *Current Opinion in Neurobiology* 49, pp. 33–41. DOI: 10.1016/j.conb.2017.10.023.

Sweeney, Yann and Claudia Clopath (2020). "Population coupling predicts the plasticity of stimulus responses in cortical circuits". In: *eLife* 9. Ed. by Ronald L Calabrese, Blake A Richards, and Brent Doiron, e56053. DOI: 10.7554/eLife.56053.

Szczurkowska, Joanna et al. (2016). "Targeted in vivo genetic manipulation of the mouse or rat brain by in utero electroporation with a triple-electrode probe". en. In: *Nature Protocols* 11.3, pp. 399–412. DOI: 10.1038/nprot.2016.014.

Tamamaki, Nobuaki et al. (2001). "Radial glia is a progenitor of neocortical neurons in the developing cerebral cortex". en. In: *Neuroscience Research* 41.1, pp. 51–60. DOI: 10.1016/S0168-0102(01)00259-0.

Tanke, Nouk, J. Gerard G. Borst, and Arthur R. Houweling (2018). "Single-Cell Stimulation in Barrel Cortex Influences Psychophysical Detection Performance". In: *The Journal of Neuroscience* 38.8, pp. 2057–2068. DOI: 10.1523/JNEUROSCI.2155-17.2018.

Tasic, Bosiljka et al. (2016). "Adult mouse cortical cell taxonomy revealed by single cell transcriptomics". en. In: *Nature Neuroscience* 19.2, pp. 335–346. DOI: 10.1038/nn.4216.

Tasic, Bosiljka et al. (2018). "Shared and distinct transcriptomic cell types across neocortical areas". en. In: *Nature* 563.7729, pp. 72–78. DOI: 10.1038/s41586-018-0654-5.

Taverna, Elena, Magdalena Götz, and Wieland B. Huttner (2014). "The Cell Biology of Neurogenesis: Toward an Understanding of the Development and Evolution of the Neocortex". en. In: *Annual Review of Cell and Developmental Biology* 30.1, pp. 465–502. DOI: 10.1146/annurev-cellbio-101011-155801.

Telley, L. et al. (2019). "Temporal patterning of apical progenitors and their daughter neurons in the developing neocortex". In: *Science* 364.6440, eaav2522. DOI: 10.1126/science.aav2522.

Telley, Ludovic et al. (2016). "Sequential transcriptional waves direct the differentiation of newborn neurons in the mouse neocortex". In: *Science* 351.6280, pp. 1443–1446. DOI: 10.1126/science.aad8361.

Theyel, Brian B., Daniel A. Llano, and S. Murray Sherman (2010). "The corticothalamocortical circuit drives higher-order cortex in the mouse". en. In: *Nature Neuroscience* 13.1, pp. 84–88. DOI: 10.1038/nn.2449.

Thomson, Alex (2010). "Neocortical layer 6, a review". In: *Frontiers in Neuroanatomy* 4.

Thomson, Alex and Christophe Lamy (2007). "Functional maps of neocortical local circuitry". In: *Frontiers in Neuroscience* 1.

Trageser, Jason C. and Asaf Keller (2004). "Reducing the Uncertainty: Gating of Peripheral Inputs by Zona Incerta". en. In: *Journal of Neuroscience* 24.40, pp. 8911–8915. DOI: 10.1523/JNEUROSCI.3218-04.2004.

Tyler, W. A. and T. F. Haydar (2013). "Multiplex Genetic Fate Mapping Reveals a Novel Route of Neocortical Neurogenesis, Which Is Altered in the Ts65Dn Mouse Model of Down Syndrome". en. In: *Journal of Neuroscience* 33.12, pp. 5106–5119. DOI: 10.1523/JNEUROSCI.5380-12.2013.

Tyler, William A. et al. (2015). "Neural Precursor Lineages Specify Distinct Neocortical Pyramidal Neuron Types". In: *The Journal of Neuroscience* 35.15, pp. 6142–6152. DOI: 10.1523/JNEUROSCI.0335-15.2015.

Urbain, Nadia and Martin Deschênes (2007). "A New Thalamic Pathway of Vibrissal Information Modulated by the Motor Cortex". en. In: *Journal of Neuroscience* 27.45, pp. 12407–12412. DOI: 10.1523/JNEUROSCI.2914-07.2007.

Usrey, W. Martin, Jose-Manuel Alonso, and R. Clay Reid (2000). "Synaptic Interactions between Thalamic Inputs to Simple Cells in Cat Visual Cortex". en. In: *Journal of Neuroscience* 20.14, pp. 5461–5467. DOI: 10.1523/JNEUROSCI.20-14-05461.2000.

Usrey, W. Martin and S. Murray Sherman (2019). "Corticofugal Circuits: Communication Lines from the Cortex to the Rest of the Brain". In: *The Journal of comparative neurology* 527.3, pp. 640–650. DOI: 10.1002/cne.24423.

Van Der Loos, Hendrik (1976). "Barreloids in mouse somatosensory thalamus". en. In: *Neuroscience Letters* 2.1, pp. 1–6. DOI: 10.1016/0304-3940(76)90036-7.

Vangeneugden, Joris et al. (2019). "Activity in Lateral Visual Areas Contributes to Surround Suppression in Awake Mouse V1". en. In: *Current Biology* 29.24, 4268–4275.e7. DOI: 10.1016/j.cub.2019.10.037.

Veinante, Pierre and Martin Deschênes (1999). "Single- and Multi-Whisker Channels in the Ascending Projections from the Principal Trigeminal Nucleus in the Rat". en. In: *Journal of Neuroscience* 19.12, pp. 5085–5095. DOI: 10.1523/JNEUROSCI.19-12-05085.1999.

Viaene, A. N., I. Petrof, and S. M. Sherman (2011a). "Properties of the thalamic projection from the posterior medial nucleus to primary and secondary somatosensory cortices in the mouse". en. In: *Proceedings of the National Academy of Sciences* 108.44, pp. 18156–18161. DOI: 10.1073/pnas.1114828108.

– (2011b). "Synaptic Properties of Thalamic Input to Layers 2/3 and 4 of Primary Somatosensory and Auditory Cortices". In: *Journal of Neurophysiology* 105.1, pp. 279–292. DOI: 10.1152/jn.00747.2010.

– (2011c). "Synaptic properties of thalamic input to the subgranular layers of primary somatosensory and auditory cortices in the mouse". eng. In: *The Journal of Neuroscience: The Official Journal of the Society for Neuroscience* 31.36, pp. 12738–12747. DOI: 10.1523/JNEUROSCI.1565-11.2011.

Vitali, Ilaria and Denis Jabaudon (2014). "Synaptic biology of barrel cortex circuit assembly". en. In: *Seminars in Cell & Developmental Biology*. Regulated Necrosis & Modeling developmental signaling pathways & Development of connective maps in the brain 35, pp. 156–164. DOI: 10.1016/j.semcdb.2014.07.009.

Vélez-Fort, Mateo et al. (2014). "The Stimulus Selectivity and Connectivity of Layer Six Principal Cells Reveals Cortical Microcircuits Underlying Visual Processing". en. In: *Neuron* 83.6, pp. 1431–1443. DOI: 10.1016/j.neuron.2014.08.001.

Waite, Phil M. E. (1973). "Somatotopic organization of vibrissal responses in the ventro-basal complex of the rat thalamus". en. In: *The Journal of Physiology* 228.2. DOI: 10.1113/jphysiol.1973.sp010098.

Wang, Chia-Fang et al. (2017). "Lhx2 Expression in Postmitotic Cortical Neurons Initiates Assembly of the Thalamocortical Somatosensory Circuit". en. In: *Cell Reports* 18.4, pp. 849–856. DOI: 10.1016/j.celrep.2017.01.001.

Wang, Xiaoqun et al. (2011). "A new subtype of progenitor cell in the mouse embryonic neocortex". en. In: *Nature Neuroscience* 14.5, pp. 555–561. DOI: 10.1038/nn.2807.

Wang, Yun et al. (2004). "Anatomical, physiological and molecular properties of Martinotti cells in the somatosensory cortex of the juvenile rat". en. In: *The Journal of Physiology* 561.1, pp. 65–90. DOI: 10.1113/jphysiol.2004.073353.

Welker, Carol (1971). "Microelectrode delineation of fine grain somatotopic organization of SmI cerebral neocortex in albino rat". en. In: *Brain Research* 26.2, pp. 259–275. DOI: 10.1016/S0006-8993(71)80004-5.

Wen, Jing A. and Alison L. Barth (2011). "Input-Specific Critical Periods for Experience-Dependent Plasticity in Layer 2/3 Pyramidal Neurons". en. In: *Journal of Neuroscience* 31.12, pp. 4456–4465. DOI: 10.1523/JNEUROSCI.6042-10.2011.

Williams, Leena and Anthony Holtmaat (2019). "Higher-Order Thalamocortical Inputs Gate Synaptic Long-Term Potentiation via Disinhibition". en. In: *Neuron* 101.1, 91–102.e4. DOI: 10.1016/j.neuron.2018.10.049.

Williams, M. N., D. S. Zahm, and M. F. Jacquin (1994). "Differential foci and synaptic organization of the principal and spinal trigeminal projections to the thalamus in the rat". eng. In: *The European Journal of Neuroscience* 6.3, pp. 429–453. DOI: 10.1111/j.1460-9568.1994.tb00286.x.

Wimmer, Verena C. et al. (2010). "Dimensions of a Projection Column and Architecture of VPM and POm Axons in Rat Vibrissal Cortex". In: *Cerebral Cortex* 20.10, pp. 2265–2276. DOI: 10.1093/cercor/bhq068.

Woolsey, Thomas A and Hendrik Van der Loos (1970). "The structural organisation of layer IV in the somatosensory region (S1) of mouse cerebral cortex." In: *Brain Research* 17, pp. 205–242.

Wu, Chia-Shan, Carlos J. Ballester Rosado, and Hui-Chen Lu (2011). "What can we get from 'barrels': the rodent barrel cortex as a model for studying the establishment of neural circuits". en. In: *European Journal of Neuroscience* 34.10. DOI: 10.1111/j.1460-9568.2011.07892.x.

Wu, Sheng-Xi et al. (2005). "Pyramidal neurons of upper cortical layers generated by NEX-positive progenitor cells in the subventricular zone". In: *Proceedings of the National Academy of Sciences* 102.47, pp. 17172–17177. DOI: 10.1073/pnas.0508560102.

Xie, Yu-feng, Michael F Jackson, and John F MacDonald (2013). "Optogenetics and synaptic plasticity". In: *Acta Pharmacologica Sinica* 34.11, pp. 1381–1385. DOI: 10.1038/aps.2013.150.

Xu, Ning-long et al. (2012). "Nonlinear dendritic integration of sensory and motor input during an active sensing task". en. In: *Nature* 492.7428, pp. 247–251. DOI: 10.1038/nature11601.

Yao, Zizhen et al. (2021). "A taxonomy of transcriptomic cell types across the isocortex and hippocampal formation". eng. In: *Cell* 184.12, 3222–3241.e26. DOI: 10.1016/j.cell.2021.04.021.

Yoshimura, Yumiko, Jami L. M. Dantzker, and Edward M. Callaway (2005). "Excitatory cortical neurons form fine-scale functional networks". en. In: *Nature* 433.7028, pp. 868–873. DOI: 10.1038/nature03252.

Yu, Jianing et al. (2019). "Recruitment of GABAergic Interneurons in the Barrel Cortex during Active Tactile Behavior". en. In: *Neuron* 104.2, 412–427.e4. DOI: 10.1016/j.neuron.2019.07.027.

Yu, Yong-Chun et al. (2009). "Specific synapses develop preferentially among sister excitatory neurons in the neocortex". en. In: *Nature* 458.7237, pp. 501–504. DOI: 10.1038/nature07722.

Yu, Yong-Chun et al. (2012). "Preferential electrical coupling regulates neocortical lineage-dependent microcircuit assembly". en. In: *Nature* 486.7401, pp. 113–117. DOI: 10.1038/nature10958.

Yuste, Rafael et al. (2020). "A community-based transcriptomics classification and nomenclature of neocortical cell types". en. In: *Nature Neuroscience* 23.12, pp. 1456–1468. DOI: 10.1038/s41593-020-0685-8.

Zador, Anthony M. (2019). "A critique of pure learning and what artificial neural networks can learn from animal brains". en. In: *Nature Communications* 10.1, p. 3770. DOI: 10.1038/s41467-019-11786-6.

Zeng, Hongkui and Joshua R. Sanes (2017). "Neuronal cell-type classification: challenges, opportunities and the path forward". en. In: *Nature Reviews Neuroscience* 18.9, pp. 530–546. DOI: 10.1038/nrn.2017.85.

Zhang, Siyu et al. (2014). "Long-range and local circuits for top-down modulation of visual cortex processing". In: *Science* 345.6197, pp. 660–665. DOI: 10.1126/science.1254126.

Zhang, Wanying and Randy M Bruno (2019). "High-order thalamic inputs to primary somatosensory cortex are stronger and longer lasting than cortical inputs". In: *eLife* 8. Ed. by Ronald L Calabrese, e44158. DOI: 10.7554/eLife.44158.

Zhang, Z W and M Deschênes (1998). "Projections to layer VI of the posteromedial barrel field in the rat: a reappraisal of the role of corticothalamic pathways." In: *Cerebral Cortex* 8.5, pp. 428–436. DOI: 10.1093/cercor/8.5.428.

Zhu, Yinghua and J. Julius Zhu (2004). "Rapid Arrival and Integration of Ascending Sensory Information in Layer 1 Nonpyramidal Neurons and Tuft Dendrites

of Layer 5 Pyramidal Neurons of the Neocortex". en. In: *Journal of Neuroscience* 24.6, pp. 1272–1279. DOI: 10.1523/JNEUROSCI.4805-03.2004.

Zingg, Brian et al. (2014). "Neural Networks of the Mouse Neocortex". en. In: *Cell* 156.5, pp. 1096–1111. DOI: 10.1016/j.cell.2014.02.023.

"*We shall not cease from exploration*
*And the end of all our exploring*
*Will be to arrive where we started*
*And know the place for the first time.*"

T. S. Eliot